

**PHOTOACOUSTIC SPECTROSCOPY  
OF  
CHEMICAL AND BIOLOGICAL SYSTEMS**

**A THESIS  
SUBMITTED FOR THE DEGREE OF  
DOCTOR OF PHILOSOPHY**

**BY  
CH. MOHAN RAO**

**SCHOOL OF CHEMISTRY  
UNIVERSITY OF HYDERABAD  
HYDERABAD - 500 134,**

**AUGUST, 1983.**

in loving memory  
of my father  
**Dr.Ch.Seshagiri Rao**

## CONTENTS

<u>Sl.No.</u>		<u>Page No.</u>
1.	Statement	ii
2.	Certificate	iii
3.	Acknowledgements	iv
4.	Synopsis	v
5.	<u>CHAPTER I</u>	1
	The Technique	
6.	<u>CHAPTER II</u>	47
	Investigation of Catalyst Surfaces	
7.	<u>CHAPTER III</u>	68
	Study of a Solid State Photoreaction	
8.	<u>CHAPTER IV</u>	92
	On the Mode of Action of Antimalarial Drugs	
9.	<u>CHAPTER V</u>	124
	Some Ongoing Projects	
10.	Vitae	141

### STATEMENT

I hereby declare that the matter embodied in this thesis is the result of investigations carried out by me as a research student of the School of Chemistry, University of Hyderabad, Hyderabad under the supervision of Professor D. Balasubramanian.

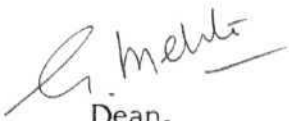
In keeping with the general practice of reporting scientific observations, due acknowledgement has been made wherever the work described is based on the findings of other investigators.


  
( CH. MOHAN RAO )



**CERTIFICATE**

Certified that the work contained in this thesis entitled  
"Photoacoustic spectroscopy of chemical and biological systems" has  
been carried out by Ch. Mohan Rao under my supervision and the same  
has not been submitted elsewhere for a degree.

  
Dean,  
School of Chemistry

  
(Professor D. Balasubramanian)  
Thesis Supervisor

## **ACKNOWLEDGEMENTS**

I express my sincere gratitude to Professor D. Balasubramanian for introducing me to Photoacoustic Spectroscopy. I appreciate his advice, encouragement and care in general, even more than his specific guidance which led to this thesis. My association with him has been very pleasant and rewarding.

I am grateful to Professor G. Mehta, Dean, School of Chemistry, and Professor A.K. Bhatnagar, Professor-in-charge, Central Instruments Laboratory, University of Hyderabad for facilities and help, and to Dr. P.M. Bhargava, Director, Centre for Cellular and Molecular Biology, for his encouragement and criticism, especially in connection with our work on malarial parasites. I am also grateful to Professor Bhinyo Panijpan, Department of Biochemistry, Mahidol University, Bangkok, for his help and friendship.

I thank my colleagues at the Schools of Chemistry and Life Sciences, University of Hyderabad and at the CCMB, and in particular Bina Chandani, Parthasarathi Mitra and M.V. Jagannadham, for their help and educative interactions, and to all my friends in various laboratories for their indulgence and feeling.

I acknowledge the assistance provided by the staff of the CIL, University of Hyderabad and the Instruments Division of CCMB. I wish to particularly thank C.S. Murthy and V.K. Sarma for their advice and help whenever the instruments refused to oblige, and for sparing time even after working hours.

I wish to thank C.Mohan Kumar and V.Giridharan for the neat typing and drawings. Financial assistance from the University Grants Commission and the Council for Scientific and Industrial Research is gratefully acknowledged.

**Ch. Mohan Rao**

## SYNOPSIS

Molecular interactions in condensed phases often result in certain features which are not observed in the solution phase of the same sample. There are certain reactions which are extremely rapid in the solid state while they do not proceed at all in solutions. Life processes are results and manifestations of several intricate molecular interactions. While many relatively simple biological functions are carried out by molecularly dispersed species in the living cell, complicated functions such as vision, the analysis, storing and retrieval of information in the brain are accomplished by critically organised molecular ensembles. It appears that solution chemistry alone might not be sufficient to understand life processes, and that it is necessary to look at living Things as they are, to the extent possible.

Optical spectroscopy is one of the oldest techniques that has been used extensively in the understanding of molecular structure and interactions. Optical spectroscopic studies of solids, surfaces and condensed biological samples are beset with several experimental difficulties such as optical opacity and light scattering. The nascent method, called 'Photoacoustic spectroscopy' has opened up new opportunities for such studies and provides additional information than what is obtained by conventional optical spectroscopy.

When a sample is exposed to radiation of appropriate wavelength, optical excitation takes place. A molecule in its excited state has several options to return to the ground state, the most general one being non-radiative decay which deposits heat in the sample. Heat thus deposited diffuses to the sample surface and causes surface temperature rise. If the radiation is intensity modulated, the excitation, decay and the consequent temperature changes will also be modulated with the same periodicity as that of the incident radiation. Thus periodic temperature change at the surface will cause a thin layer of air surrounding it to expand and contract periodically imposing a piston-like action on the rest of the gas in the cell, which leads to pressure oscillations. If the intensity modulation is in the range of 40 Hz to 2000 Hz, then the resulting pressure oscillations will constitute acoustic waves.

A microphone can then be used as a transducer to monitor optical absorption in the samples. Monitoring this acoustic signal over a wavelength region constitutes Photoacoustic Spectroscopy (PAS). Since it is the sound strength that is measured and not the transmitted photon intensity, this method is suitable for optically opaque and light-scattering materials. One can get optical absorption spectra of virtually any sample using PA method. Thus this technique makes biological samples amenable to spectral study without disturbing the molecular organisation in the material. The PA signal is a complex one that contains information regarding optical and thermal properties of the sample along with the lifetimes of the excited states and the depth of the chromophore in the sample. We have undertaken a project to understand and explore the potential of this technique in the study of some chemical and biological systems.

The first chapter of the thesis presents a review of the current understanding of the technique in terms of the theory and some experimental aspects as well. A description of two commercial instruments and the modifications we have incorporated in them for our purposes are also presented.

The second chapter deals with a successful application of this technique in the monitoring of the surface acidity of catalysts. The surface acidity of a catalyst has a major role to play in deciding the kinetics and the nature of the products formed in, e.g., the petroleum cracking reactions. There is no simple and convenient method available for monitoring the surface acidity of the catalyst used. We have used an indicator dye as a reporter of the surface acidity. The PA spectral features of the reporter molecule on the catalyst (Silica-alumina) provided information regarding acidic sites. Three kinds of acidic sites were found and their relative abundance estimated.

The third chapter deals with a study of a solid state photoreaction. Diacetylenes,  $R-C\equiv C-C\equiv C-R$ , polymerize in the solid state upon exposure to heat, uv, or  $\gamma$  radiation, to yield fully conjugated one-dimensional polymers  $[=RC\equiv C-CR=]_n$ . We have chosen such a diacetylene monomer, 3BCMU (4,6-decadiyne-1, 10-bis [(n-butoxycarbonyl) methylurethane]) and studied its polymerization in situ. The polymerization does not appear to be autocatalytic in nature. The absorption spectrum, the conformation, and the linear dichroism spectrum of the polymer have been determined. The polymer is in the planar conformation, and the chains are aligned along the major axis of the crystal.

The action spectrum of the photoreaction has been determined by a new method employing PAS and found to closely correspond to the absorption spectrum. The photocalorimetry of the polymerization has also been followed. The decrease in the contribution to the PA signal arising from the heat evolved in the reaction appears to be counterbalanced by that due to increased photon absorption by the sample as polymerization proceeds.

The fourth chapter deals with the in situ study on the action of antimalarial drugs on the malaria parasite. It was thought that the antimalarial drugs intercalate to the DNA of malaria-causing parasites and impair their metabolism, eventually killing the parasite. Recent observations are not in agreement with this idea and implicate hemozoin, the malaria pigment, in the mechanism of drug action. The malarial parasite degrades the hemoglobin of the host's red blood cells for its metabolic needs. The residual heme is toxic to the parasite due to its membrane-lytic property. Parasites handle this toxic substance, presumably, by sequestering with proteins and storing this complex as a pigment known as hemozoin. Heme aggregates and heme bound to proteins do not lyse the membrane. PAS studies on the parasite, its hemozoin pigment and drug-treated parasites have proved to be useful in study of this problem particularly in the light of the convenience the method offers with respect to sample preparation and handling. The spectral changes observed between free heme on one hand and the pigment and the parasite itself on the other constitute the first direct observation, in situ of the pigment spectral features in the parasite and offer an actual proof for the suggestion that heme in the parasite is in the bound form. PAS study on the parasites, isolated from mouse blood that was treated with antimalarial

drugs, shows spectral features which suggest that in the parasite a hemin-drug complex is accumulated, which is an efficient lytic agent of the parasite membranes. On the basis of the PAS results and certain earlier suggestions a scheme for the mode of action of the quinoline class of antimalarial drugs is proposed. These observations have been corroborated by results obtained using other spectral methods, e.g., circular dichroism and fluorescence of binary mixtures of hemin and the drug in solution.

We conclude the thesis with a brief discussion on possible future studies in the light of some of our ongoing projects. One of the projects is a study of photodamage that occurs to some vitamins in the solid state, particularly vitamin B<sub>1</sub>. PAS has been able to show that B<sub>1</sub> and some of its derivatives undergo photochemical reactions in the solid state yielding a new spectral band (around 350 nm). Current efforts are directed towards the isolation and characterization of this photoproduct. The second project is the study of photosynthesis in isolated chloroplasts and the effect of orientation on their photosynthetic efficiency. Chloroplasts were oriented in a 13 kG magnetic field, in a suitable buffer which also contained acrylamide, and it was possible to trap them in that orientation in the polyacrylamide gel that was formed when the magnetic field was on. We were able to observe linear dichroism with such samples. Attempts are being made to achieve orientation to substantial degree so that the problem can be studied in detail.

We hope that this new technique will become one of the extensively used spectroscopic tools, especially for the study of solid state chemistry and biological phenomena. This thesis is our first step in that direction.

## CHAPTER I

### THE TECHNIQUE

#### 1.1 ABSTRACT:

Photocoustic Spectroscopy is a newly emerged non-destructive absorption spectroscopic tool particularly suitable for studying solids, gels and biological materials. The photoacoustic signal contains information regarding the optical and thermal properties of the sample; information about the life time of the excited states and a depth profile of chromophores in the sample can also be obtained in some cases. The theoretical treatments of the photoacoustic effect, the effect of three dimensional heat flow and of the mechanical vibration of the sample on the PA signal are briefly described. Theoretical aspects of some nonconventional PA experiments, such as the measurement of nonradiative lifetimes of the excited states, dichroism and quantification of the PA signal are also briefly described. Some developments in the experimental techniques; the two commercial spectrometers used in the present study, and the modifications that we have incorporated in them for better performance are also described.



## 1.2 Introduction

It is our aim in this chapter to provide a brief and contextual overview of the theoretical and experimental aspects of photoacoustic spectroscopy (PAS). Although we begin with the discovery and proceed towards the present state of the art of the technique, we would have certainly missed a few aspects or given lesser emphasis than what they deserve. This is largely due to our own interest, governed by the problems we set ourselves to tackle. Rosencwaig (1) has described the theoretical aspects of the technique in detail while its applications to problems of interest in biology (2, 3) and in the study of solids and surfaces (4) have been recently reviewed.

## 1.3 The discovery

Alexander Graham Bell's letter of 2nd November, 1880 to his associate, Summer Tainter, describes the first photoacoustic (PA) experiment. Bell had described the discovery of the effect in a brief account given to the American Association for Advancement of Science a few months earlier (5). This was followed by a series of papers published by Bell (6), Tyndall (7), Roentgen (8), Mercadier (9) and Preece (10).

Photophone is a device to communicate speech (sound) using light as carrier. Sound is converted to a light signal by deflecting a beam of sun light, over a knife edge or a narrow slit, by a voice-activated mirror, making it possible to translate the pressure modulation of speech into an intensity modulation of light. Since the electrical conductivity of selenium changes with the intensity of light falling in it, this can be used to convert a light signal into an electrical signal, which in turn can reproduce the acoustic signal. While experimenting with such a system, Bell was able to hear sound without

any electrical means. An intensity modulated beam of light, upon impinging on a thin diaphragm, produces sound. This is the "sound produced by light" or the "photoacoustic phenomenon". Bell continued experimenting on this phenomenon (6) and found that such an effect could be realised with liquid and gas samples as well. He also inferred that this effect is due to the absorption of light, and proportional to the light intensity. Larger signals were produced from loose, porous materials, and those that have strong colors. Lampblack the dark spongy solid gave a strong audible signal. Bell attempted to explain this phenomenon as follows:

"When a beam of sunlight falls upon the mass, the particles of lampblack are heated, and consequently expand, causing a contraction of the air-spaces or pores among them. Under these circumstances a pulse of air should be expelled, just as we would squeeze water out of a sponge. The force with which the air is expelled must be greatly increased by the expansion of the air itself, due to contact with the heated particles of lampblack. When the light is cut off, the converse process takes place. The lampblack particles cool and contract, thus enlarging the air spaces among them, and the enclosed air also becomes cool. Under these circumstances, a partial vacuum should be formed among the particles, and the outside air would then be absorbed as water is by a sponge when the pressure of the hand is removed. I imagine that in some such manner as this a wave of condensation is started in the atmosphere each time a beam of sunlight falls upon the lampblack, and a wave of rarefaction is originated when the light is cutt off" (6).

However, the photophone effect remained for quite a while only a matter of scientific curiosity and the initial excitement of the discovery faded off soon. It was only about 50 years later, when sensitive microphones were available, that photoacoustic (PA) experiments were revived, but this time with only gaseous systems. Viengerov (11), Pfund (12) and Luft (13) were the first few pioneering workers in the field of gas phase PAS. Gorlik (14) was the first one to consider the possibility of extracting rate data from the phase of the PA signal. It was followed by Slobodskaya's (15) experimental realisation of obtaining the rates of energy transfer from the phase difference.

Although with gaseous samples the PA method appeared quite successful, it took a further 40 years for the 'rediscovery' of PA effect with solid samples. Though Bell's explanation of the PA effect is quite convincing, it turned out to be only partly true. Rosencwaig (1) considers that the explanations given by Mercadier (9) and Preece (10) were closer to the present day understanding of the effect. In the year 1973, Parker (16) observed a small signal from the cell windows in his gas PAS experiments and developed the theoretical basis for calculating the PA signal from transparent windows. Though Parker's theory was developed for a specific case, the modern theories for the PA effect have several common features with this theory.

#### **1.4 Photoacoustic Effect - The Parker Theory**

Parker (16) was investigating the collisional deactivation of singlet oxygen by the photophone technique. His system consisted of a closed high pressure gas cell with two windows and a microphone fixed on the side wall, half way between the ends of the cell, as shown in the Figure 1.1 .

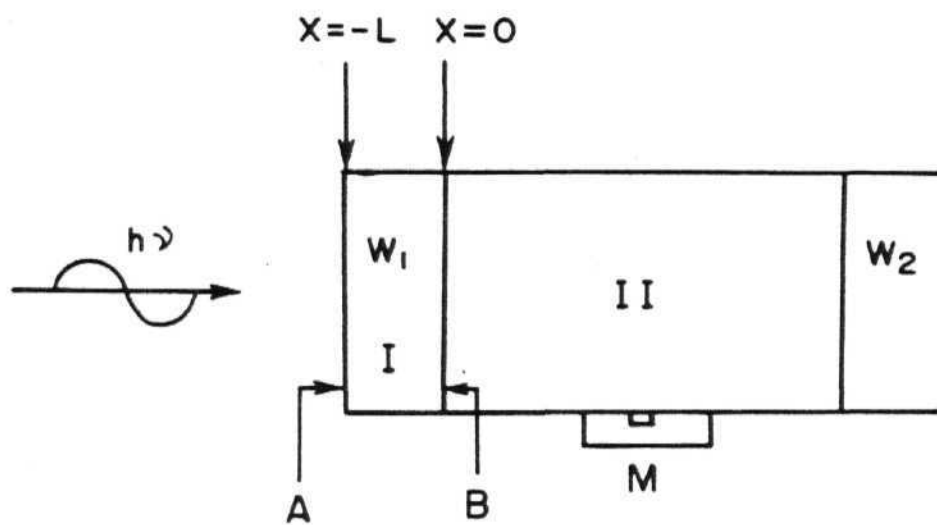


Figure 1.1 Cross-sectional view of Parker's Photoacoustic cell  
 $W_1$  and  $W_2$  = Cell windows;  $M$  = Microphone.

Oxygen was contained in the cell and the pressure increase upon irradiation was monitored by the microphone. In the course of the study, it was observed that nonabsorbing gases like nitrogen and neon also gave strong audio signals. To isolate the source of the signal generation, Parker blocked the light entry into the cell by covering the front surface of the (side A) entrance window with a metal foil and found that there was no detectable signal. When the light entry was blocked by covering the same window, but from the rear surface (side B), one could detect a strong signal. Thus it was possible to recognise that the signal originates from the window, apparently due to heating caused by light absorption. Parker, subsequently carried out a theoretical analysis of this heat production and transport.

Heat equations can be applied to the glass (region I) and to the gas (region II) as

$$-k_1 \nabla^2 T_1 + j\omega C_1 T_1 = \beta I_0 \quad 1$$

where  $K_1$  is the thermal conductivity of the glass,  $C_1$  is the specific heat per unit volume,  $\beta$  is the absorption coefficient and  $I_0$  is the incident light intensity. In the region II, i.e., the gas phase,

$$k_2 \nabla^2 T_2 - j\omega C_{p2} T_2 = -j\omega P_e \quad 2$$

where  $K_2$  is the thermal conductivity of the gas,  $C_{p2}$  is the specific heat at constant pressure per unit volume, and  $P_e$  is the differential pressure. The requirement of temperature and heat flux continuity defines the boundary conditions as:

$$T_1(0, t) = T_2(0, t) \quad \& \quad k_2 \left( \frac{dT_2}{dx} \right) = k_1 \left( \frac{dT_1}{dx} \right)$$

Invoking the equation of state and imposing the boundary conditions, an expression for  $P_e$ , the differential pressure can be obtained in terms of the absorption coefficient, the intensity of the incident light, the modulation frequency and the thermal properties.

$$P_e(l/2) = -\left(\frac{\gamma-1}{\omega l}\right) \left[ j \left( \frac{C_p k_2}{\omega} \right) \right]^{1/2} \left( \frac{\beta I_0}{C_1} \right) \quad 3$$

Equation 3 describes the differential pressure at the centre of the cell (the microphone is fixed mid way between the ends of the cell). This expression is derived with the assumption that  $\beta$ , the optical absorption coefficient, is the same throughout the length of the window.  $P_e$  calculated from eq. 3 turned out to be much less than the experimental value. To account for this discrepancy, it was assumed that absorption at the surface is higher than that at the bulk, and that the heating must take place in a thin layer at the surface. The heat equations are altered accordingly and the expression for  $P_e$  is obtained as

$$P_e(l/2) = -j \left( \frac{\gamma-1}{\omega l} \right) \left( \frac{k_2 C_p}{k_1 C_1} \right)^{1/2} \beta_L I_0 \quad 4$$

with  $\beta_L$ , the absorption coefficient in a thin layer  $L$ . Such an assumption gave a better agreement with the experimental value. In summary, the important features of the Parker theory are: 1. A thin layer of the sample absorbs light and converts it to heat; 2. the heat thus generated is communicated to the gas by thermal conduction; 3- the signal magnitude is predicted to vary as  $\omega^{-1}$  was so observed; 4. the role of the thermal properties of the filler gas on the signal is well described.

The Parker theory has been further extended to explicitly include the size of the PA cell and the finite thermal conductivity in the cell walls. The dependence of the PA spectrometer sensitivity to the cell size has been investigated; and the experimental results agree well with the extended Parker theory (17).

### **1.5 Photoacoustic effect; The Rosencwaig and Gersho (RG) theory (18):**

When a sample is exposed to radiation of appropriate wavelength, optical excitation takes place. A molecule in its excited state has several options to return to ground state, the most general one being a nonradiative decay which deposits heat in the sample. The heat thus deposited diffuses to the sample surface and causes a small increase in the surface temperature. If the incident radiation is intensity modulated with a certain periodicity, the excitation, decay and the consequent surface temperature rise will also be modulated with the same periodicity. This periodic temperature changes at the surface will cause a thin layer of air surrounding it to expand and contract periodically, imposing a piston-like action on the rest of the gas in the cell; this leads to pressure oscillations in the closed cell. If the intensity modulation frequency is in the audiorange (say 40 Hz to 15 KHz), the resulting pressure oscillations can be measured by a gas microphone. The monitoring of this acoustic signal over a wavelength region of the incident light constitutes photoacoustic spectroscopy (PAS). A theoretical analysis of the PA effect can be divided into 3 stages. The first stage is an estimation of the heat deposited in the sample as a function of position and time, in terms of the optical absorption coefficient  $\beta$  of the sample, the efficiency of the nonradiative decay  $\eta$  and the intensity of the incident radiation. The second stage is to set up and to solve the differential equations for the thermal diffusion from the

solid to the surface, to the backing material, and in the gas. The third stage is to calculate the volume changes in the thin layer of gas and the consequent pressure oscillations in the cell.

Rosencwaig and Gersho (18) use a one-dimensional heat flow model for the analysis in a cylindrical cell as given in Fig. 1.2. The cell has a diameter  $D$  and length  $L$ . It is assumed that the length  $L$  is small compared to the wavelength of the acoustic signal and that the microphone will detect the average pressure produced in the cell. The sample is considered to be in the form of a disk having a diameter  $D$  and length  $L$ . The length of the backing material is  $l_b$ , and the length of the gas column  $l_g$ , which is equal to  $L - l - l_b$ . The thermal diffusivity of the sample is defined as  $\alpha = k_i / \rho_i C_i$  where  $k$  is the thermal conductivity of the material  $i$ . The damping of the heat waves is defined as thermal diffusion coefficient  $a_i = (\omega / 2\alpha)$ , where  $\omega$  is the modulation frequency. The inverse of the thermal diffusion coefficient  $1/a_i$  gives the thermal diffusion length  $\mu_s$  in cm.

**1.5.1 The production of heat:** The heat produced in the sample is governed by the intensity of the incident radiation  $I_0$ , the optical absorption coefficient  $\beta$  and the efficiency of the non radiative decay  $\eta$ : the expression for the heat density produced can be written as

$$H(x) = I_0 \beta e^{\beta x} \cdot \eta \quad 5$$

The intensity of the sinusoidally modulated monochromatic beam is given by

$$I = \frac{1}{2} I_0 (1 + \cos \omega t) \quad 6$$



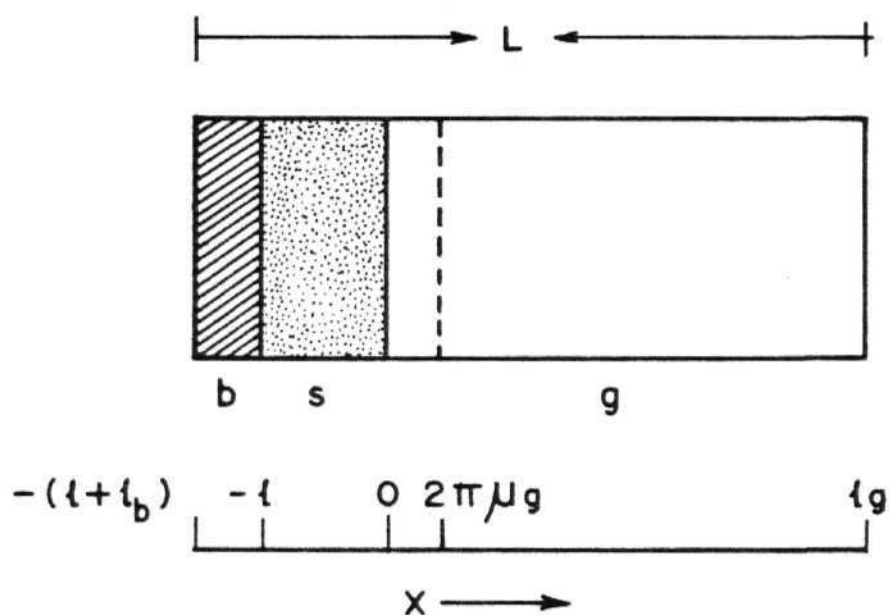


**Figure 1.2** Cross-sectional view of Photoacoustic cell (RG)

**b = backing material, s = sample, g = gas column**

where  $I_0$  is the incident monochromatic light flux (watts/cm<sup>2</sup>), and  $\omega$  is the modulation frequency in radians. The heat density produced with the modulated light assuming  $\eta = 1$ , can be written as:

$$H(x, t) = \frac{1}{2} I_0 \beta e^{\beta x} (1 + \cos \omega t) \quad 7$$

where  $x$  takes on negative values since the solid extends from  $x = 0$  to  $x = -l$

**1.5.2 Thermal diffusion equations:** It follows from the Fourier heat conduction equation that the rate of change of temperature ( $\partial \phi / \partial t$ ) is equal to the thermal diffusivity,  $\alpha$ , times the derivative of the temperature gradient;

$$\frac{\partial^2 \phi}{\partial x^2} = \frac{1}{\alpha} \cdot \frac{\partial \phi}{\partial t} \quad 8$$

In the case of the PA effect the heat source is distributed in the solid; taking this distributed heat source into account thermal diffusion equation can be written as:

$$\frac{\partial^2 \phi}{\partial x^2} = \frac{1}{\alpha_i} \cdot \frac{\partial \phi}{\partial t} - A e^{\beta x} (1 + e^{j\omega t}) \quad -l \leq x \leq 0 \quad 9$$

Where  $A = \left( \frac{\beta I_0 \eta}{2ks} \right)$  and  $\phi$  is the temperature. Similar equations can be written for the backing material and the gas, excluding the heat source term since there will be no light absorption and hence no heat production.

$$\frac{\partial^2 \phi}{\partial x^2} = \frac{1}{\alpha_b} \cdot \frac{\partial \phi}{\partial t} \quad -l-l_b \leq x \leq -l \quad 10$$

$$\frac{\partial^2 \phi}{\partial x^2} = \frac{1}{\alpha_g} \cdot \frac{\partial \phi}{\partial t} \quad 0 \leq x \leq l_g \quad 11$$

The real part of the complex valued solution of equation 9 to 11 is the solution of physical interest and represents the temperature in the cell relative to the ambient temperature as a function of position and time. These equations

are solved with appropriate boundary conditions, in terms of the optical and thermal properties of the sample. The explicit solution for  $G$ , the complex amplitude of the periodic temperature at the solid gas boundary, is given by:

$$\theta = \frac{\beta I_0}{2k_s(\beta^2 - \sigma_s^2)} \left\{ \frac{(\gamma-1)(b+1)e^{\sigma_s l} - (\gamma+1)(b-1)e^{-\sigma_s l} + 2(b-\gamma)e^{-\beta l}}{(q+1)(b+1)e^{\sigma_s l} - (q-1)(b-1)e^{-\sigma_s l}} \right\} \quad 12$$

$$\text{where } b = k_b a_b / k_s a_s ; \quad q = k_g a_g / k_s a_s$$

$$\gamma = (1-j)\beta / 2a_s ; \quad \sigma_s = (1+j)a_s$$

Thus the above equations can be evaluated for specific parameters, yielding a complex number whose real and imaginary parts,  $\theta_1$ , and  $\theta_2$ , respectively, determine the in phase and quadrature components of the periodic temperature variations at the surface of the sample. The actual temperature at the surface as a function of time is given by:

$$T(0, t) = \phi + \theta_0 + \theta_1 \cos \omega t - \theta_2 \sin \omega t \quad 13$$

where  $\phi$  is the ambient temperature and  $\theta_0$  is the increase in temperature due to the steady state component of the absorbed heat.

**1.5.3 Pressure oscillations:** The temperature changes at the surface cause volume changes in a thin layer of gas surrounding it. This volume of air acts as a piston on the rest of the gas in the cell, resulting in pressure oscillations. The periodic temperature variations in the gas are given by the sinusoidal component of the solution ( eq. 9 to 11)

$$\phi_{ac} = \theta \cdot e^{-\sigma x} + j\omega t$$

It is shown, by plotting the real part of the solution of equation 14 as a function of  $X$ , that the thermal wave in the gas gets completely damped within a distance  $2\pi\mu_g$  from the surface of the sample. Hence the gas layer of thickness  $2\pi\mu_g$  can be considered as an acoustic piston. The displacement of this piston can be calculated from the spatially averaged temperature within  $2\pi\mu_g$  as a function of time and using the ideal gas laws. This spatially averaged temperature of the gas in the piston, as a function of time, is obtained by evaluating the integral

$$\bar{\Phi}(t) = \frac{1}{2\pi\mu_g} \int_0^{2\pi\mu_g} \phi_{ac}(x,t) dx \quad 15$$

substituting the solution for  $\phi_{ac}(x,t)$ , and integrating over the limits, one gets:

$$\Phi(t) = \frac{1}{2\sqrt{2}\pi} \cdot \theta e^{j(\omega t - \pi/4)} \quad 16$$

The displacement caused by this temperature change can be estimated by ideal gas laws, and is given by

$$\delta x = \frac{\theta\mu_g}{\sqrt{2}T_0} e^{j(\omega t - \pi/4)} \quad 17$$

The rest of the gas responds to the action of the piston adiabatically. The acoustic pressure is derived from the adiabatic gas law  $PV^\gamma = K$ ;

$$\delta P(t) = Q \cdot e^{j(\omega t - \pi/4)} \quad 18$$

$$\text{where } Q = \frac{\gamma P_0 \theta}{\sqrt{2} l_g \alpha_g T_0} \quad 19$$

Thus  $Q$  specifies the complex envelope of the sinusoidal pressure variation in the cell, which can be written as

$$Q = Q_1 + jQ_2 = q e^{-j\psi} \quad 20$$

where  $Q_1$  and  $Q_2$  are the real and imaginary parts of  $Q$ , and  $q$  and  $\psi$  are the magnitude and phase of  $Q$ . The complete expression for  $Q$  after substituting the expression for  $\Theta$  is given by

$$Q = \frac{\beta I_0 \gamma P_0}{2\sqrt{2} k_s l_g \alpha_g T_0 (\beta^2 - \sigma_s^2)} \left\{ \frac{(\gamma-1)(b+1)e^{\sigma_s l} - (\gamma+1)(b-1)e^{-\sigma_s l} + 2(b-\gamma)e^{-\beta l}}{(\gamma+1)(b+1)e^{\sigma_s l} - (\gamma-1)(b-1)e^{-\sigma_s l}} \right\}$$

- 21

Equation (21) may be evaluated for the magnitude and phase of the acoustic signal. The complexity of the expression for  $Q$  makes it difficult to get a physical insight of the phenomenon in terms of various parameters like  $\beta$ ,  $\omega$  and  $\alpha$ . These three parameters determine the optical absorption length  $\mu_\beta, (1/\beta)$  and thermal diffusion length  $\mu_s, [(\alpha/2\omega)]$  which in turn determine the PA signal phase and magnitude and their dependence on the modulation frequency  $\omega$ . Rosencwaig & Gersho have considered six special cases where the expression for  $Q$  can be made simple. Table 1.1 presents such simplified special cases.

## 1.6 Contribution of mechanical vibrations to the PA signal

Absorption of chopped light causes periodic heating in the sample: this causes the expansion and contraction of the sample itself depending on the thermal expansion coefficient of the sample. The simultaneous periodic heat flow to the gas also causes expansion and contraction within a thin boundary layer of gas next to the sample. The net pressure changes in the cell then can be attributed to the 'composite piston' which is the result of the superimposition of thermal and mechanical effects. McDonald and Wetsel, Jr. (19, 20) have considered this situation, and extended the PA theory to include the contribution from the mechanical vibrations of the sample.

TABLE I.1

Optical absorption length $\mu_\beta = \beta^{-1}$	Thermal diffusion length $\mu_s = (2\kappa/\omega)^{1/2}$	P.A. Intensity
<b>1. Optically transparent</b>		
$\mu_\beta > L$	(i) Thermally thin $\mu_s \gg L ; \mu_s > \mu_\beta$	$I_{PA} \propto \beta L$
	(ii) Thermally thin $\mu_s \gg L ; \mu_s < \mu_\beta$	$I_{PA} \propto \omega^{-1}$
	(iii) Thermally thick $\mu_s < L ; \mu_s \ll \mu_\beta$	$I_{PA} \propto \beta \mu_s ; \propto \omega^{-3/2}$
<b>2. Optically Opaque</b>		
	(i) Thermally thin $\mu_s \gg L ; \mu_s > \mu_\beta$	$I_{PA}$ Independent of $\beta$ (PA Saturation)
	(ii) Thermally thick $\mu_s \sim L ; \mu_s > \mu_\beta$	$I_{PA} \propto \omega^{-1}$
	(iii) Thermally thick $\mu_s \ll L ; \mu_s < \mu_\beta$	$I_{PA} \propto \beta \mu_s ; \propto \omega^{-3/2}$

$\beta$  = Optical absorption coefficient in  $\text{cm}^{-1}$

$L$  = Sample thickness

$\omega$  = Modulation frequency

$\kappa$  = Thermal diffusivity (= Thermal conductivity / density x specific heat)

The coupled equations are solved and the simplified expression for the gas pressure  $P$  in the cell due to the combined effect of thermal and mechanical pistons for the thermally thick sample is obtained as:

$$P_g = - \frac{j r \rho_c I_0}{\omega l_g 2 \rho_s c_{ps}} \left[ \frac{\beta}{\sigma_g T_0 (g+1)(r+1)} + \beta_T (1 - e^{-\beta l}) \right] \quad 22$$

where  $\beta_T$  is the thermal expansion coefficient of the sample. The second term in the parentheses arises due to the mechanical vibrations. This treatment suggests that the acoustic coupling does not alter the linear relation between the PA signal and  $\beta$ , when  $fti_s \ll 1$ . The relative effect of coupling increases as  $\omega^2$  if  $\mu_\beta > \mu_s$ . Increase in coupling effect with  $\omega$  is due to the decrease in thermal diffusion length: only light absorbed within a thermal diffusion length can contribute to RG piston, whereas surface vibration is proportional to the total energy adsorbed in the sample. The relative contribution of the latter may be significant for thermally thick samples where  $\mu_\beta > \mu_s$ .

The composite piston model is applicable for liquids and solids. But, since the coefficient of thermal expansion is smaller for solids, the acoustic coupling becomes less significant. Nevertheless, including the acoustic coupling terms makes this theory more general and the interpretation of data becomes more accurate.

### 1.7 Effect of three dimensional heat flow

Both the RG and the McDonald and Wetsels' theories assume a one dimensional heat flow, which is found to be acceptable in most of the experimental situations. However, Powell et al. (21) and Quimby and Yen (22) have carried out experimental investigations and have observed departures

from the one-dimensional predictions, in regard to the frequency dependence of the PA signal and the phase change. Powell et al. (21) have observed a  $\omega^{-n}$  dependence of the PA magnitude for a thermally thick sample where  $n$  is less than 3/2 and greater than 1. Some theoretical ideas have been proposed by Quimby and Yen (23) and McDonald (24). McDonald has suggested that the one-dimensional model gives precisely the same result as that of the three-dimensional model provided the thermal waves, transverse to the incident beam, do not reach the cell wall. Quimby and Yen (23) also consider that the inclusion of the three-dimensional heat flow effect does not change **the** predicted PA signal, provided the thermal diffusion length in the gas is much less than the radius of the sample chamber.

Chow (25) has developed a rigorous theory of the three-dimensional photoacoustic effect, which imposes no restriction on the size of the sample, the geometry and the beam profile. For sufficiently high modulation frequencies, or for samples with large lateral dimensions, this signal is found to be smaller than its one-dimensional counterpart. Departure from one-dimensional theoretical predictions occur at modulation frequencies for which the thermal diffusion length of the gas is of the order of the lateral dimension of the sample. Beam spot size plays a relatively insignificant role in affecting the signal. McDonald (26) has extended the three-dimensional heat flow treatment to a situation in which thermal conduction to the side walls may be insignificant. The effect of this is to cause a decrease in the PA signal, when compared to the one-dimensional model, or to the three-dimensional model with **the** assumption that thermal waves do not reach the cell wall. Chow, in a latter publication (27), has presented a detailed study on the modulation frequency dependence of the PA signal in one-dimensional and three-dimensional cases.



McDonald (28, 29) has shown that PA signal is accurately given by one-dimensional model for short, wide cells, viz., cells with dimensions small compared to the acoustic wavelength, and radius large enough to avoid any appreciable thermal transport to the side wall.

### **1.8 Theoretical aspects of some nonconventional PA experiments**

From the foregoing, it can be seen that the theory of PA signal generation is fairly well understood. In this section we describe briefly the theoretical aspects of a few nonconventional PA experiments which interest us.

**1.8.1. Nonradiative lifetime measurements:** PA signal originates after the decay of the excited state, and thus the delay between excitation and signal contains information regarding nonradiative lifetime. The relaxation times associated with radiationless decay processes have been studied using frequency domain PAS by Powell et al. (30-32) and the lifetime is calculated from the expression

$$\tau\omega = \tan \psi \quad 23$$

The validity of this expression for solids is very limited. Mandelis and Royce (33) have developed theoretical treatment for time domain PAS. Aamodt and Murphy (34) have also considered excited state lifetime in their treatments for the time domain PAS. Royce and Mandelis (35) use one-dimensional model similar to that of RG and, derive an expression for spatial and temporal temperature distribution in the gas, including the finite excited-state relaxation time in the sample.

A complex expression for the pressure change in the cell for a modulated light source is obtained, which shows that the phase depends on the optical absorption coefficient, the physical dimensions of the sample, the ratio of thermal properties of the sample and the gas, and the relaxation time. In the case of a thermally thick and optically opaque sample, the expression can be simplified to

$$\psi(\tau, \omega) \approx \frac{\pi}{4} + \tan^{-1}(\omega \tau) \quad 24$$

which can be used to calculate  $\tau$ . The expression for the time-dependent temperature variation at the surface and the pressure in the cell are obtained for pulsed excitation. The plots of the computed pressure as a function of time show an inflection point at  $t = \tau$ , provided  $\tau$ , the lifetime, is short compared to the thermal transit time of the cell, but long compared to  $\tau_p$  the duration of the pulse. This expression can be used to measure the relaxation times only after accounting for the transfer function of the microphone, which relates the electric output of the microphone to the pressure. Mandelis and Royce (33) have considered these effects and suggested a limitation on the range of the existed state lifetime measurements, the range being between  $10^{-5}, 10^{-1}$  sec. However it may be possible to improve this by using a Piezo electric detector.

Malkin and Cahen have considered one and two step photochemical processes, with special emphasis on photosynthesis in green plants. The in phase component of the signal as a function of  $\omega$  (in Hz) shows an inflection point, while quadrature component maximises at  $\omega$  corresponding to the rate constant of the process: rate of the process equals to  $\omega^{-1}$  (36).

**1.8.2 Quantitative PAS:** One of the major drawbacks of the PAS technique is the difficulty in quantification. As it can be seen, the PA signal depends, apart from  $\beta$ , on sample dimensions, and thermal properties of the sample and the coupling gas (and sometimes on the backing material). Empirical quantification methods (determining the standard plot for certain set of conditions and using it for determining the concentration of unknown samples under identical conditions) have met with reasonable success (37-45). Monahan and Nolle (46) have undertaken a systematic study of the dependence of PA signal on the optical absorption coefficient  $f_i$ , with a known uniform particle size. They have shown that the PA signal is proportional to  $\beta$  if the sample is thermally thick and optically nontransparent. When the sample is thermally thin, Melamed's analysis of diffuse reflection absorption is to be applied for getting the correct  $\beta$  value. Many researchers could obtain the optical absorption coefficient by measuring PA signal as a function of  $\omega$  (e.g. see 47-49).

Bennett and Forman (50) have shown that the phase lag between the PA signal with respect to light modulation can be used to distinguish surface and bulk absorption coefficients. As  $\beta$  increases, light penetration into the sample will decrease, and hence the heat deposited will be nearer to the surface. The time taken for this heat to diffuse to surface will be less, causing a decreased phase lag when compared to the phase lag obtained with the sample with low  $\beta$ . Roark et al. (51) have used the phase data to compute quantitative absorption spectra. They obtain, for thermally thick samples,

$$\psi = \tan^{-1} \left[ \frac{-\beta^3 + 2\beta - 4}{\beta^3 - 2\beta^2 - 2\beta} \right]$$

where  $B = \beta\mu_s$ . This equation enables one to calculate  $\beta$  (if the  $\mu_s$  is known) from  $\psi$ . This equation gives satisfactory results even for samples with very high  $\beta$  values. It was noted that measured phase angle differs from theoretical one due to various problems associated with phase measurement. The experimentally determined phase lag,  $\psi_{exp}$ , can be written as

$$\psi = \psi_c + \psi_{exp} \quad 26$$

$\psi_c$  is obtained by measuring  $\psi_{exp}$  for a sample whose optical absorption is known. The PA phase angle spectrum is recorded for 0.2 M  $\text{Fe}(\text{bipy})_3\text{Br}_2$  solution and  $\beta(\lambda)$  computed according to the equation 25. The computed  $\beta(\lambda)$  spectrum, at all modulation frequencies, agrees very well with the transmission data.

Poulet et al. (52) have developed a theoretical model within the framework of the RG theory and obtained an expression for the phase of the PA signal in terms of  $\beta\mu_s$  as

$$\psi = -\pi + \tan^{-1}(\beta\mu_s) \quad 27$$

These authors also have realised that the experimental phase angle and theoretical value differ as:

$$\psi_{exp} = \psi_{th} + \psi_{app} \quad 28$$

$\psi_{app}$  is attributed to the three-dimensional heat flow and is estimated from the phase lag produced by a black body ( $\beta\mu_s \gg 1$ ) in which case  $\psi_{exp}$  is given by

$$\psi_{exp} \approx \psi_{app} \quad 29$$

Mechanical coupling suggested by McDonald and Wetsel (19, 20) complicates the situation at low  $\beta$  values. For the samples with  $\beta\mu_s < 1$  the present theory gives values of  $\beta$ , which are far from the experimental values. These authors suggest the use of the amplitude of the product of the PA signal and  $\omega$  (i.e.  $\Delta P(t)\omega$ ) for low values of  $\beta\mu_s$ , and phase of  $\Delta P(t)\omega$  for high values of  $\beta\mu_s$ .

Teng and Royce (53) have used the magnitude data to compute the correction term, which can be used to calculate the correct phase angle  $\psi(\beta)$ . This  $\psi(\beta)$  can be used to compute  $\beta(\lambda)$ .

The optical absorption spectrum, i.e.  $\beta(\lambda)$ , is obtained from the measured phase and amplitude for 0.6 M potassium permanganate solutions, in the range of 300-600 nm. The spectrum thus obtained agrees well with the transmission spectrum. This method needs only a single scan at one modulation frequency, and no auxiliary measurement of  $\beta$  at a chosen wavelength is necessary.

Burggraf and Leyden (54) have combined the phase and magnitude information to arrive at a combined response function given as

$$C\beta/\mu_s = \frac{\sqrt{2} q_n}{\sin(\psi - \pi/4)} \quad 30$$

where  $C$  is a constant that depends on the thermal properties of the sample and gas. Thus by measuring  $q_n$  and  $\psi$  it is possible to measure  $\beta$  provided  $\mu_s$  and  $C$  are known. This treatment has also been extended to include light scattering in particulate samples, by considering the light distribution in the sample.

From the foregoing, it appears that an adequate theory exists for quantitative PAS. But in all cases, the samples were assumed to be thermally thick and optically non-transparent. These assumptions are seldom valid in case of powder samples, where the particle diameter may become much smaller than  $\mu_\beta$  or  $\mu_s$ .

We believe that the phase lag due to nonradiative relaxation should also be considered when one measures  $\beta$  from  $\psi$ . Though this contribution is negligibly small, it is necessary for generalizing the theory and to interpret the data more precisely.

$$\psi_e = \psi_i + \psi_T + \% \quad 31$$

where  $\psi_e$  is the experimental phase lag,  $\psi_i$  the phase lag due to the instrument,  $\psi$  due to the finite nonradiative relaxation time, and  $\psi$  due to the optical absorption coefficient. The contribution of  $\psi_\beta$  to  $\psi_e$  is recognised and accounted for by Royce et al. in deriving the expression for lifetimes in the time domain PAS. But in all the attempts to obtain  $\beta$  from  $\psi$ , the contribution of  $\psi_r$  is neglected. Though this is acceptable in many a case, there are, however, some instances where  $\psi_{rT}$  is not negligible. We have observed that the  $\psi$  of naphthalene is altered significantly when benzophenone is added (optical absorption of benzophenone at the chosen wavelength is negligible). It could be due to the rapid and efficient energy transfer from the naphthalene singlet  $S_1$  state to the benzophenone triplet ( $T_1$ ) state, which relaxes to ground state slowly, leading to the increased phase lag. This observation points out the necessity of incorporating the  $\psi_{rT}$  term in the expression for  $\psi_{re}$  especially if an energy transfer phenomenon is under study. The difficulties associated with measuring accurate phase lag mask the significance of  $\psi_{rT}$  contribution to  $\psi$ .

**1.8.3 Dichroism measurements:** If the sample is optically anisotropic, one can use polarized radiation to study the linear dichroism of the sample by PA method. We have incorporated a polarizer in the light path of the PA spectrometer which enabled us to obtain linearly polarized PA spectra. The details are discussed later in this thesis in Chapter 3. Fournier *et al.* (55) have constructed a PA spectrometer to measure linear and circular dichroic PA spectra of samples. In this system, light exhibits a periodic change of its polarization instead of intensity. PA signal then becomes proportional to  $\Delta\beta = \beta_1 - \beta_2$ , where  $\beta_1$  and  $\beta_2$  are the absorption coefficients for the two orthogonal polarizations. They have demonstrated the performance of the setup by recording linear dichroic and magnetic circular dichroic spectra of a  $\text{NdMoO}_4$  single crystal. The polarization modulation frequency was 300 Hz for linear dichroism and 3000 Hz for circular dichroism. Saxe *et al.* (56) have presented a theoretical analysis of the circular differential PA effect (CDPA). A polarization modulated beam may be considered as the superimposition of two intensity modulated beams which are phase shifted by  $180^\circ$ . Thus it is possible to treat the CDPA effect in terms of the superimposition of two conventional PA experiments, and the pressure changes in the cell  $\Delta P(t)$  is given by:

$$\Delta P(t) = \Delta P_L(t) + \Delta P_R(t) \quad 32$$

$$\text{where } \Delta P_L = R \operatorname{Re} \{ G_L a_L e^{j(\omega t - 1/4\pi)} \} \quad 33$$

$$\text{and } \Delta P_R = R \operatorname{Re} \left\{ G_R a_R e^{j(\omega t - 1/4\pi)} \right\} \quad 34$$

These can be combined to write

$$\Delta P(t) = \text{Re} \left\{ \Delta Q e^{j(\omega t - 1/4\pi)} \right\} \quad 35$$

where,  $\Delta Q = Q_L - Q_R$ .

$Q_L$  and  $Q_R$  both independently are equal to the value of  $Q$  given by the RG theory. Hence

$$\Delta Q = \Delta Q_1 + j\Delta Q_2 \quad 36$$

and the PA signal

$$AP(t) = \Delta Q e \quad 37$$

The expression for  $\Delta Q$  is obtained from RG analysis and six limited cases as described by RG are considered. it was shown that in all the six cases  $AP(t)$  is proportional to  $\Delta\beta$ , i.e.,  $\beta_L - \beta_R$ . Thus CDPAS can be used to obtain the CD spectrum of virtually any sample. The modulation frequency dependence of the signal can be used to further characterize the sample in terms of its thermal parameters. The signal varies as  $\omega^{-1}$  for optically transparent and thermally thin samples and as  $\omega$  for thermally thick samples. In the case of optically opaque samples,  $\omega$  dependence is expected for thermally thin samples and  $\omega^{-3/2}$  dependence for thermally thick samples. Fournier's sample (55) falls into the optically and thermally thick case and indeed shows  $\omega^{-3/2}$  dependence. CDPAS is expected to be extremely useful in the study of the conformation of membrane-bound proteins and similar matrix-embedded systems.



### 1.9 Developments in Experimental Techniques

Photoacoustics and photoacoustic spectroscopy are finding increasing applications in a wide variety of research and industrial problems. This has been mainly due to a better understanding of the technique and improvements in the experimental techniques. We briefly describe some of the significant improvements in the experimental techniques.

The detector for Bell's first PA experiment was the human ear, while the light source was the sun. The advent of sensitive microphones nearly half a century later has made PAS of gases more attractive. The PAS of gases is fairly well understood and is being extensively used. In regard to its experimental aspects, PAS has two major advantages over other spectral techniques. Firstly the PA signal is proportional to the intensity of incident radiation and hence the signal can be increased to very high levels, provided the sample is not photodamaged. The problem of detecting a small difference between large signals does not arise in PAS. Secondly the technique is not detector-limited, and can therefore be extended to some other parts of the electromagnetic spectrum with ease. There are significant developments in these two aspects. Tungston lamps are replaced by high pressure arc lamps. With the advent of laser sources, the sensitivity of the technique has been greatly enhanced (for example see 44, 45, 57, 58). HorduiK and Schlossberg (59) were the first to utilise a strain transducer directly in contact with the solid sample. They have used a PZT-5H piezoelectric device, a laser for light source and could detect optical absorption coefficients of  $1 \times 10^{-5}$  to  $10^{-6}$  cm, a truly enhanced sensitivity. They have also developed a theory to derive the functional dependence of the strain generated by light absorption. Wetsel (60) and Eyring et al. (61) have also considered the theoretical schemes for

piezoelectric PAS. Jackson and Amer (62) have developed the theory for piezoelectric PAS of condensed matter and experimentally verified their theoretical predictions. Tam and Patel (63) have used a pulsed dye laser, a piezoelectric transducer directly coupled to the sample, and gated PA detection. With this system the weak visible absorption band of benzene near 607 nm has been detected, and the sensitivity limit goes down to  $10^{-7} \text{ cm}^{-1}$ . Low temperature PAS (at 77° K) has been reported by Aamodt and Murphy (64), who dipped the whole PA cell in liquid nitrogen. A microphone which is kept outside is coupled to the cell by a narrow channel. Robin and Kuebler (65), Smith and Laguna (66) and Videl (67) have carried out of PA measurements at liquid helium temperatures while Durgaryan and Fahim have developed a PA cell for high temperature studies (68). A very high sensitivity superconducting microphone for low temperatures is a significant development towards low temperature PAS (69).

Boccara et al. (70) have developed a thermooptical method wherein the microphone is replaced by a probe beam. The periodic temperature gradient in the gas near the surface of the sample gives rise to a refractive index gradient suitable for periodically deflecting a probe beam propagating along the surface of the sample. The magnitude of this deflection is proportional to the optical absorption in the sample and depends on the thermal properties of the sample and the gas. This has been termed as detection by the mirage effect.

In regard to the second aspect, namely, the possibility to extend to other regions of electromagnetic spectrum, some important developments are IRPAS, PA detection of micro wave absorption and PA Raman spectroscopy.

Low and Parodi (71) have carried out PA studies in infrared region. Fourier transform techniques have been developed for PAS in IR region to overcome the problems associated with the availability of intense IR sources (72-75). The detection of ferromagnetic resonance (FMR) in films of Fe, by the PA method was first reported by Nunes et al. (76). They have monitored the microphone signal while the sample was exposed to chopped microwave radiation of 11.6 GHz. The variation of the microphone signal as a function of the external magnetic field gives the FMR. Similar studies on Fe and Ni films using a Helmholtz resonant cell has also been reported (77), and paramagnetic resonance of DPPH ( $\alpha$ - $\alpha$  diphenyl- $\beta$ -picryl-hydroxyl-hydrozyl) crystals has been detected by the PA method (78). The piezoelectric and photothermal detection methods have also been introduced to enhance the sensitivity (79). Netzelmann et al. (80) have adopted a pulsed excitation mode for detecting EPR signals. The sensitivity of the PA method for detecting paramagnetic resonance is not greater than the conventional methods, but this method offers a depth profiling of paramagnetic species in the sample, which is not possible by conventional methods.

It has also been possible to carry out Raman spectroscopy of gaseous methane by the PA method (81). A laser beam of 514.5 nm wavelength ( $\omega_p$ ) is chopped at 573 Hz and focussed in to the PA cell which contains methane gas. Another laser beam ( $\omega_s$ ), is also focussed in to the PA cell, where the beams superimpose.  $\omega_s$  is chosen so as to make  $\omega_p - \omega_s = \Delta \omega = 2916.7 \text{ cm}^{-1}$  ( $\nu_1$ , symmetric stretch of methane). The PA signal was detected by the lock-in analyser tuned to 573 Hz; while  $\omega_p$  causes pulsed excitation due to chopping,  $\omega_s$  will stimulate the Raman scattering. The PA signal is detected only when  $\omega_s$  precisely equals  $\omega_p - \Delta \omega$ . Thus monitoring the PA signal by scanning the  $\omega_s$  one obtains the Raman spectrum.

Wong et al. (82) have developed the sanning PA microscopy method. An intense laser beam is focussed to a point of diameter  $30\mu$  and the PA signal is recorded as the beam scans the surface. Repeated scans, with the beam translation, will give the image of the sample. Important features of this technique are: it is non-destructive, locates chromophores of different characteristic absorption wavelengths, and a depth profiling of chromophore is possible by adding the third dimension, i.e. the modulation frequency. A high laser power density at the small point of excitation is necessary for a good signal to noise ratio, this requirement can be overcome by adopting the Hadamard transform technique (83).

Fourier transform PAS is a successful combination of the Bell's photoacoustic effect (1881) and Michelsons' inteferometer (1882) that was achieved in the year 1978. The recombined beam from the two arms of the interferometer may be in phase or out of phase, depending on the optical path difference achieved by translation of one of the mirrors. Each frequency comes in and out of phase at a characteristic optical path difference and the superimposition of all frequencies produces interferogram. The equivalent of an interferogram results if the beam is allowed to impinge on the PA cell and the PA signal is recorded as a function of optical path difference. This, upon Fourier transforming, gives the PA spectrum (uncorrected).

The output from the Michelson interferometer is focussed on to a PA cell. The PA signal is collected as a function of the path difference (which is twice the difference between the distance of the two mirrors from the beam splitters). This constitutes the interferogram.

$$PA(x) = \int_0^{\infty} PA(\lambda) \cos(2\pi x \lambda) d\lambda$$

where  $PA(\lambda)$  is the signal strength at wavelength  $\lambda$  and  $PA(x)$  the observed signal at a path difference ( $x$ ). This upon inverting gives the spectral distribution of  $PA(\lambda)$ , as:

$$PA(\lambda) = \int_0^{\infty} PA(x) \cos(2\pi x \lambda) dx \quad 39$$

The detected  $PA(\omega)$  signal is due to the composite effects of the spectral distribution at that ( $\lambda$ ). Thus, FTPA spectrum is obtained after collecting  $PA(x)$  at various discrete  $X$  values, and transforming the data to  $PA(\lambda)$ . To achieve sampling at exact spacings in  $x$ , another interferometer is used, one arm of which is common with the source interferometer. The fringes from the second interferometer provide the trigger pulses for sampling. Farrow et al. (84) have reported the FTPAS for solids in the visible range using such a device.

Recently, single pulse PA technique has also been developed (85-86). The PA effect in water, using nanosecond and picosecond laser pulses has been reported by Sladky et al. (87). PA detection of nanosecond pulse-induced optical absorption (88, 89) and time resolved PAS in the picosecond region (90) are some of the significant developments in the time domain PA technique.

### 1.10 Instruments used in this study

We have used two commercial instruments in the present study, with some modifications and improvements in each, in order to suit our purposes.

**1.10.1 P.A.R. model 6001 Spectrometer:** The EG&G Princeton Applied Research, model 6001 photoacoustic spectrometer, that we have used in our studies uses a 1 KW high pressure xenon arc lamp as the source in the uv, visible and

near infrared regions. The lamp current is sinusoidally modulated at a set frequency (40-2000 Hz) to achieve intensity modulation. The modulated light, reflected by an ellipsoidal reflector enters the grating monochromator through an entrance slit. Three concave holographic gratings, one each for the uv, visible and the near infrared regions, are mounted on a turret. The dispersion of the gratings used in the 200-800 nm region is 0.25 mm/nm, while the grating used in the region above 800 nm has a dispersion of 0.0625 mm/nm. Thus the minimum spectral bandwidth in the region below 800 nm is 2 nm with a 0.5 mm slit width, and 16 nm with a 4 mm slitwidth. The output from the monochromator passes through an order filter and is focussed on the sample by an off axis ellipsoidal reflector. About 8% of the beam is reflected back on to the centre of the reflector where the pyroelectric detector is located. The PA cell consists of an outer jacket with a fused silica window and a fused silica sample holder with a rectangular sample tray (4 mm x 8 mm x 2 mm), and coupled to a microphone. The preamplified signal from the microphone, is fed to a dual phase lock-in-amplifier, while the preamplified signal from pyroelectric detector is similarly fed to another dual phase lock-in-amplifier. A voltage controlled oscillator gives a sine wave at a set frequency, which is applied to the current modulator and to the lock-in amplifiers as the reference signal through a phase shifter which allows a phase shift of the reference signal with respect to the modulation signal through  $360^\circ$  in steps of  $0.1^\circ$ . The pyroelectric detector signal is used to compensate for the spectral distribution of the source intensity as well as for a real time correction for temporal fluctuation.

The inphase and quadrature components from the lock-in amplifiers are digitized by a 14 bit ADC and stored. A TMS 9900 microprocessor is used to carry out the computations and system controlling. It is possible to record the phase and magnitude of the signal as well as inphase and quadrature components separately (Figure 1.3).

The reference signal for the lock-in amplifier in the model 6001 spectrometer is derived from the voltage controlled oscillator, and the same signal is applied to the lamp current modulator. With this configuration it is possible to acquire correct magnitude spectra at any frequency. However, correct measurements of phase angle, and the magnitude of in phase and the quadrature components is possible only if there is no lag between the modulation of the lamp current and the lamp output. It can be safely assumed that the pyroelectric detector outputs the signal in phase with the modulation of the light intensity striking it. Thus it is possible to monitor the lag between the lamp current and the lamp output by measuring the phase lag between reference signal and pyroelectric signal. Figure 1.4 shows the plot of the phase as a function of the modulation frequency. It can be seen that this phase lag is appreciable even at 40 Hz and becomes very high at higher frequencies. This plot can be used to correct the measured phase angles. The correct phase angle is given by the sum of measured phase at a given frequency  $\omega$  and the phase of pyroelectric signal at the same  $\omega$ .

We have incorporated an oriel uv standard polarizer (model no. 2540-2) mounted on a three axis precision rotator (model no. 1641) into the light path of the model 6001 PA spectrometer. Two separate spectra were recorded for orthogonal polarizations, the dichroism can be computed from this data.





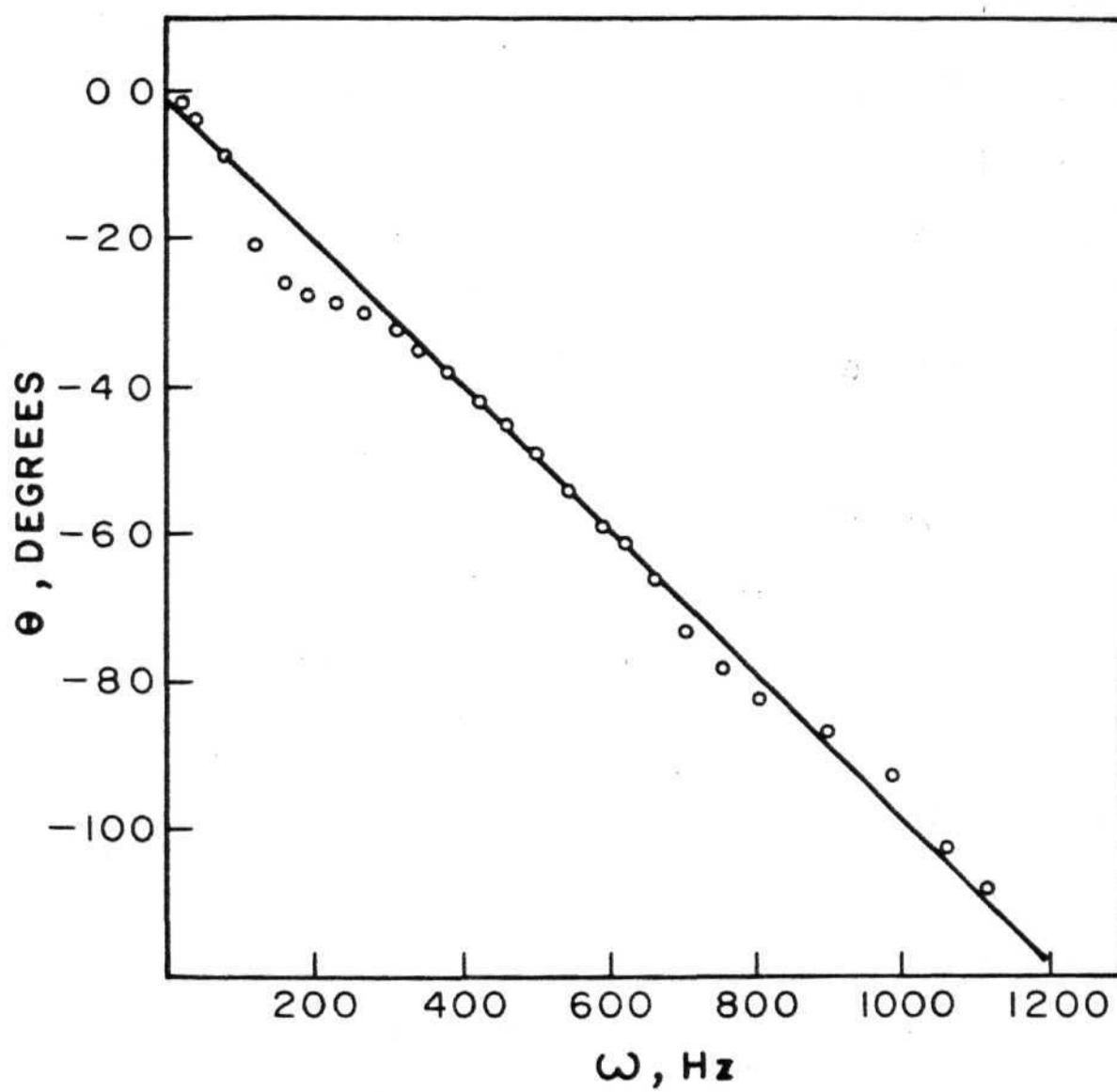


Figure 1.4

Phase angle as a function of modulation frequency for the sample carbon black

Unfortunately, polarization of the beam is a common feature of many reflection optics. In the case of an optically isotropic sample, polarization in the monochromator makes very little or no difference. But for optically unisotropic samples the recorded spectrum depends on the optical absorption coefficient  $\beta(\lambda)$  and monochromator polarization  $P$ , which is also wavelength dependent parameter. We have been able to obtain  $\beta(\lambda)$  by recording the source-compensated spectra for carbon black samples with orthogonal polarizations. An experimental situation encountered is described in Chapter 3.

In this instrument, two 12-bit digital-to-analog converters convert the digital memory contents to analog signals that drive the X, Y recorder; thus a monitoring of the signal with time is not possible. However, since one can extract the X and Y output from the instrument, we incorporated a Hitachi model 056-4006 stripchart recorder and could monitor the time profile of the signal. The example of a solid state photoreaction in this connection is described in Chapter 3.

**1.10.2 EDT OAS 400 Spectrometer:** The other commercial instrument used is the model OAS 400 made by Edt research, England. This is also a single beam PA spectrometer and employs a 300 W high-pressure short-arc xenon lamp with an integral parabolic reflector and a sapphire window. Radiation from the xenon source is focussed onto the plane of rotation of the chopper, which chops the radiation at preset frequencies of 10, 20, 40, 80, 160 and 240 Hz. The monochromator employs two plane holographic gratings, one for the uv and visible region (1200 lines/mm) and the other for the near infrared region (300 lines/mm). The minimum spectral bandwidth below 800 nm at 0.5 mm slit is 2 nm. Fraction of the light is reflected onto the pyroelectric

detector while the remaining light impinges on the sample. The PA cell consists of a metal jacket with a fused silica window and incorporates a microphone and its preamplifier circuit. The sample holder is made of aluminium with a sample tray whose dimensions are 15 mm x 5 mm x 2 mm. The signal from the microphone is preamplified and fed to tuned amplifiers, the output of which is fed to a single phase lock-in-amplifier. The resultant output is ratioed against the pyroelectrical signal similarly treated, but without lock-in-detection. The ratioed signal is plotted against the wavelength in the manual operation mode. The OAS 400 also uses a CBM 4032 microcomputer along with a CBM 4020 dual floppy disc drive; in this computer assisted mode, the signal is digitised and sent to the computer through an IEEE 488 interface. Normalization of the spectra with a pre-recorded carbon black spectrum is necessary in this mode. This is because only the lock-in-output without ratioing against the the pyroelectric signal is sent to the computer to avoid the problem of reference overloading around 750 nm. Thus on the OAS 400 spectrometer, with a CBM 4032 computer, it is possible to acquire the signal at one of the six frequencies at the set phase angle. Maximizing the signal at the peak absorption of the sample is recommended but this cannot be acceptable over a wide wavelength region, since phase angle is also a wavelength dependent parameter. In order to obtain a normalized magnitude spectrum, one has to acquire the spectrum in the required range with the phase set to  $0^\circ$  and store the data and then acquire the spectrum without altering any parameters, except setting the phase to  $90^\circ$  and store the data. Then one needs to compute the magnitude spectrum from the stored inphase ( $0^\circ$ ) and quadrature ( $90^\circ$ ) components, and normalize this with the carbonblack spectrum previously computed in the same way. The phase can be computed by taking the inverse tangent of the ratio of quadrature to inphase signals (  $\tan^{-1} Q/I$  ), with a phase accuracy of about  $\pm 3^\circ$ .

And, acquiring the inphase or quadrature signal is not possible if the signal is negative with respect to the ground. To obviate these drawbacks, we have incorporated an absolute value operator circuit (figure 1.5) after the lock-in-amplifier and before the AD converter. This has enabled us to acquire the absolute value of the signal irrespective of its sign. (Since the computation of magnitude requires squaring the components, dropping the sign does not alter the magnitude data). In order to improve the sensitivity, phase resolution and to overcome the various problems mentioned earlier, we have incorporated a few more modifications in the OAS 400, as shown in figure 1.6. Firstly the pyroelectric detector is disengaged and the output from the microphone preamplifier is fed into a EG&G PAR dual phase lock-in-amplifier level. The output of the 5206 lock-in-analyzer is connected to the input of AD converter through the absolute value operator circuit. A high resolution graphics board is installed in the CBM 4032 in order to achieve a graphic display of the spectrum, and the entire system controlling software rewritten. With these modifications on line display of the normalized, magnitude spectrum was made possible, with several other improvements. Table 1.2 compares the performance of the OAS 400 spectrometer before and after our modifications.

Photoacoustics and photoacoustic spectroscopy are still in their formative stages. We hope that the next few years promise to be an exciting period of growth for the rediscovered spectroscopy.

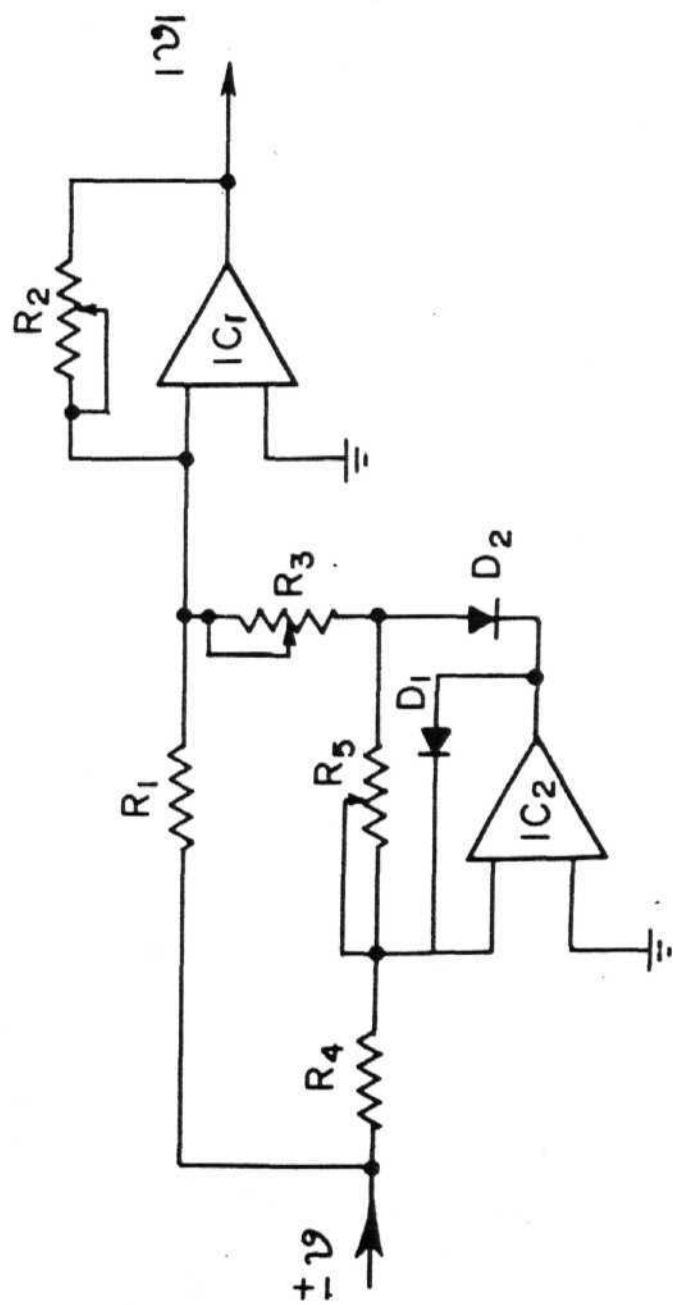


Figure 1.5 Absolute value operator circuit

IC<sub>1</sub> and IC<sub>2</sub> = 741; R<sub>1</sub> = R<sub>2</sub> = R<sub>4</sub> = R<sub>5</sub> = 10 K;  
R<sub>3</sub> = 5 K; D<sub>1</sub> = D<sub>2</sub> IN 4001.

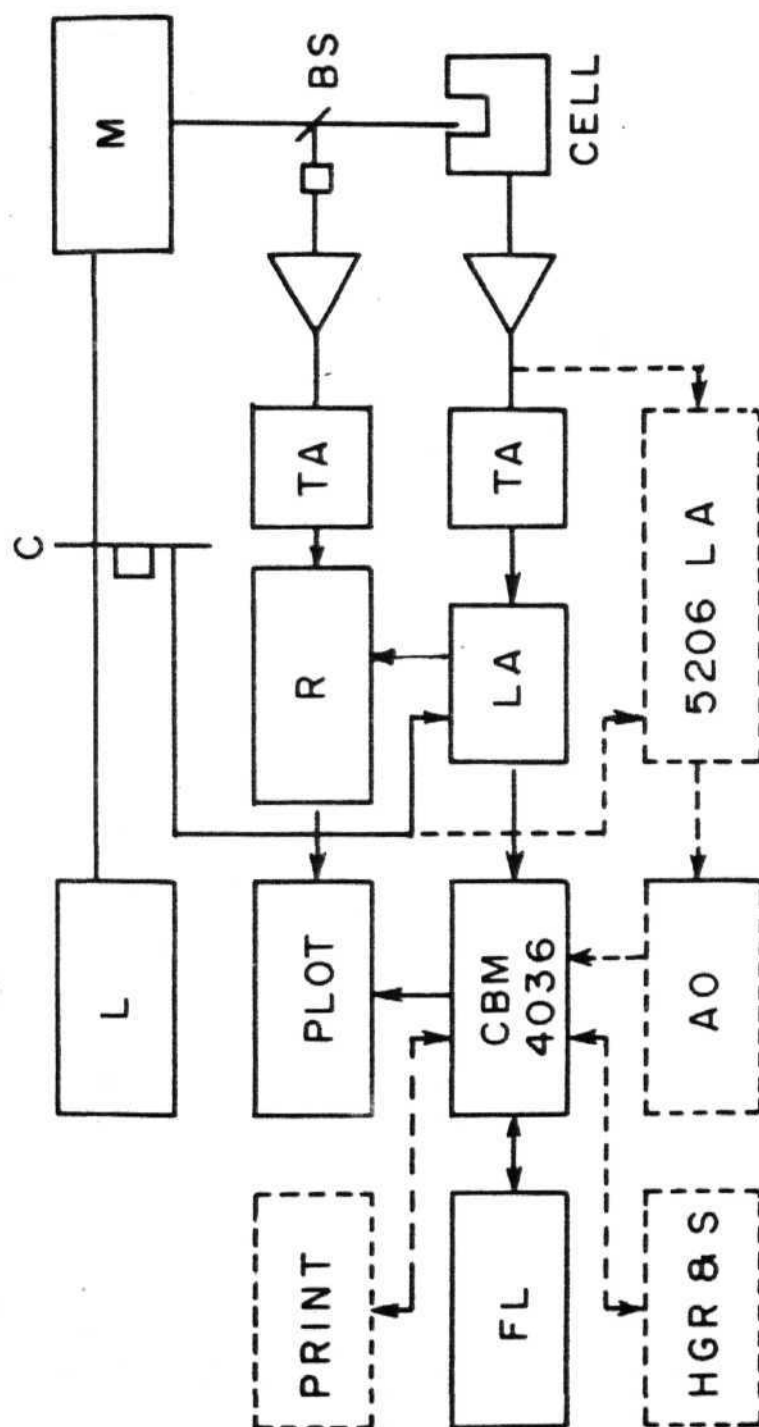


Figure 1.6 Schematic diagram of Edt OAS 400 Photoacoustic Spectrometer

L = Lamp; C = Chopper; M = Monochromator; BS = Beam splitter  
 TA = Tuned amplifier; R = Ratimeter; LA = Lock-in-amplifier  
 AO = Absolute value operator; HGR&S = High resolution graphics  
 and system software; FL = Floppy disk drive. Dotted lines indicate  
 our modifications.

TABLE 1.2 COMPARISON OF THE PERFORMANCE OF OAS 400 SPECTROMETER

## BEFORE AND AFTER MODIFICATIONS

Before Modification	After Modification
1. It is possible to acquire signal at a preset phase (i.e. inphase or quadrature only one component at a time), provided the signal is not negative.	1. It is possible to acquire inphase, quadrature components and computed magnitude or phase irrespective of the sign of the signal.
2. Phase resolution is $\pm 3.0^\circ$ (approx.) Phase setting: continuously variable, marking at $5^\circ$ interval	2. Phase resolution is $\pm 0.1^\circ$ Phase setting : in steps of $0.025^\circ$
3. Sensitivity maximum : $10\mu\text{V}$ full scale	3. Sensitivity : maximum $100\text{mV}$ full scale
4. Normalization to be done after acquiring and computing magnitude data by pre-recorded carbon black magnitude spectrum.	4. On line normalization with pre-recorded carbon black magnitude spectrum.
5. Displays spectral data in numbers. Intensity data displayed are only of one component of the signal along with the source spectral distribution.	5. Graphic display of the (320 x 200 resolution) normalized magnitude spectrum.
6. Minimum time required for recording a magnitude spectrum (in the range 200-800 nm) is 24 min. (+ computation time)	6. Minimum time required is 3 min including computation time.

## REFERENCES

1. A. Rosencwaig, 'Photoacoustics and Photoacoustic spectroscopy', John Wiley, New York, 1980.
2. T.A. Moore, Photochem, Photobiol. Rev., 7, 187 (1983).
3. D. Balasubramanian and Ch. Mohan Rao, Current Sci., 51, 111 (1982).
4. P. Ganguly and C.N.R. Rao, Proc. Indian. Acad. Sci. (Chem. Sci.), 90, 153 (1981).
5. A.G. Bell, Am. 3. Sci., 20, 305 (1880).
6. A.G. Bell, Philos. Mag., 11, 510 (1881).
7. 3. Tyndall, Proc. Roy. Soc. Lond., 31, 307 (1881).
8. W.C. Roentgen, Phios. Mag., 11, 308 (1881).
9. M.E. Mercadier, C.R. Hebel, Serv. Acad. Sci., 92, 409 (1881).
10. W.H. Preece, Proc. Roy. Soc. Lond., 31, 506 (1881).
11. M.L. Veiengerov, Dokl. Akad. Nauk. SSSR., 19, 687 (1938).
12. A.H Pfund, Science, 90, 326 (1939).
13. K.F. Luft, Z. Tech. Phys., 24, 97 (1943).
14. G. Gorelik, Dokl. Akad. Nauk. SSSR., 54, 779 (1946).
15. P.V. Slobodskaya, Izv. Akad. Nauk. SSSR. Ser. Fiz., 12, 656 (1948).
16. 3.G. Parker, Appl. Opt., 12, 2974 (1973).



17. L.C. Amodt, 3.C. Murphy and 3.G. Parker, 3. Appl. Phys., 48, 927 (1977).
18. A. Rosencwaig and A. Gersho, 3. Appl. Phys., 47, 64 (1976).
19. F.A. McDonald and G.C. Wetsel 3r., 3. Appl. Phys., 49, 2313 (1978).
20. G.C. Wetsel Jr. & F.A. McDonald, Ultrasonic Symp. Proc., 347 (1977).
21. R.C. Powell, D.P. Neikirk and D. Sardar, 3. Opt. Soc. Am., 70, 486 (1980).
22. R.S. Quimby and W.M. Yen, Appl. Phys. Lett., 35, 43 (1979).
23. R.S. Quimby and W.M. Yen, 3. Appl. Phys., 51, 1252 (1980).
24. F.A. McDonald, Appl. Phys. Lett., 36, 123 (1980).
25. H.C. Chow, 3. Appl. Phys., 51, 4053 (1980).
26. F.A. McDonald, 3. Appl. Phys., 52, 381 (1981).
27. H.C. Chow, 3. Appl. Phys., 52, 3712 (1981).
28. F.A. McDonald, 3. Photoacoustics, 1, 21 (1982).
29. F.A. McDonald, Third Int. Conf. on Photoacoustic and Photothermal Spectroscopy, Paris, April 1983.
30. L.D. Merkle and R.C. Powell, Chem. Phys. Lett., 46, 303 (1977).
31. L.D. Merkle, R.C. Powell and T.M. Wilson, 3. Phys., CU, 3103 (1978).
32. R.G. Peterson and R.C. Powell, Chem. Phys. Lett., 53, 366 (1978).
33. A. Mandelis and B.S.H. Royce, 3. Appl. Phys., 51, 610 (1980).

34. **L.C. Aamodt** and **J.C. Murphy**, 3. Appl. Phys., 49, 3036 (1978).
35. **A. Mandelis** and **B.S.H. Royce**, 3. Opt. Soc. Am., 70, 475 (1980).
36. **S. Malkin** and **D. Cahen**, Photochem. Photobiol., 29, 803 (1979).
37. **A. Hordvik** and **H. Schlossberg**, Appl. Optics, 16, 101 (1977).
38. **S. Oda**, **T. Sawada**, **M. Nomura** and **H. Kannada**, Anal. Chem., 51, 686 (1979).
39. **D. Hursh** and **T. Kuwana**, Anal. Chem., 52, 646 (1980).
40. **S. Ikeda**, **Y. Murakami** and **K. Akatsuka**, Chem. Lett. 3, 363 (1981).
41. **S.L. Castleden**, **C.M. Elliott**, **G.F. Kirkbright** and **D.E.M. Spillane**, Anal. Chem., 51, 2152 (1979).
42. **A. Rosencwaig** & **S. Hall**, Analyt. Chem., 47, 548 (1975).
43. **S. Kawamoto**, **Y. Yokoyama** & **I. Shigero**, Buneki Kagaku., 28, 142 (1979).
44. **S. Oda**, **T. Sawada** and **H. Kamada**, Bunseki Kagaku., 27, 269 (1978).
45. **T. Sawada**, **S. Oda** and **H. Kamada**, Proc. Jpn. Acad. Ser. B., 54, 189 (1978).
46. **E.M. Monahan, Jr.** and **A.W. Nolle**, 3. Appl. Phys., 48, 3519 (1977).
47. **H.S. Bennett**, **R.A. Forman**, App. Opt., 15, 2405 (1976).
48. **J.M. McDavid**, **K.L. Lee**, **S.S. Yee**, **M.A. Afromowitz**, 3. Appl. Phys., 49, 6112 (1978).
49. **F.A. McDonald** and **G.C. Wetsel Jr.**, 3. Appl. Phys., 49, 255 (1978).

50. H.S. Bennett and R.A. Forman, 3. Appl. Phys., 48, 1432 (1977).
51. J.C. Roark, R.A. Palmer and J.S. Hutchison, Chem. Phys. Lett., 60, 112 (1978).
52. P. Poulet, J. Chamborn and R. Unterreiner, 3. Appl. Phys., 51, 1738 (1980).
53. Y.C. Teng and B.S.H. Royce, 3. Opt. Soc. Am., 70, 557 (1979).
54. L.W. Burggraf and D.E. Leyden, Anal. Chem., 53, 759 (1981).
55. D. Fournier, A.C. Boccara and J. Badoz, Appl. Phys. Lett., 32, 640 (1978).
56. J.D. Saxe, T.R. Faulkner and F.S. Richardson, Appl. Phys., 50, 8204 (1979).
57. G. Stella, J. Gelford & W.H. Smith, Chem. Phys. Lett., 39, 146 (1976).
58. T. Sawada, S. Oda, S. Hiromichi and H. Kamada, Anal. Chem., 51, 688 (1979).
59. A. Hordvik and H. Schlossberg, Appl. Optics, 16, 101 (1977)
60. G.C. Wetsel Jr., 'Topical meeting on Photoacoustics,'<sup>1</sup> Iowa State University, Ames, 1979.
61. M.M. Forrow, R.K. Burnhan, M. Auzanneau, S.L. Olsen, N. Purdie and E.M. Eyring, Appl. Opt., 17, 1093 (1978).
62. W. Jackson and M. Amer, 3. Appl. Phys., 51, 3343 (1980).
63. A.C. Tam and C.K.N. Patel, Appl. Phys. Lett., 34, 467 (1979).
64. J.C. Murphy and L.C. Amodeo, 3. Appl. Phys., 48, 3502 (1977).

65. M.B. Robin & N.A. Kuebler, 3. Chem. Phys., 66, **169** (1977).
66. 3.B. Smith and G.A. Laguna, Phys. Lett., 56(A), 223 (1977).
67. F. Vidal, C.R. Acad. Sci. (Paris)., 285, 93 (1977).
68. A.A. Durgaryan, M. Fahim, Fiz. Trend. Tela (Leningrad)., 18, 600 (1976).
69. P.C. Ribeiro, M. Labrunie, J.P. Von der Weid and O.G. Symko, 3. Appl. Phys., 53, 8378 (1982).
70. A.C. Boccara, D. Fournier and 3. Badoz, Appl. Phys. Lett., 36, 130 (1980).
71. M.3.D. Low & G.A. Parodi, Spectros. Lett., 11, 581 (1978).
72. G. Busse and B. Bullemer, Infrared Phys., 18, 225 (1978).
73. M.G. Rockley, Chem. Phys. Lett., 68, 455 (1979).
74. D.W. Vidrine, Appl. Spectros., 34, 314 (1980).
75. B.S.H. Royce, 3. Enns and Y.C. Teng, Bull. Am. Phys. Soc., 25, 408 (1980).
76. O.A.C. Nunes, A.M.M. Monteiro and K.S. Neto, Appl. Phys. Lett., 35, 656 (1979).
77. C. Evora, R. Landers and H. Vargas, Appl. Phys. Lett., 36, 864 (1980).
78. I. Hirabayashi, K. Morrigaki and Y. Sono, 3ap. 3. Appl. Phys., 20, L208 (1981).
79. R.C. Du Varney, A.K. Garrison and G. Busse, Appl. Phys. Lett., 38, 675 (1981).
80. V. Netzelmann and 3. Pelzi, 'Third Int. Conf. on Photoacoustic and Photo-thermal Spectroscopy,' Paris, April 1983.

81. **3.3. Barret, M.3. Benny**, Appl. Phys. Lett., 34, 144 (1979).
82. Y.H. Wong, R.L. Thomas and G.F. Hawkins, Appl. Phys. Lett., 32, 538 (1978).
83. H. Coufal, V. Moller and S. Schreider, Appl. Opt., 21, 116 (1982).
84. M.M. Farrow, R.K. Barnham and E.M. Eyring, Appl. Phys. Lett., 33, 735 (1978).
85. D.M. Cox, Opt. Comm., 24, 336 (1978).
86. S.L. Chin, D.E. Evans, R.D. Alpine, F.K. Mc Clusky and E.B. Selkirk, Opt. Comm., 31, 235 (1979).
87. P. Sladky, R. Dannelins, V. Siratkaitis & M. Bondys. Czech. J. Phys., B27, 1075 (1977).
88. Y. Bae, 3.3. Song and Y.B. Kim, Appl. Opt., 21, 35 (1982).
89. M.G. Rockley and J.P. Delvin, Appl. Phys. Lett., 31, 24 (1977).
90. M. Bernstein, L.3. Rothberg and K.S. Peters, Chem. Phys. Lett., 91, 315 (1982).

## CHAPTER II\*

### INVESTIGATION OF ACIDITY OF CATALYST SURFACES

#### 2.1 ABSTRACT

The surface acidity and the distribution of acidic sites play a major role in deciding the kinetics and the nature of the product formed in several reactions promoted by heterogenous catalysts. A simple method to monitor the surface acidity employing photoacoustic spectroscopy is described. The indicator dye methyl red, which changes its electronic absorption features upon interacting with acidic solids, has been used as a probe of surface acidity of silica-alumina, one of the extensively used catalysts in the petrochemical industry. Photoacoustic spectra of adsorbed indicator dye as a function of the surface neutralization are used to determine the acidity of the catalyst. Acidic sites with three different acid strengths have been detected and their relative abundance estimated.

---

\*Part of the work reported in this chapter has been published in Spectroscopy Letters, 13, 329 (1980).

### 2.2.1 Introduction

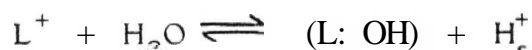
The catalytic activity at the surface of a solid catalyst is largely due to adsorption, chemisorption or physisorption, which organises at least one of the reactant molecules into a form in which it can very readily undergo reaction. Typically, the catalyst is a solid body with a characteristic structure and a definite boundary surface that might not be completely represented by its bulk stoichiometry or molecular formula. The actual chemical species and the architecture of the accessible surface are of great importance in understanding catalysis and in tailormaking catalysts.

The binary composite of silica and alumina is one of the extensively used catalysts in the petrochemical industry. Neither silica nor alumina alone is effective in promoting catalytic cracking reactions. A catalyst having an appreciable cracking activity is obtained only when prepared from the hydrous oxides, followed by partial dehydration (1, 2). It was considered for long that the silica-alumina catalyst is a combination of the two oxides, alumina and silica. It was not readily obvious which physical or chemical property of the combination of the two oxides should be responsible for its high activity (3). Alkali metal ions and nitrogen-containing organic basic compounds were found effective in deactivating these catalysts to a significant extent. This observation led Mills et al. (4) to conclude that it is the acidic characteristics of the cracking catalysts that are fundamental to their activity.

In the cracking of petroleum, the silica-alumina catalyst performs many other functions besides cracking in the sense of breaking the C-C bond. Thus, at the usual cracking temperatures of around 450-550°C, other concomitant reactions, such as double bond migration in the olefins formed, cyclization

and skeletal isomerisation, hydrogen transfer and polymerization to coke-like polymeric materials, also occur. At temperatures below those of cracking, these catalysts promote various other hydrocarbon reactions, such as the polymerization of olefins, and certain alkylation reactions (3). The reaction that will be catalysed by a particular catalyst under a given set of conditions depends on the strength of the acidic sites participating in the process. For example, dehydration of alcohols can be observed by weak acidic sites, while skeletal isomerisation of alkenes requires stronger acidic sites (5).

The surface of solids may have two kinds of acidic sites, the Lewis and the Bronsted sites. As with molecular Lewis acids, a Lewis acid site on a solid is a site which has an unoccupied orbital with a high affinity for an electron pair. A Bronsted acid site is one which has a tendency to give up a proton. In many cases, the two can be related by the presence of water:



where  $L^+$ , the Lewis site, shares an electron pair with  $OH^-$  ion from water molecule and the remaining proton  $H^+$  is adsorbed on the surface, but can be easily removed in a chemical reaction. Thus the Lewis acidity converts to Bronsted acidity (6). The origin of acidity in a silica-alumina catalyst is attributed to at least three kinds of structural features: (i) the aluminum cations substituting for silicon cations in a tetrahedral coordination; (ii) aluminum cations in a perturbed tetrahedral arrangement and (iii) silicon in a perturbed tetrahedral arrangement (7). In these perturbed tetrahedral arrangements, at least one among the four oxygen atoms might be displaced, partially exposing the cations to the surface. In the case of silica-alumina catalyst, features of type (i) may be responsible for the Bronsted acidity while type (iii) could provide the



source of Lewis acidity (7). Clearly the heterogeneous system is very complex, and sites with whole distribution of electron or proton affinity can be expected, with coordination deficiencies and imperfections of various types causing them, and relocation of ions tending to neutralize them. Both Brønsted and Lewis acidic sites are active in catalytic reactions. However, due to the differences in the mechanisms between a Brønsted acid and a Lewis acid site, it is sometimes found that they catalyze different reactions. For example, with a silica-alumina catalyst, it is shown that only the Brønsted acidic sites will polymerise propylene (8) whereas the decomposition of isobutane correlates with the density of Lewis acid sites (9). In the case of the isomerisation of cis-2-butene on a silica-alumina catalyst, it was shown that both types of sites were active, but with different rates and different detailed mechanisms {10, 11}.

From the foregoing it can be seen that the surface acidity and distribution of acidic sites play a major role in deciding the kinetics and the nature of the products formed. There has hence been considerable interest in detecting and quantifying the types and the abundance of acidic sites on a catalyst surface, and several methods to determine these have been suggested.

### **2.2.2 Measurement of surface acidities**

Various methods, such as the titration of suspensions of solid catalysts with organic amines using adsorbed indicators, electronic absorption spectral measurements of adsorbed indicators and IR spectral studies of adsorbed organic bases have been adopted to determine the surface acidity, and the acid strength of solid catalysts. Bonardet et al. have suggested a NMR method for the determination of acid strengths.

G.N. Lewis was the one who first reported the titration of a solid using an indicator dye to determine the end point. He had shown that  $AlCl_3$  suspended in carbon tetrachloride could be titrated with an amine solution using crystal violet as the indicator (q.v. 12). The basic indicator forms a coloured conjugate with the acid sites on the surface; upon addition of the titrating base (which must be a stronger base than the indicator) the indicator base is displaced by the titrating base, and the colour changes or fades. Johnson (12) has developed a method for the determination of the acidity of solid surfaces which involves the titration of the solid suspended in benzene with *n*-butylamine, using *p*-dimethylaminobenzene as the indicator. Hammett and Deyrup (13) have developed a measure for describing the acid strength of concentrated acids, known as the Hammett acidity function.

$$H_0 = pK_{BH^+} - \log \frac{C_{BH^+}}{C_B}$$

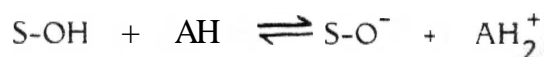
where  $H_0$  is the Hammett acidity function,  $pK_{BH^+}$  is the ionisation constant of the conjugate acid  $BH^+$ , and  $C_{BH^+}$  and  $C_B$  are the concentrations of the conjugate acid, and the unprotonated base respectively. Benesi (14) has used Hammett indicators to measure the acid strengths of solid surfaces. If the solid has acidic sites with acidic strength (on the Hammett scale) less than the  $pK_a$  of the indicator, a colour change can be seen. By using several indicators with differing  $pK$  values, it is possible to estimate the acid strengths of surface sites. For example, if a solid gives yellow colour with benzalacetophenone ( $pK_a = -5.6$ ), and does not show any colour change with anthraquinone ( $pK_a = -8.2$ ), it can be concluded that the solid surface has acidic sites with  $H_0$  values bracketed, or ranging between,  $-5.6$  and  $-8.2$ .

A complete description of the surface acidity requires the determination of the acid strength as well as the number of acidic sites or acidity. The estimation of the acid strength is possible by the use of an adsorbed Hammett indicator. Benesi (15) combined his acids strength bracketing technique with titration and could determine the acidity of groups of sites differing in their acidic strength. The solid surface is titrated with a base using various Hammett indicators. The amount of base required to observe the colour change of a particular Hammett indicator is proportional to the number of acidic sites (or acidity) having  $H_o$  less than or equal to the  $pK_a$  of that indicator. Yamanaka and Tanabe (16) have developed a method of determining the basicity of a solid surfaces at various basic strengths by titrating the solid suspended in benzene with trichloroacetic acid using a series of Hammett indicators. This method makes it possible to determine the basic strength expressed by a Hammett acidity functions and, hence, the acid base strength distribution of a solid surface on a common scale.

Electronic absorption spectra of adsorbed indicators provide a means of determining the acidic or basic nature of the surface (17, 18). This method has been developed by Kobayashi et al. for determining both the acid strength and the total acidity of solids (19, 20). The  $\pi-\pi^*$  band of pyridine is known to redshift a little upon adsorption. Protonated pyridine and hydrogen bonded pyridine show characteristic vibrational structures in their electronic absorption peak at 256 nm, while pyridine coordinated to Lewis acid sites shows a broad band, which is red shifted compared to the protonated one. This method has the advantage of being able to detect small amounts of adsorbed pyridine, due to the large molar absorption coefficient of the transition (21). Similarly, the infrared absorption spectra of adsorbed ammonia (22) and of pyridine (23) have

also been used for determining the acidity of solid surfaces. The spectrum of pyridine coordinated to the surface is markedly different from that of the pyridinium ion. This again permits the differentiation of acidic type on the surface.

Bonardet et al. (24), have used an NMR method for determining the Bronsted acid strengths of solid surfaces. NMR peaks for the solid samples are very wide and prevent any accurate chemical shift measurements. But if the surface proton participates in a heterogeneous equilibrium with an adsorbed proton acceptor molecule, AH, as



where S-OH is a surface hydroxyl. The chemical shift will be altered by the acid proton if the rapid exchange occurs between the proton of the surface S-OH and the adsorbed AH. The experimentally observed high resolution NMR spectrum should then contain only a single line with a chemical shift due to the coalescence of the lines  $\delta_{\text{AH}}$ ,  $\delta_{\text{AH}_2^+}$  and  $\delta_{\text{OH}}$ . The observed chemical shift,  $\delta_{\text{obs}}$ , is then given by:

$$\delta_{\text{obs}} = P_{\text{OH}} \delta_{\text{OH}} + P_{\text{AH}} \delta_{\text{AH}} + P_{\text{AH}_2^+} \delta_{\text{AH}_2^+}$$

where  $P_i$  is the concentration of hydrogen atoms in the group i. If the chemical shifts of the two nuclear types in the AH and  $\text{AH}_2^+$  species (e.g.  $^1\text{H}$  and  $^{15}\text{N}$ ) are known, the relative concentrations of AH and  $\text{AH}_2^+$  can be calculated, and the chemical shift of the surface proton (OH) can also be deduced.

### 2-2. 3 The Photoacoustic Method

From the foregoing, it can be seen that the surface acidity - the ability of the surface to convert an adsorbed neutral base to its conjugate acid - can be measured by titrating the solid suspensions in nonaqueous media using appropriate indicators. The use of spectrophotometry to monitor the colour changes associated with the titration should enormously increase the accuracy of measurement. A major obstacle in using electronic spectroscopy in these systems is the heterogeneous phase and the associated scattering problems. In this context, we have explored the idea of using PAS to circumvent these difficulties.

The method is rather simple. An organic dye molecule, which changes its electronic absorption features upon interaction with acidic solids, adsorbed on the surface of the catalyst serves as the reporter of the acidity of the surface. Recording the PA spectrum of this sample as a function of the surface neutralization, achieved by adding varying amounts of a base, provides an accurate titre value for calculating the acidity.

The dye chosen should exhibit distinct changes in its optical absorption features in its acidic and basic forms. Methyl red is a satisfactory choice as such a reporter; since it absorbs at 515 nm in the acidic form and at 410 nm in the basic form. Thus the PA signal strength at 515 nm can be taken as a measure of the acidic form of the indicator, provided the PA signal strength at 515 nm varies linearly with the concentration of the dye on the surface. The base chosen for the neutralization of the surface was n-butylamine in benzene.

### 2.3 Materials and Methods

The silica-alumina catalyst,  $\text{SiO}_2\text{-Al}_2\text{O}_3$  (5% silica), prepared by calcining the mixtures of hydrous oxides was provided by Prof. Kuriacose of the department of Chemistry, Indian Institute of Technology, Madras, and the sample was used without any pre-heating. Methyl red and butyl amine were laboratory grade reagents and benzene was spectral grade. About 50 mg of the solid catalyst was taken in each of several preweighed glass stoppered graduated tubes, the exact weights determined, and 0.5 ml of benzene was added to each of the tubes to wet the sample. Varying amounts of dye solution (12 mg of methyl red dissolved in 30 ml of benzene) in the range of (5-150  $\mu\text{l}$ ) was added to each tube and shaken for a minute. The walls of the tube were washed down with 1 ml of benzene, and the total volume was made up to 3 ml and left for several hours for equilibration. The supernatant liquid was decanted and preserved for estimating the concentration of the unadsorbed dye and the residual samples dried under vacuum and stored in a dry vacuum desiccator containing a small amount of  $\text{P}_2\text{O}_5$  until spectral measurements were made. The spectra of these samples were used for monitoring the linearity of the PA signal strength with the amount of adsorbed dye.

About 50 mg of the solid catalyst was taken as in the previous case and the exact weight of the sample determined. The required amount of the indicator in benzene was added, maintaining the same amount of the indicator (ca. 125  $\mu\text{l}$ /60 mg of the solid) per unit weight of the solid. Varying amounts of (0 to 12  $\mu\text{l}$ /mg in 1  $\mu\text{l}$ /mg steps) the titrant (0.04 mM/ml, n-butyamine in benzene) were added, the tubes shaken, and left for 24 hours for equilibrium. The supernatant liquid was decanted, the samples were dried under vacuum, and stored in a vacuum desiccator over  $\text{P}_2\text{O}_5$ . The samples were transferred to the PA cell in a dry box.

All the spectra were corrected for blank absorption and normalized using a prerecorded carbon black spectrum. This normalization corrects the observed spectrum for the power variation of the source over the spectral region of interest. A high modulation frequency of 300 Hz was used to avoid problems of nonlinearity due to PA saturation, if any. The spectra were recorded with 2.0 mm slits, giving a spectral band width of 8 nm, and at a scan speed of 100 nm/min. The optical density of the supernatant liquids were measured on a Shimadzu 200S u v -vis spectrophotometer.

## **2.4 Results and Discussion**

Methyl red adsorbed on the solid surface was found to absorb at 515 nm in the acidic form and at 410 nm in its basic form. As the surface is neutralized, the absorption, and hence the PA signal strength at 515 nm decreases, while the signal strength at 410 nm increases. The sample that shows no band at 515 nm is the one that is fully neutralized and the amount of the titrant butylamine added in this case is the volume required to neutralize the surface. The acidity of the surface is then expressed as milli-equivalent of the titrant per gram of the catalyst.

As discussed before, this method requires that PA signal strength should vary linearly with the amount of the chromophore adsorbed on the surface. Figure 2.1 shows the plot of PA signal strength at 515 nm versus the amount of methyl red adsorbed on the sample. The amount of the methyl red absorbed on the sample is determined by equilibrating the solid with a methyl red solution of known concentration and estimating the unadsorbed dye in the supernatant. The PA signal varies linearly with the amount of the adsorbed dye, at low concentrations and becomes independent at higher concentrations. This could be due

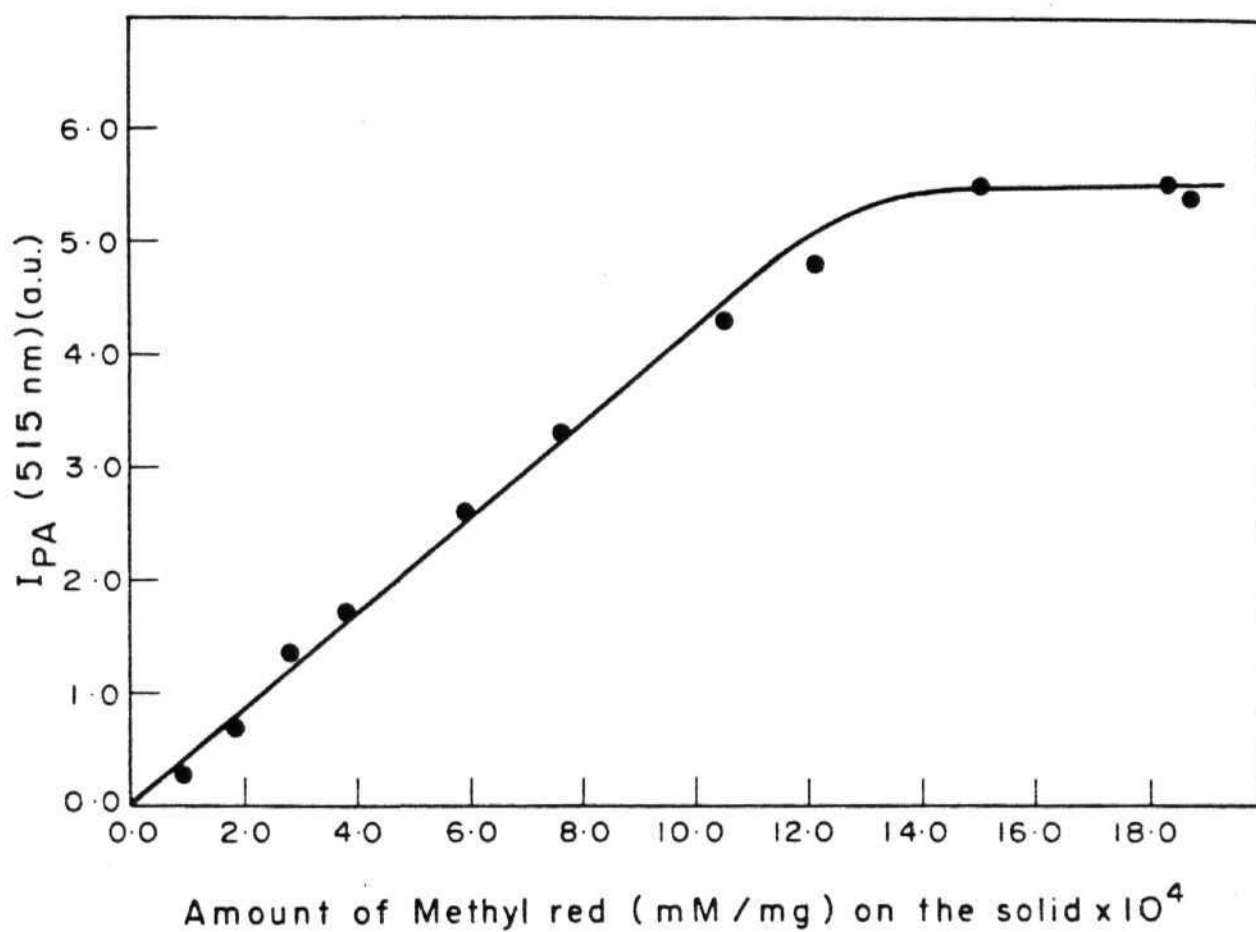


Figure 2.1 PA signal intensity at 515 nm versus amount of methyl red on silica-alumina.



to PA saturation or due to the complete coverage of all the acidic sites on the surface and hence further absorption of indicator causes very little or no increase in the absorption at 515 nm. (methyl red adsorbed on chromatography grade neutral alumina samples (Sigma and BDH) does not absorb at 515 nm. Methyl red adsorbed on neutral silica gel also does not absorb at 515 nm.)

In the case of highly absorbing samples, most of the radiation will be absorbed within one optical absorption length  $\mu_s^{-1} = 1/\beta$ , where  $\beta$  is the optical absorption coefficient) small compared to the thickness of the sample,  $l$ . If the thermal diffusion length  $\mu_s$  (given by  $(2\alpha/\omega)^{1/2}$ ); where  $\alpha$  is the thermal diffusivity and  $\omega$  the modulation frequency) is more than the sample thickness,  $l$  and optical absorption length  $\mu_s^{-1}$  then the sample is photoacoustically opaque and signal becomes independent of  $\beta$  and varies as  $\omega^{-1}$  (Case 2(i) of Table 1.1). Signal saturation can be overcome by increasing the modulation frequency which will decrease  $\mu_s$ . When  $\mu_s < \mu_s^{-1}$  and less than 1, then the PA signal will be proportional to  $\beta\mu_s$  and vary as  $\omega^{-3/2}$  (case 2(iii) of Table 1.1). In the case of finely divided powder samples as the present ones, the thickness of the sample is equal to the diameter of the particle and since the particle diameter is much smaller than  $\mu_s$  &  $\mu_s^{-1}$ , PA signal saturation is seldom encountered for fine powders. Figure 2.2 shows a plot of the logarithm of PA signal strength at 515 nm versus the logarithm of  $\omega$ , the modulation frequency. The slope is found to be -1.0 and does not vary even at 550 Hz. Taking  $\mu_s$ , the thermal diffusivity of alumina to be  $0.083 \text{ cm}^2 \text{ s}^{-1}$  (TPRC Data Series Volume 10, Thermal diffusivity<sup>1</sup>, Y.S. Toulkian (Ed.), Plenum, New York, 1970) and assuming that 5% silica does not alter the thermal properties of alumina significantly, the thermal diffusion length for silica-alumina can be calculated. The calculated values for  $\mu_s$  vary from  $2.5 \times 10^{-2} \text{ cm}$  at 40 Hz to  $6.9 \times 10^{-3} \text{ cm}$  at 550 Hz.

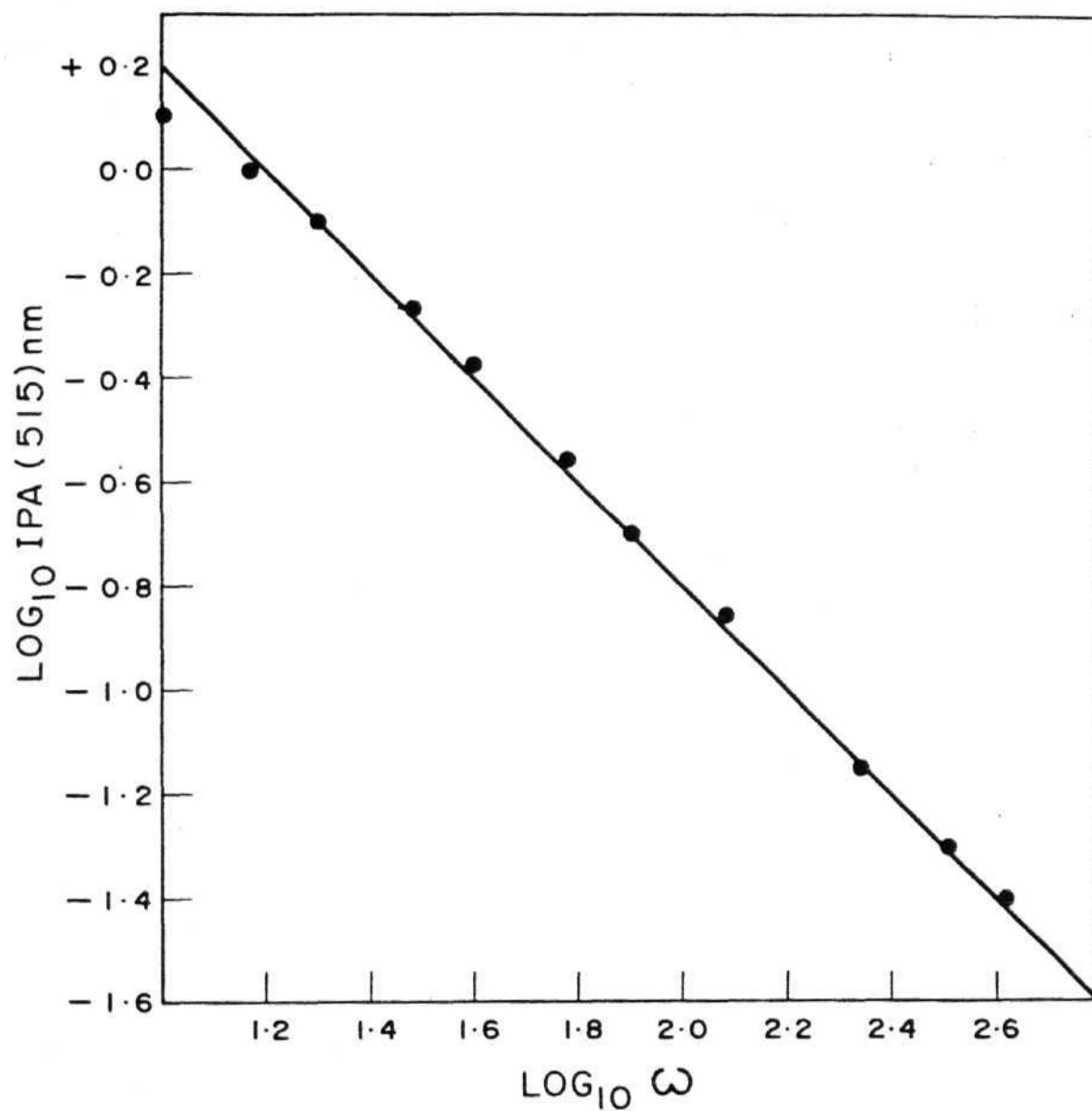


Figure 2.2 A log-log plot of the PA signal for methyl red adsorbed on silica-alumina versus **modulation frequency**; showing the  $\omega^{-1}$  dependence.

If the near plateau region of Figure 2.1 is due to the onset of PA saturation, one would expect a change of slope to  $-1.5$  at high frequencies. Thus it is clear from Figure 2.2 that the situation is not due to PA saturation. The independence of the PA signal with respect to the amount of adsorbed methyl red can be attributed to a complete coverage of all the acidic sites. Thus, the plot also provides an estimate of the concentration of the indicator dye required to completely cover the acidic sites on the given solid surface.

Figure 2.3 shows the PA spectra of a few samples of the catalyst neutralised to varying extents by the amine. It can be seen that the band at 515 nm due to acidic form of the indicator decreases while the band at 410 nm due to basic form of the indicator increases progressively with the surface neutralization. An interesting feature of the figure is the presence of an isosbestic point near 445 nm through which most of the curves pass. It can however be seen that two curves deviate a little from the isosbestic point.

This deviation, we believe, is due to the presence of trace amounts of water in the two samples, which will decrease the PA signal by robbing the thermal energy deposited in the sample due to the nonradiative deexcitation process. Also, possible differences in the surface concentration, if any, of the indicator may lead to deviations. In this connection Figure 2.4 shows the effect of exposure of the sample to the atmosphere on the PA signal strength. The first spectrum is of the sample transferred to the PA cell in a dry box. The second spectrum is also of the same sample transferred to the PA cell in the open, exposing the sample to the atmosphere (25°C and 60% RH) for about 2 minutes. It can be seen that there is a reduction in the peak height and also a slight change in the band shape. This difference is observed only for the samples that are neutralised to some extent. The peak heights at 515 nm were measured after

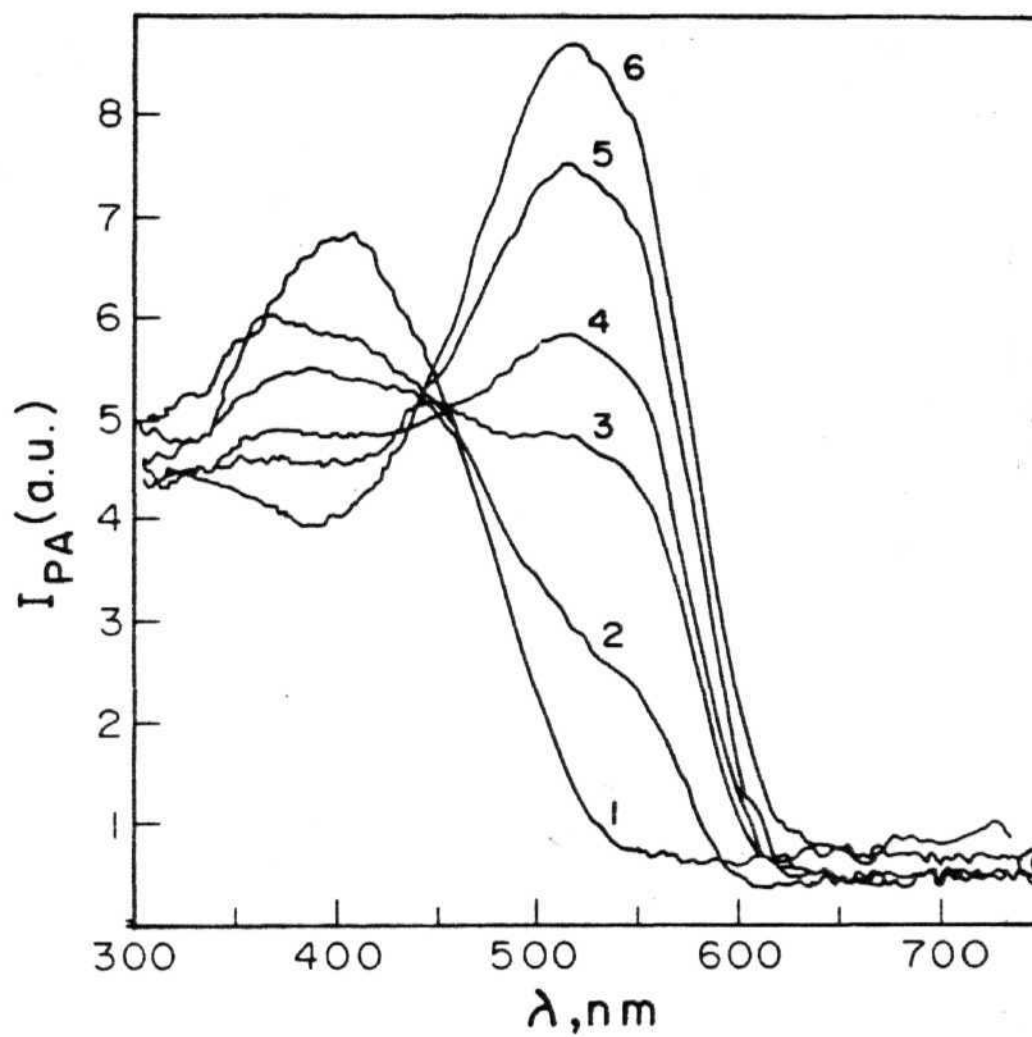


Figure 2.3 PA spectra of methyl red adsorbed on silica alumina containing increasing amounts of n-butylamine in  $\mu\text{L/mg}$ . Curve (1) 1.0; Curve (2) 2.0; Curve (3) 3.0; Curve (4) 4.0; Curve (5) 9.0; Curve (6) 10.0.

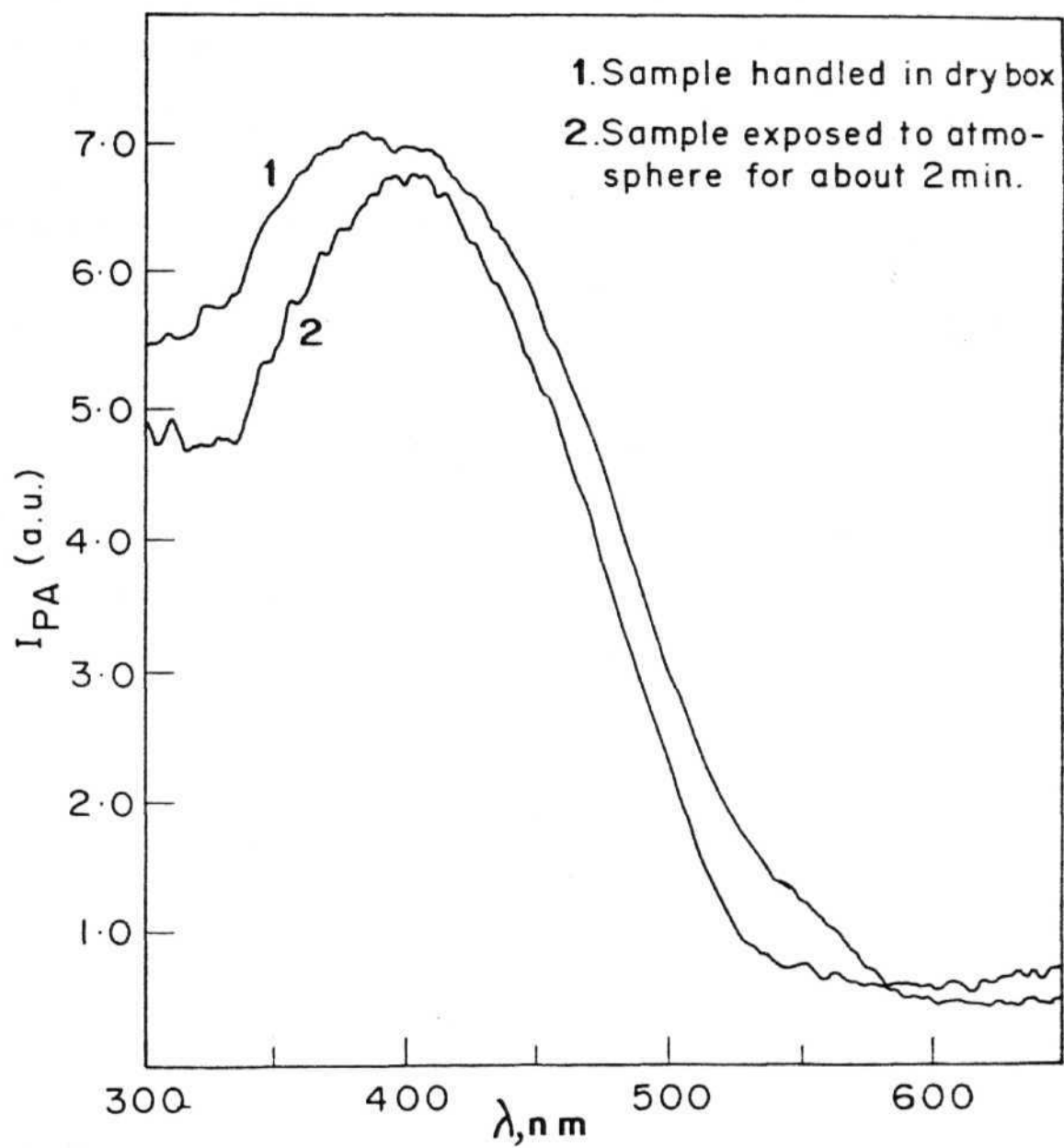


Figure 2.4 PA spectra of methyld red on neutralized silica-alumina showing the effect of sample exposure to the atmosphere.

normalization at 445 nm, where all the spectra should have the same signal strength; this accounts for small variations of signal strengths from sample to sample if any.

The PA signal strength at 515 nm is plotted against the volume of the titrant added, in order to determine the neutralization point. Interestingly the plot shows three inflection points; an observation that has been confirmed by six independent experiments. The surface of silica-alumina is known to have at least three different groups of acidic sites with varying acid strengths (25). This point is reflected in our titration plots. Figure 2.5 is plot of the quotient  $\Delta S / \Delta v$  versus  $\bar{v}$ , where  $\Delta S$  is the difference in the signal strength at 515 nm between two consecutive volumes ( $v_1, v_2$ ) of the added amine, and  $\Delta v = v_1 - v_2$  and  $\bar{v}$  is the average volume  $((v_1 + v_2) / 2)$  of the amine added. Such a derivative plot is made to accentuate the inflection points and shows two distinct peaks and a shoulder. The relative amounts of the strong, moderately strong and the weak acid sites on the surface under investigation are found to be 1.0: 1.3: 1.09 respectively, on the basis of the relative amounts of the titrant. And the total acidity is found to be 0.39 milli-equivalent per gram of the solid.

## 2.5 Conclusion:

The work reported here, though preliminary in nature, demonstrates for the first time the potential of PA spectroscopy in the study of surface acidity of catalysts. Apart from the surface acidity, it has also been possible to monitor the distribution of various acidic sites on the surface. Because of its simplicity, this method appears particularly suitable for screening catalysts prepared in the laboratory and for making rapid surveys of the catalysts used in some industrial processes, where the surface acidity is the key factor.

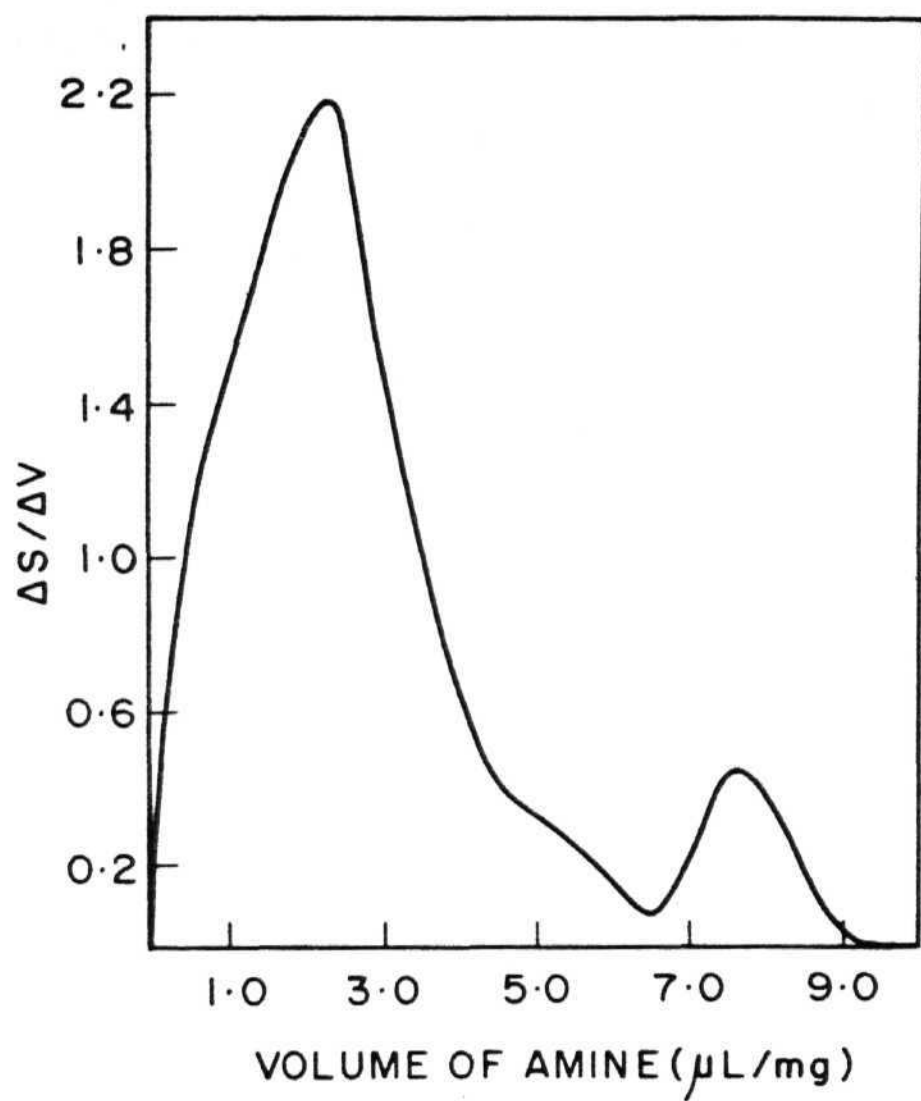


Figure 2.5 Derivative plot of the the titration of catalyst surface with n-butylamine.

We have used here a single indicator that allows the measurements of the total (or at least all the sites of interest) acidity. The extension of this work, with the use of a series of Hammett indicators, as reported by Benesi (15) in his visual titration method, is evident. Such a study should be able to provide precise information not only regarding the total acidity and the distribution of acidic sites but also acid strengths of each group of sites. Indeed, such a study has been reported by Ganguly and Rao (26) and more extensively by Jagannathan et al. (27). The IR spectra of certain organic bases coordinated to the surface are markedly different from that of the protonated species. It should be also possible to distinguish between Lewis and Bronsted acid sites by extending the study into the near infrared and infrared spectral regions.



### References;

1. W.A. Gruse and R. Stevens, 'Chemical Technology of Petroleum<sup>1</sup>', McGraw-Hill, New York, 1960, p 388.
2. R.C. Hansford, P.G. Waldo, L.C. Drake and R.E. Honig, Ind. Eng. Chem., 44, 1108 (1952).
3. M.W. Tamele, Disc. Faraday Soc., 8, 270 (1950).
4. G.A. Mills, E.R. Boedeker and A.G. Oblad, J. Amer. Chem. Soc., 72, 1559 (1950).
5. K. Tanabe, 'Solid Acids and Bases', Acad. Press, New York, 1970.
6. H. Pines and S. Maassem, Adv. Catal., 16, 49 (1966).
7. T.T. Kazto and M. Masaji, Bull. Chem. Soc. Japan, 44, 1534 (1971).
8. V.C.F. Holm, G.C. Bailey and A. Clark J. Phys. Chem., 63, 129 (1959).
9. M. Sato, T. Aonumo and T. Shiba Proc. 3rd Int. Congress on Catalysis", Vol. I, paper 17, Amsterdam 1964.
10. D. Ballivet, D. Barthomenf and Y. Tranbonze, J. Catal., 26, 34 (1972).
11. D. Ballivet, D. Barthomenf and Y. Tranbonze, J. Catal., 34, 423 (1974).
12. O. Johnson, J. Phys. Chem., 59, 827 (1955).
13. L.P. Hammett and A.J. Deyrup, J. Am. Chem. Soc., 54, 2721 (1932).
14. H.A. Benesi, J. Am. Chem. Soc., 78, 5490 (1956).
15. H.A. Benesi, J. Phys. Chem., 61, 970 (1957).

16. T. Yamanaka and K. Tonabe, 3. Phys. Chem., 79, 2409 (1975).
17. H.P. Leflin and M.C. Hobson, Jr., Adv. Catal., 14, 115 (1963).
18. A.N. Terenin, Adv. Catal., 15, 227 (1964).
19. S. Kobayashi, Nippon Kagaku Zasshi., 84, 21, 25 (1963); 82, 288 (1961); 80, 1399 (1959).
20. S. Kobayashi and I. Higuchi, Shokubai (Tokyo), 10, 123 (1968).
21. Y. Kageyama, T. Yotsuyanagi and K. Aomura, 3. Catal., 36, 1, (1975).
22. S.E. Mapes and R.R. Eischens, 3. Phys. Chem., 58, 1059 (1954).
23. E.P. Parry, 3. Catal., 2, 371 (1963).
24. S.L. Bonardet, J.P. Fraissard and L.C. de Menorval, 'Proc. Sixth. Int. Congr. on Catalysis' (Imperial College, London), 12-16 July, p 633 1976.
25. H. Yoshizumi, Y. Shimada and T. Shirasaki, Chem. Lett., 2, 107 (1973).
26. P. Ganguly and C.N. R. Rao, Proc. Ind. Acad. Sci. (Chem. Sci.), 90, 153 (1981).
27. K. Jagannathan, P. Ganguly and C.N.R. Rao, 3. Catal., 75, 262 (1982).

## CHAPTER III\*

STUDY OF A SOLID STATE PHOTOREACTION3.1 ABSTRACT

There is a considerable current interest in organic solid state photochemical reactions, their energetics, kinetics and topochemical factors in order to exploit them for specific molecular transformations. PAS appears to be a useful method in this connection not only because it is a convenient spectrophotometric tool for solids but also because of its selective sensitivity for the nonradiative deexcitation channel. A successful application of PAS to monitor several features of a solid state photoreaction is described in this chapter. The reaction chosen is ultraviolet radiation induced polymerization of a diacetylene to produce a fully conjugated linear polydiacetylene. The time profile, the wavelength dependence and the calorimetric features of the reaction have been investigated.

Polarized PA spectra suggest a laminar alignment of the polymer chains in the crystal. A method has been described for obtaining the action spectrum of the photoreaction, which is simple, more convenient than the conventional sampling method and which appears to be of general use

---

Parts of the work reported in this chapter have been published in the *Journal of Physical Chemistry*, **86**, 939 (1982); and presented at the annual meeting of the American Chemical Society, New York City, August 1981.

### 3.2 Introduction

The most remarkable feature in the solid state is the tendency of its constituent atoms or molecules to arrange themselves in an ordered periodic pattern. As a consequence of the decreased translatory freedom, the reactions in the solid state occur with a minimum amount of atomic or molecular movements. The crystalline matrix provides an extraordinary spatial control on the initiation and progress of organic reactions, leading to the formation of products that could be difficult, if not impossible, to make by conventional solution methods. A given compound can react differently in the solid state and in the solution or gas phases; chemically closely related compounds can show significant differences in their chemical behaviour even in the solid state; the same compound, in different polymorphic modifications, has been shown to undergo different transformations (1). The underlying cause for all these observations is the influence of the crystalline matrix. Such a matrix influence is termed as "topochemical" influence (2). The molecule of interest can be tailor-made with a remarkable selectivity and stereospecificity if one can manipulate these topochemical factors. The importance of the study of solid state reactions is evident in order to augment our understanding of these subtle structural and geometrical factors involved. Photoacoustic spectroscopy would appear to be a useful method in such studies not only because it is a convenient spectrophotometric tool for solids but also because of its selective sensitivity for nonradiative decay processes.

In this context, we illustrate a comprehensive use of PAS in studying several features of a solid state photo reaction such as the wavelength dependence of the photo reaction, time profile of the reaction, conformation of the product, orientation of the product in the solid and photocalorimetry.

The reaction chosen is the ultraviolet radiation-induced polymerization of a crystal of a diacetylene monomer to produce the polydiacetylene.

Diacetylenes,  $R-C \equiv C-C \equiv C-R$ , where R is a monovalent substituent group, polymerise in the solid state either upon heating or upon exposure to uv or radiation, to yield a fully conjugated, one-dimensional polymer crystal. Current interest in the solid state polymerization of diacetylenes has mainly been due to the initial work of Wegner (3-6). Most of polydiacetylenes are insoluble in common organic solvents, but after the recent synthesis of a new class of polydiacetylenes by Patel (7), that are highly soluble in organic solvents (chloroform, acetic acid, dichlorobenzene, dimethyl formamide etc.). Considerable interest has been generated on the conformational features of the polymers in solution. The molecular weights, conjugation lengths, optical properties and conformational features of such polymers have been reported (8, 9). There has also been a great deal of recent interest in the optical properties of polydiacetylenes crystals, mainly due to the one-dimensional nature of the polymer (10-13), and their possible optogalvanic applications. Various techniques have been employed to study the solid state polymerization and optical properties of the polydiacetylenes. The most commonly used technique for monitoring the polymerization is monomer extraction (14-16), which is a tedious gravimetric method that requires large amounts of the material. Finite solubility of the polymer in the solvent chosen for the exclusive removal of monomer leads to an underestimation of the polymer conversion; conversely, any trapped monomer in the polymer lattice, especially at high conversion, can lead to an overestimation of the polymer conversion. Patel et al. have recently reported a new technique for determining the extent of polymer conversion (17). One of them is differential scanning calorimetric method, the principal requirement

of which is that the material should display separate monomer and polymer melting endotherms. The other is a simple and accurate spectroscopic method which requires the polymer to be soluble. The method of diffuse reflectance spectroscopy has also been used for an in situ study of the thermal and uv polymerization (13). Specular reflections were minimised by using a set of crossed polarisers in the optical path, and the spectra recorded in 2.5 nm steps over the desired spectral range. 20 separate measurements were made and averaged at each wavelength. The absorption spectrum was then obtained by the use of the Kubelka-Munk method of treating the data.

Considering the inherent difficulties involved in the calorimetric and the diffuse reflectance methods, and the efforts involved in treating the data in order to obtain the absorption spectrum, it would appear that photoacoustic spectroscopy would be superior, more convenient and of general use; the requirement here would be that the absorption spectra of the monomer and the polymer be well separated.

### 3.3 Materials and Methods

The monomer 3BCMU (4,6-decadiyn-1,10-bis[(n-butoxy carbonyl)methyl urethane]) has the structure  $R-C\equiv C=C\equiv C-R$ , where  $R = -(CH_2)_3OCONHCH_2COOC_4H_9$  and produces upon polymerization the polymer hereafter referred to as poly (3BCMU). 3BCMU was the generous gift of Dr.G.N. Patel of Allied Chemical Corporation, Solvay, N.Y., USA. The monomer was purified by first dissolving in acetone and filtering off any traces of the polymer, and then by repeated recrystallization from acetone-hexane mixtures and stored in the dark below 10°C.

Photoacoustic spectra were recorded on a EG and G Princeton Applied Research model 6001 instrument. All PA measurements were done using a modulation frequency of 40 Hz, unless otherwise stated. Optical absorption spectra were recorded using a Cary 17D spectrophotometer. Polymerization of the monomer crystals was done using the source lamp of the PAS instrument, and, when necessary, using a model UV SL-25 multiband UV 'gun' made by Ultraviolet Products, USA.

In situ polymerization of 3BCMU was carried out on samples of the monomer adsorbed (from acetone solutions and subsequent solvent evaporation) on to filter paper strips, or on thin crystal platelets, using light from the source Xe lamp of the spectrometer ( $\sim 5 \text{ mW}/\text{cm}^2$ ). However, in experiments designed to monitor the time-dependent growth of the PA signals, a strip chart recorder attached to the instrument was used to follow the 630 nm and 580 nm peaks, and the sample in the PA cell was illuminated with an external UV-gun.

For photocalorimetry, the procedure suggested by Chance and coworkers<sup>(15,16)</sup> was followed. The monomer in the crystalline or adsorbed state was placed in the cell with the light blocked, and the excitation wavelength for polymerization was chosen for the experiment (210, 225, 240 or 252 nm). The PA signal at the chosen wavelength obtained upon unmasking the sample cell was recorded as a function of time using a strip chart recorder.

For linear dichroism measurements, an Oriel UV-standard polarizer (model No. 2540-2) along with a precision rotator (model No. 1641) was incorporated into the optical path of the instrument and the PAS of the sample crystal recorded at 0° and 90° polarizer angles (with respect to the major c axis of

the 6 mm x 2 mm crystal platelet). Polarization of the emerging beam is always a problem associated with reflection optics. The polarization of a small fraction of the total radiation incident on the sample does not make any difference in the observed spectra for optically isotropic samples, provided the detector is not sensitive to the polarization of light. Thus PA signal will be proportional to the product  $\beta(\lambda)I_0(\lambda)$ ; the second term  $I_0(\lambda)$  is taken care of by normalizing the observed spectrum with the spectrum obtained for the carbon black sample. However, if the sample were optically anisotropic, then in spite of correcting for  $I_0(\lambda)$  the spectrum would show an increased absorption when the plane of polarization of the incident light coincides with the orientation of the transition dipole of the sample, i.e. now the observed spectrum would be proportional to the product  $\beta(\lambda)I_0(\lambda)P(\lambda)$  where  $P(\lambda)$  is polarization factor at  $\lambda$ .

Indeed we have observed a spurious band at 425 nm with a crystal of poly(BCMU) in the EG&G PA spectra. Poly(BCMU) has no absorption maximum at 425 nm. The observed signal is due to the polarization of light incident on the sample. This could pose a problem if one attempts to record polarized PA spectra. We could solve this problem by normalizing the spectrum with carbon black spectrum recorded with a polariser with the same angle set in the optical path. Introducing the polarizer in the optical path, while recording the carbon black sample, will translate the change of the plane of polarization into a change of light intensity. Figure 3.1 shows the carbon black spectrum recorded with polarized light. These spectra were used for normalizing sample polarized spectra.

The approach taken to determine the action spectrum was to expose the monomer to radiation of a chosen wavelength in the instrument for a fixed period of time and to monitor the extent of polymerization by measuring the



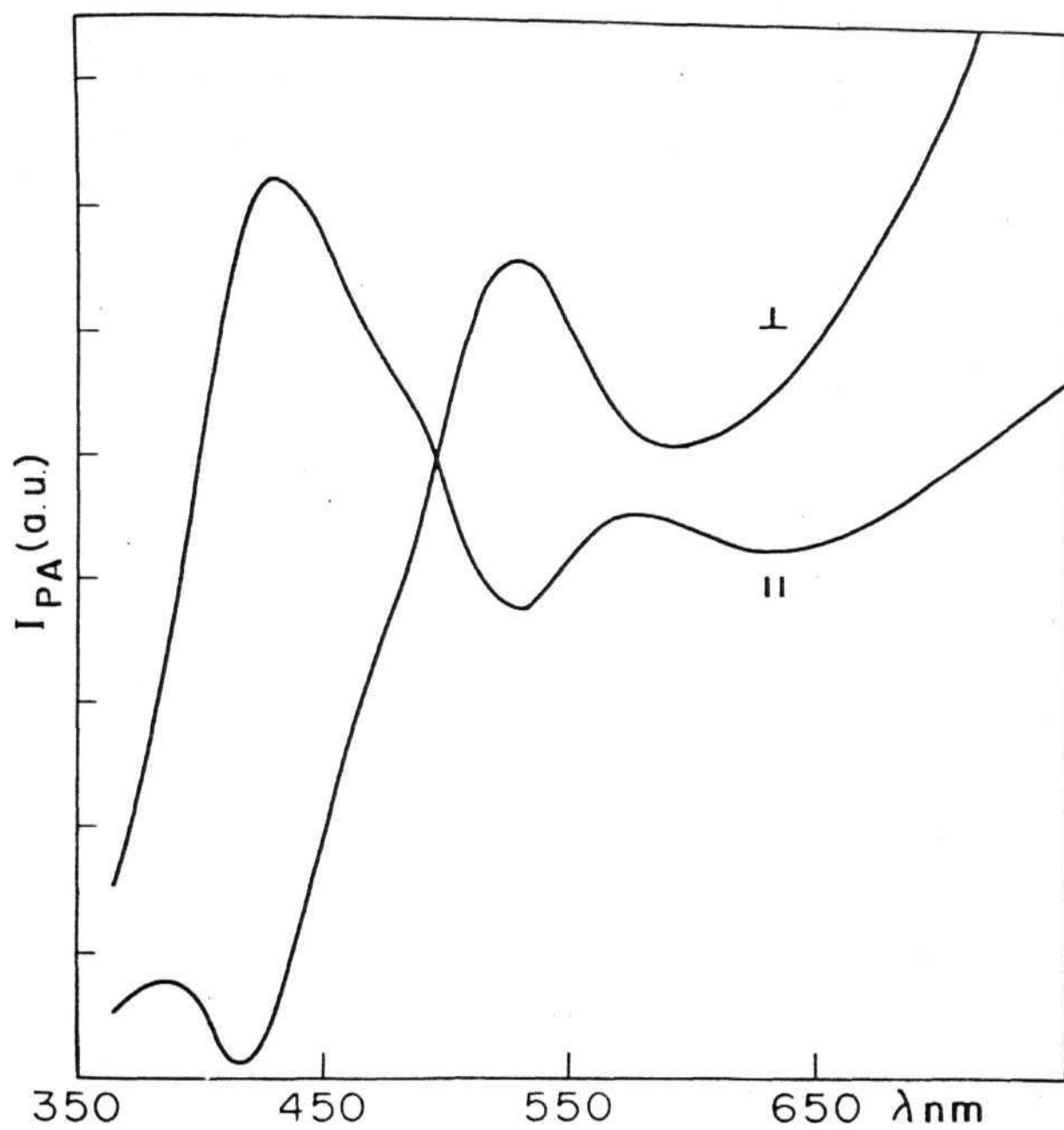


Figure 3.1 PA spectra of carbon black recorded with polarized light.

polymer PA signal strength in the visible region 630 nm and or 580 nm. The monomer has no absorption and hence no PA bands above 300 nm. A direct comparison between two samples exposed to different wavelengths is prone to error due to variations in the sample size, and due to the variation of the source intensity with wavelength. These problems were overcome by two steps. Sample variation was minimized by dissolving 3BCMU in acetone and dipping filter paper strips (3 mm x 7 mm, Whatman No.1) in the solution and drying them, all in the dark and below 10°C. Then a given paper strip containing the adsorbed 3BCMU was irradiated at a chosen wavelength for 10 s, and the PA spectrum in the region 700-200 nm was recorded (curve a). Next, the same sample was irradiated with the external wide-band UV gun for several minutes to allow for complete polymerization and the spectrum of the fully polymerized sample was recorded in the same region (curve b). The fraction of the monomer that had polymerized upon 10 s exposure with the chosen wavelength was calculated from the ratio of the areas under the polymer band profiles (630,580 nm) of curves a and b. The variation in the spectrometer source intensity with wavelength was accounted for by normalizing the fraction (a/b) obtained to the light intensity at a given wavelength. This extent of polymer formed, corrected for power variation, was taken as the action parameter at the chosen wavelength, and plotted against wavelength to give the action spectrum of the photo-reaction.

A method of determining the action spectrum employing PAS has been used, and is described in the section on Results and Discussion. Briefly this uses the fact that in thermally thin ( $\mu_s \gg l$ ) and optically transparent ( $\mu_a \gg l$ ) samples, the ratio of the optical absorption (OA) spectrum to the photo-acoustic (PA) spectrum would be a wavelength-independent constant if the

molecules of the sample return to the ground state solely by nonradiative decay. If the sample were to fluoresce or undergo photoreactions as well, the OA/PA ratio would show wavelength dependence corresponding to the photo action. In this method, therefore, the OA spectrum of the monomer 3BCMU is compared with its PA and the ratio plotted.

### 3.4 RESULTS AND DISCUSSION

#### 3.4.1 In situ polymerization:

Figure 3.2 shows the PAS record of the in situ polymerization of 3BCMU adsorbed on filter paper. The experiment was started by uncovering the light mask from the sample chamber and scanning the spectrum from 700 nm to 200 nm at a scan rate of 200 nm/min. Curve 1 is the spectrum of the pure monomer, and displays no bands in the visible region. Exposure of the monomer during this run to UV-radiation in the 300-200 nm region for 30 s is sufficient to start the polymerization; curve 2 reveals the presence of signals at 630 nm and 580 nm which correspond to the absorption bands of poly (3BCMU) reported by Chance et al. (20). Curves 3 to 7 show the progressive intensification of these bands, suggesting further photopolymerization of the sample. Curve 7 is essentially identical to curve 6 and suggests that, under these conditions, exposure of the monomer to UV radiation for a period of about 3 minutes was enough to polymerize the sample to the conversion limit.

In situ polymerization of a thin crystal shows exactly the same features but differs in the time required for reaching the conversion limit. Attenuation of the source power falling on the sample by introducing quartz plates in the light path led to the expected increase in the time required for reaching conversion limit. Use of a thicker crystal caused difficulties in measurements due to an increase in the sample thickness  $l$  relative to the optical absorption length  $\mu$ , which resulted in PA saturation.

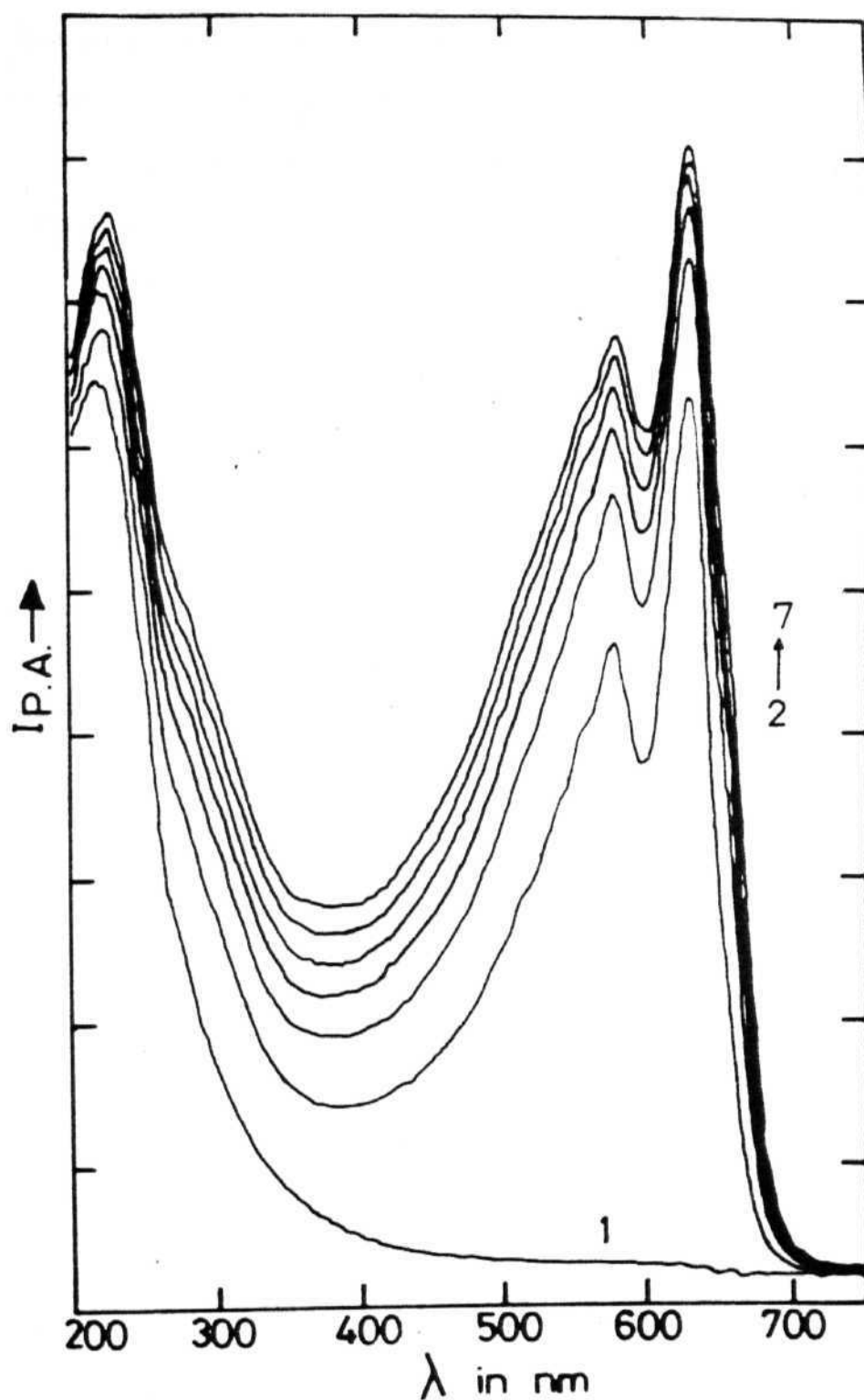


Figure 3.2 In situ photopolymerization of 3BCMU adsorbed on a filter paper strip. Curve 1 in the first run and 2-7 are subsequent ones on the same sample. Runs started at 750 nm and stopped at 200 nm.

The bands seen at 630 nm and 580 nm correspond to the planar conformation of poly (3BCMU); the band at 475 nm, seen in solution (20) and attributed to the nonplanar form of the polymer, is not seen in our experiments in the solid state.

That UV-radiation is needed for photopolymerization of 3BCMU was established by the following experiment. The monomer was exposed to radiation from 700 nm down to 200 nm during the first run in the instrument, leading to some polymerization. Subsequent runs were stopped at 300 nm, cycled in the range 700-300 nm, and the strength of the 630 nm (and 580 nm) band monitored. The absence of any increase in these signal strengths revealed that polymerization proceeds only when the monomer is exposed to UV-radiation. This observation was further confirmed in pulse excitation experiments, wherein the time variation of the 630 nm band was monitored as the external UV-illumination was turned on and off periodically. The results of such an experiment are illustrated in Figure 3.3 a which shows the PA signal to increase during the periods when the illumination is on and invariant during the dark.

#### **3.4.2 Time profile of the reaction:**

Wegner had studied (14) the UV-polymerization of a related diacetylene, PTS (where the substituent R group is p-toluene Sulfonyl), and concluded that the UV-polymerization is not autocatalyzed. However, reinvestigation of the reaction using diffuse reflectance spectroscopy by Chance and Patel (16) revealed that the reaction was autocatalytic and that the effect would be effectively masked in such UV experiments unless the optical absorption depth  $\mu_p (=1/\beta)$  where  $\beta$  is the optical absorption coefficient in  $\text{cm}^{-1}$ ) of the crystal is comparable to or larger than the crystal thickness  $l$ . In this connection, PAS would appear

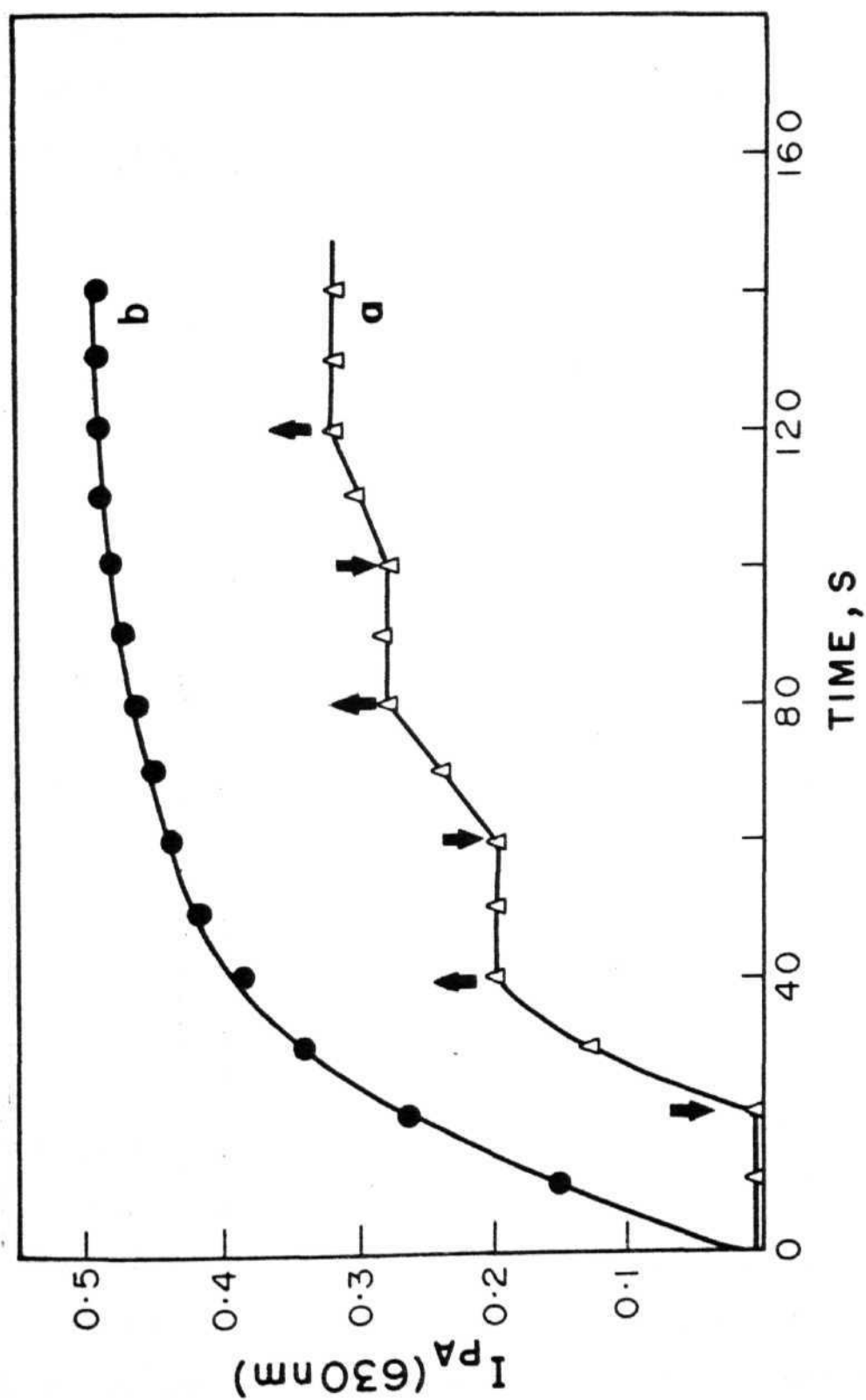


Figure 3.3 (a) Variation of the PA intensity at 630 nm with time, as the external uv-gun illumination was switched on and off every 20 seconds. (b) Time-dependent growth of the 630 nm PA signal when the sample, 3BCMU (on filter paper), was constantly illuminated by an external uv-gun.

to be a convenient method to study this feature of the reaction under appropriate conditions.

In Chapter I, Table 1.1, we had considered six limiting cases concerning the relative magnitude of  $\mu_\beta$ ,  $\mu_s$  and  $l$ , and the dependence of the PA signal on  $l$  in some detail. The particular case of interest here is that of an optically transparent sample ( $\mu > 1$ ) which is also thermally thin ( $\mu > \mu_s > 1$ ) where the PA signal  $I_{PA}$  is proportional to  $l$ , parallels the wavelength dependence of  $\beta$ , and varies as the inverse power of the modulation frequency ( $\omega^{-1}$ ). In the present case of 3BCMU in the crystalline and adsorbed phases, it is clear that  $\mu_\beta > 1$  and  $\mu_s > 1$ , since the PA spectra in Figure 1 reveal well-resolved bands at 630 and 580 nm, PA saturation does not occur and the spectra parallel the absorption spectra in the wavelength dependence of  $\beta$ . We have also confirmed the dependence of the PA signal on  $l$  by using samples of different thicknesses, and their  $\omega^{-1}$  dependence by measuring the spectra at several modulation frequencies. Thus we are dealing with samples which meet the criterion for detecting any autocatalysis. The time evolution of the polymer PA signal at 630 nm is shown in Figure 3.3 b. The time profile of the reaction illustrated in the figure shows no features suggestive of autocatalysis, and confirms the earlier suggestion that photopolymerization of 3BCMU is not autocatalytic (17).

### 3.4.3 Photocalorimetry:

Chance and Shand (18) have devised a PA photocalorimetric method to measure the heat energy involved in the photopolymerization of some diacetylenes. The time-dependent variation of the PA signal at the exciting wavelength was analyzed using a kinetic model that was shown to agree with experimental results. In PA photocalorimetry, the time profile of the heat liberated,

arising from the exothermic photoreaction as well as that due to photon absorption by the sample, is measured. The calorimetric curve shown in Figure 3.4 for 3BCMU polymerization was prosaic, exhibiting a sharp rise in the PA<sub>225</sub> signal (upon unblocking the light) which stayed essentially invariant (negligible rise) with time. Identical results were obtained when other excitation wavelengths were tried, such as 210, 240 or 252 nm (absorption peaks of monomer). This is in contrast to the curve for the higher homolog 4BCMU, where the signal showed a gradual fall with time after the instantaneous rise upon unmasking the light (18).

As the polymerization reaction proceeds, the amount of the polymer, which absorbs stronger than the monomer, increases, resulting in an increase of the signal with time. On the other hand, since the polymerization rate falls with time, the heat liberated due to polymerization, and hence the PA signal, should decrease with time. The experimentally measured signal would be a result of the above two factors. The heat liberated per photon absorbed may be represented as  $h\nu + nq\Delta H$ , where  $h\nu$  is the photon energy,  $n$  the length of the polymer repeat units produced per photon,  $q$  the probability of the excited state initiating a polymer chain, and  $H$  the heat liberated per polymerized unit. In the case of 4BCMU,  $q$  has been estimated to be  $3 \times 10^{-3}$ ,  $n$  as 2400, and  $\Delta H$  as 1.6 eV, while for 3BCMU  $n$  has been estimated to be 1000.

If one assumes the values of  $q$  and  $\Delta H$  to be the same as in 4BCMU, then, the heat liberated in the polymerization of 3BCMU would be expected to have a value that is 1000/2400 times that of the polymerization of 4BCMU. The near constancy of the photocalorimeter curve for 3BCMU polymerization



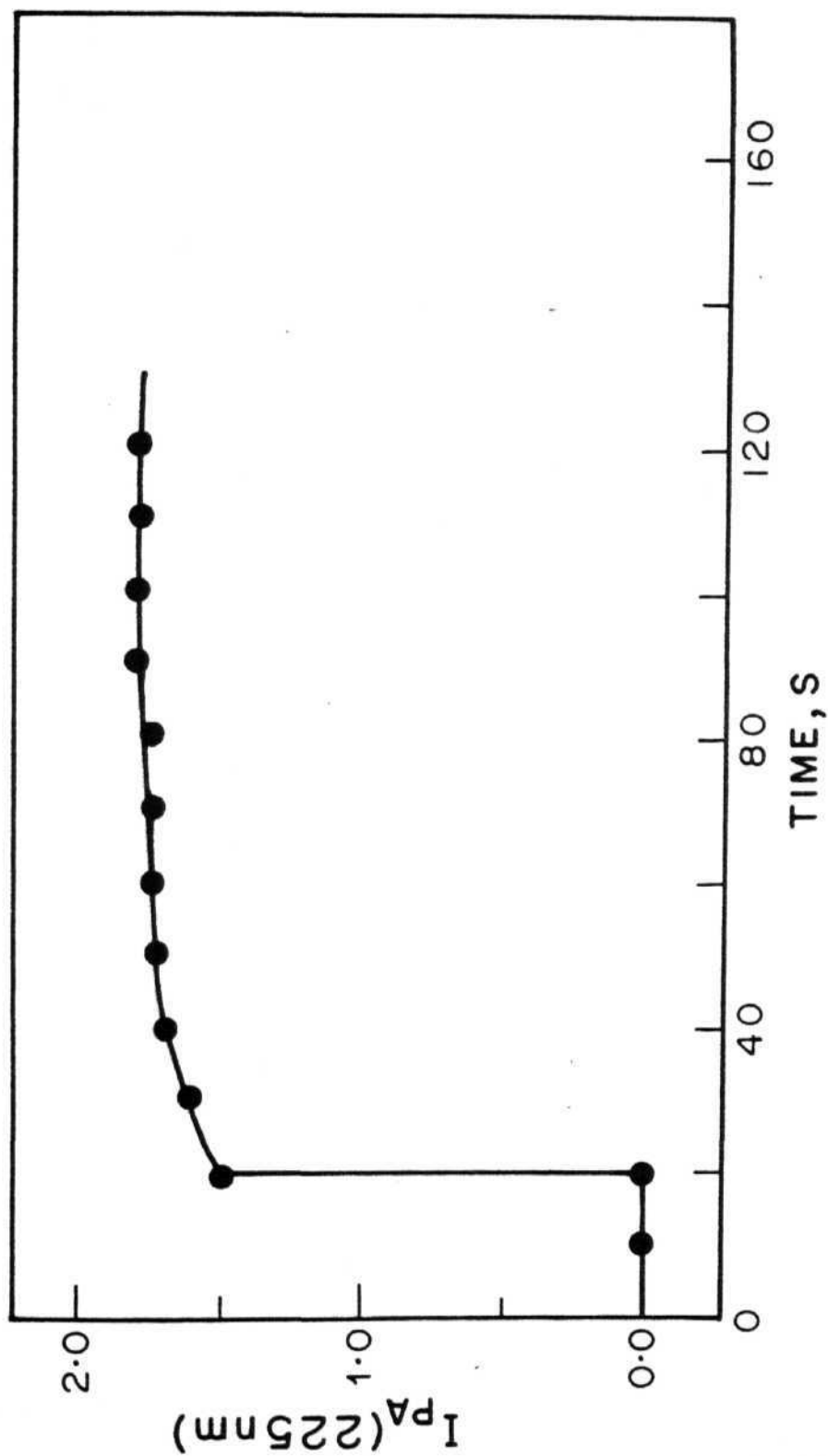


Figure 3.4 Photocalorimetric profile of 3BCMU photopolymerization. PA signal intensity of the photopolymerization-initiating wavelength (225 nm) was followed with time upon the removal of the light-mask from the sample cell.

with time would then suggest that the contribution **due** to the heat of the reaction is **effectively** balanced by that due to the increased photon absorption by poly (3BCMU). The related diacetylene DCHD (where the substituent R group is methyl carbazole) also displays an essentially time-invariant PA photocalorimetric profile (19).

It is, however, possible that the parameter  $q$  need not be the same for 3BCMU as for its homolog 4BCMU. While these two monomers show essentially the same absorption characteristics and initiate photopolymerization from the same excited states, their molecular structures differ by a methylene group. Even such a subtle difference could reflect in the corresponding crystal packing and lead to different values of the chain initiation probability  $q$  for 3BCMU and 4BCMU. In the light of the near-constancy of the measured photocalorimetric curve for the polymerization of 3BCMU (Figure 3.4), it is also possible to conclude that the product  $nq$  is much smaller for 3BCMU compared to its higher homolog. The differences in 1, if any, are more than overcome by the large differences in  $n$  between two monomers.

Changing the modulation frequency between 40-200 Hz had no significant effect on the nature of photocalorimetric curve, except to decrease the magnitude of the initial signal. This is to be expected, since such a change would about equally affect both the factors that contribute to the photocalorimetric signal.

#### **3.4.4 Action spectrum;**

We next turn our attention to the measurement of the action spectrum of the photoreaction. In essence, an action spectrum describes the wavelength (energy) dependence of photo-action. In conventional methods, the amount

of the photoproduct formed is monitored as a function of the wavelength of excitation of the reactant. On the other hand since PAS measures the extent of partitioning of the absorbed energy into heat dissipation, it should be possible to exploit PAS to measure the action spectra of such molecules where no other competing deexcitation processes, such as luminescence, occur. We have tried both the approaches to determine the action spectrum of the 3BCMU photoreaction. In the first, a sample of the monomer adsorbed on filter paper strip was irradiated for a period of 10 s in the PA cell, using the PA spectrometer lamp and tuning the monochromator to UV-radiation of a chosen wavelength, and the PA spectrum in the 700-200 nm region was recorded. The experiment was repeated with several samples, each irradiated for the same time with light of a different wavelength. The data were analyzed, after correcting for the wavelength variation of the source power as described in the Materials and Methods section.

In the second method (21), we exploit the fact that the PA signal of an absorbing or optically transparent sample  $I_{PA}$ , will be proportional to the incident power absorbed by the sample ( $P_{abs}$ ) and will depend on the efficiency,  $\eta$ , of the nonradiative decay to the ground state while the optical absorption signal  $I_{OA}$  is indicative of  $P_{abs}$ . For a sample that neither fluoresces nor undergoes any photochemical reactions,  $\eta = 1$  and the PA spectrum will parallel the optical absorption (OA) spectrum in the entire spectral range; i.e. a plot of the ratio of the absorption and PA signals  $[I_{OA}/I_{PA}]$  against wavelength will be a flat curve of zero slope. If, however, a part of the adsorbed energy were to be utilized towards emission or any photoreaction, the ratio  $I_{OA}/I_{PA}$  would be expected to change with the wavelength, displaying the maximum changes at those wavelengths corresponding to the particular excited states from which emission or photoreaction occur. We have tested this with  $KMnO_4$ ,

$K_2Cr_2O_7$  and the dye thymol blue, compounds which neither fluoresce nor undergo any phototransformation, and in each case the ratio  $I_{\text{un}}/I_{\text{PA}}$  was seen to be independent of wavelength (figure 3.5 a). With the fluorescing dye Rhodamine 6G, such a plot displayed a peak at 525 nm indicating that the excited state corresponding to absorption at 525 nm was being deexcited partly through the fluorescence mode (Figure 3.5 a). Now, since diacetylenes such as 3BCMU do not fluoresce at room temperature but photopolymerize, the ratio  $I_{\text{OA}}/I_{\text{PA}}$  as a function of wavelength in the UV-range would be expected to reflect the extent of photochemistry that occurs and thus yield the action spectrum.

This method of obtaining the action spectrum of a photoprocess by PAS is being explored in greater detail in our laboratory. Figure 3.6, plot (a), shows the action spectrum obtained by the conventional method while plot (b) is the action spectrum obtained by the  $I_{\text{OA}}/I_{\text{PA}}$  ratio method; the resemblance between the two curves is gratifyingly close. Cahen and coworkers have utilized a similar method to monitor photoprocesses other than nonradiative decay in biological systems (22-24).

### 3.4.5 Linear dichroism;

Figure 3.7 shows the polarized PA spectra of poly (3BCMU) obtained by polymerizing the monomer crystal in situ. The bands at 630 nm and 580 nm are seen to have much higher intensities when the polarization is parallel to the major axis of the crystal than when it is perpendicular, suggesting that the transition dipoles of these bands in the highly conjugated system of the polymer lie along the major axis of the crystal. This observation is consistent with reports using normal incidence reflection spectra (20) on this class of polydiacetylenes, and indicates that the polymer chains are aligned along the c axis of the crystal. When the samples were taken as adsorbates on filter paper rather than crystals, no dichroism was observed on the resultant polymer suggesting random orientation on the paper surface.

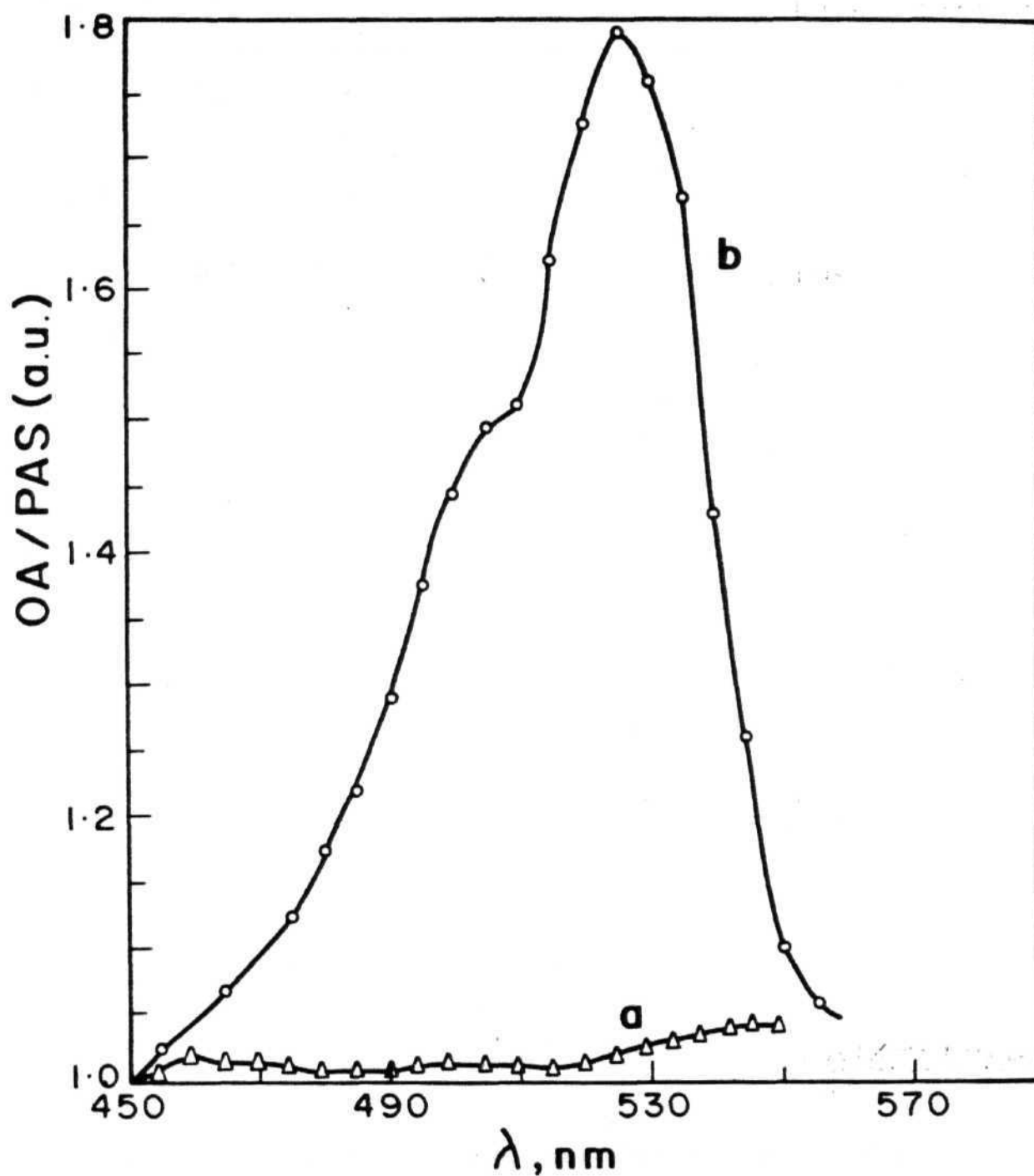
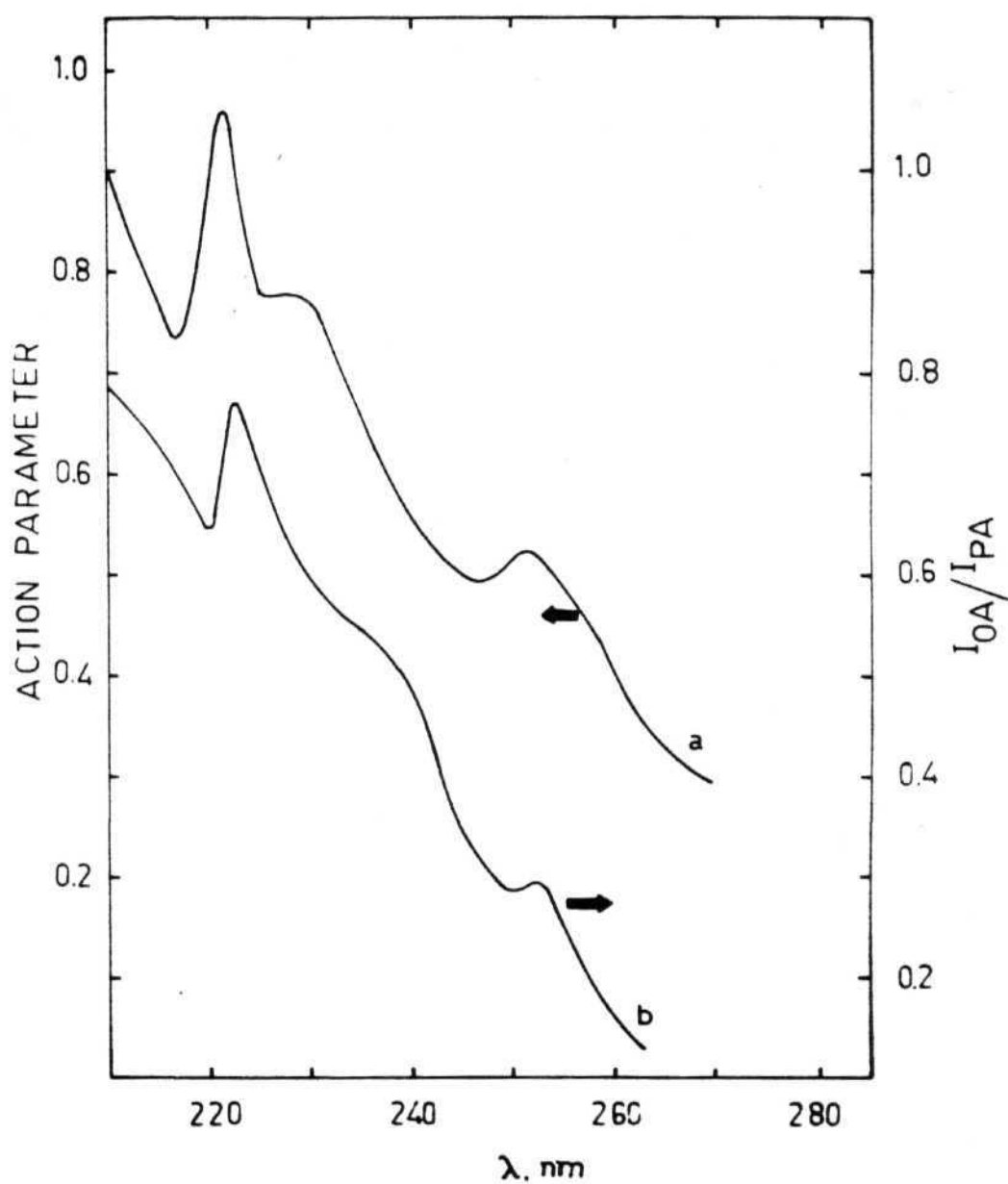


Figure 3.5 Plot of the ratio of the optical absorption (OA) and PA signal (PAS) against wavelength for the aqueous solutions of (a) Thymol blue (b) Rhodamine 6G.



**Figure 3.6** Action spectra of the photopolymerization of 3BCMU (a) using the conventional method and (b) by  $I_{OA}/I_{PA}$  method described in the text.

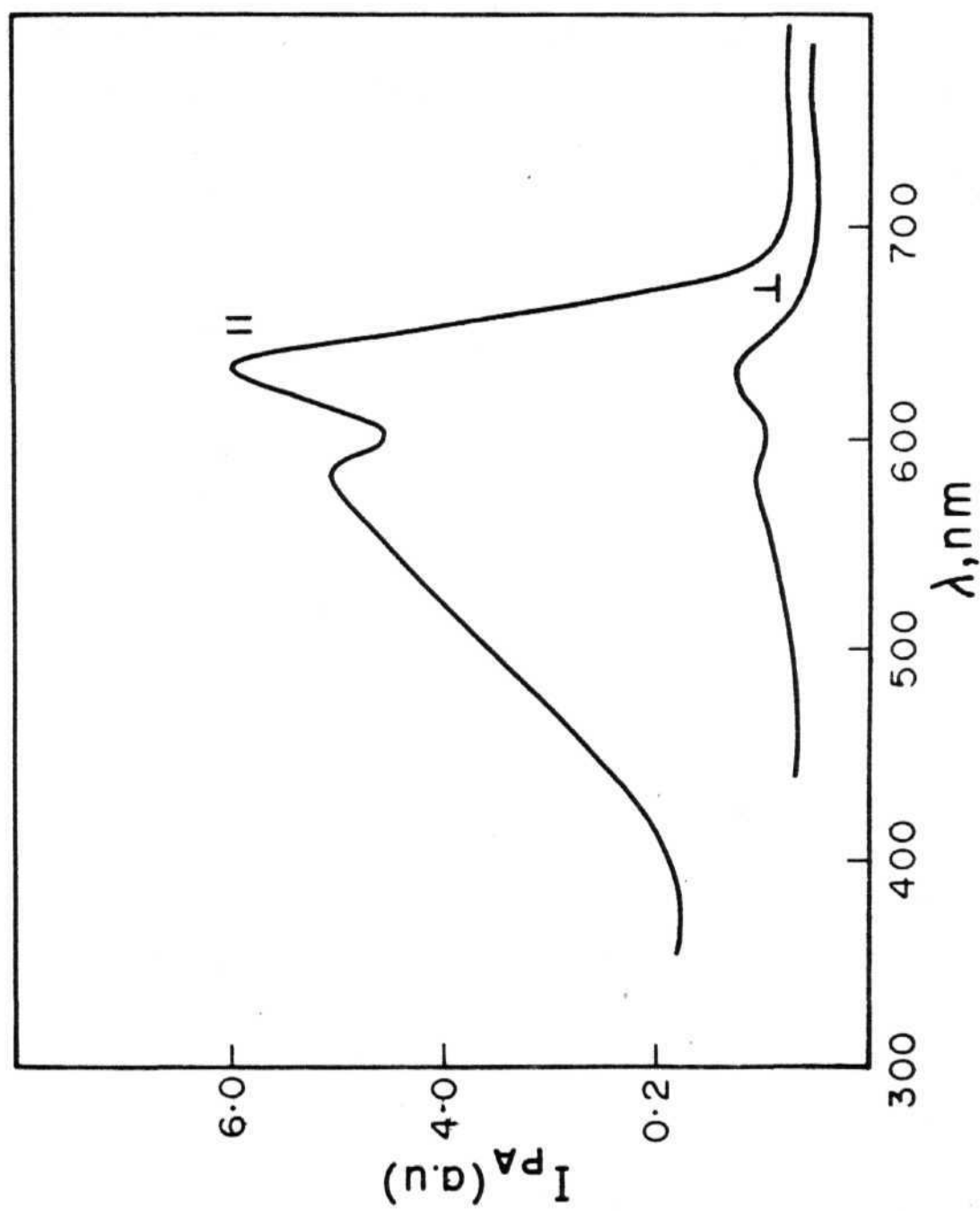


Figure 3.7 Polarized PA spectra of poly (3BCMU) with the plane of polarization parallel ( $||$ ) and perpendicular ( $\perp$ ) to the major axis of the crystal.

### 3-5 Conclusion:

We have shown that PAS can be conveniently used to monitor several features of a solid-state reaction (i) the wavelength dependence of the photo-reaction, i.e. the action spectrum (ii) the time profile of the reaction (iii) the conformation of the product polymer (iv) the linear dichroism and orientation of the polymer in the solid and (v) the photocalorimetry of the reaction. The approach opens up the possibility of studying various organic photoreactions in the solid state and to understand the reactions in terms of the energy states involved in the reaction, and the effect of subtle geometric and structural changes on the course of the reaction. The method described here for the determination of the action spectrum of the photoreaction appears to be simpler and more convenient than the conventional sampling method.



**REFERENCES:**

1. M.D. Cohen and G.M. Schmidt, 3. Chem. Soc., 1916 (1964).
2. E. Hertel, Z. Electrochem., 37, 536 (1931).
3. G. Wegner, Z. Naturforsch., 24, 824 (1969).
4. G. Wegner, Makromol. Chem., 154, 35 (1972).
5. G. Wegner, in 'Chemistry and Physics of one dimensional metals', H.3. Keller (Ed.), 297-314, Plenum Publication Corp., New York, 1977.
6. R.H. Baughmann, in 'Contemporary Topics in Polymer Science', E.M. Pearce and J.R. Schaefgen (Eds.), Plenum, New York, 1977, Vol.2, p 205.
7. G.N. Patel, Polym. Prepr. Am. Chem. Soc. Div. Polym. Chem., 19, 154 (1978).
8. G.N. Patel, R.R. Chance and J.D. Witt, Polym. Prepr. Am. Chem. Soc. Div. Polym. Chem., 19, 160 (1978).
9. G.N. Patel and E.K. Walsh, 3. Polym. Sci. Polym. Lett. Ed., 17, 203 (1979).
10. R.R. Chance, R.H. Baughmann, C.3. Eckhardt and H. Miller, 3. Chem. Phys., 67, 3616 (1977).
11. H. Muller, C.3. Eckhardt, R.R. Chance and R.H. Baughmann, Chem. Phys. Lett., 50, 22 (1977).
12. D. Bloor and F.H. Preston, Phys. Stat. Sol. A, 40, 279 (1977).
13. H. Muller and C.3. Eckhardt, 3. Chem. Phys., 67, 5386 (1977).
14. G. Wegner, Makromol. Chem., 145, 85 (1971).

15. D. Bloor, L. Koshi, G.L. Stevens, F.H. Preston and D.J. Ando, 3. Mater. Sci., 10, 1678 (1975).
16. R.R. Chance and G.N. Patel, 3. Polym. Sci., Polym. Phys. Ed., 16, 859 (1978).
17. G.N. Patel, Y.P. Khanna, D.M. Ivory, 3.M. Sowa and R.R. Chance, 3. Polym. Sci. Polym. Phys. Ed., 17, 899 (1979).
18. R.R. Chance and M.L. Shand, 3. Chem. Phys., 72, 948 (1980).
19. M.L. Shand, R.R. Chance and A. Prock, 'Ultrason. Symp. Proc.\*', 664-667 (1980).
20. R.R. Chance, G.N. Patel and 3-D. Witt, 3. Chem. Phys., 71, 206 (1979).
21. D. Balasubramanian, Ch. Mohan Rao and B. Panijpan, paper presented at the 7th International Biophysics Congress, Mexico City, Mexico, August 1981, Abstr. No. 11 TH-p3.
22. S. Malkin and D. Cahen, Photochem. Photobiol., 29, 803 (1978)
23. D. Cahen, G. Bults, H. Garty and S. Malkin, 3. Biochem. Biophys. Methods, 3, 293 (1980).
24. N.L. Ross, S. Malkin and D. Cahen, Biochim. Biophys. Acta., 593, 330 (1980).

## CHAPTER IV\*

### ON THE MODE OF ACTION OF ANTIMALARIAL DRUGS

#### 4.1 ABSTRACT

It was thought that antimalarial drugs intercolate to DNA of malaria causing parasites and thus mediate chemotherapeutic action. Recent observations are against this idea and implicate endogenous hemin in the malaria parasite in the mode of action of drugs. We have monitored the status of endogenous hemin and the effects of added drugs on it by a direct study of the parasites by PAS. Suci. a study has provided the first spectral evidence for the presence of hemin self-aggregates in the parasites. The malaria pigment, hemozoin, is shown to be a hemin-protein complex. PA spectra of drug-treated parasites suggest that the drug interacts with endogenous hemin. It appears that (i) the endogenous hemin exists predominantly as self-aggregates and as hemozoin pigment; (ii) antimalarial drugs bind to transient hemin; and (iii) a drug-hemin complex accumulates which eventually leads to lysis of the parasite. On the basis of the PAS results and certain earlier suggestions, a scheme for the mode of action of quinoline class of antimalarial drugs is proposed. Drug-sensitive and resistant parasites show distinct differences in their PA spectra.

---

\* Parts of the work reported in this chapter are (i) published in Current Science, 51, 111 (1982) (ii) presented at the "Third International Conference on Photoacoustic and Photothermal Spectroscopy", Paris, April 1983 and (iii) being published.

## 4.2 Introduction

In the year 1955, the World Health Organization began a global malaria eradication programme, one of the massive programmes ever launched by the organisation. This has resulted in the eradication of malaria from the United States, most of Europe and the Middle East. Taiwan and Mauritius, where malaria incidence was the highest, were completely freed from the disease by 1960. Success seemed at hand. But since the last decade malaria is tragically resurgent in Asia and certain other parts of the world. In our country the incidence of malaria was reduced from several million cases per year to 50,000 in the year 1961, but has unfortunately assumed endemic proportions recently; 30 million cases were reported in 1977. Nearly half of child mortality in the tropical countries has been attributed to malaria. According to current estimates, at least 10% of malaria cases lead to death of the patient. The setback in the apparently successful malaria eradication programme can be attributed to, besides several socioeconomic reasons, at least two scientific aspects; one is the resistance of malaria-transmitting mosquitos to insecticides while the other more recent phenomenon is the resistance of the malaria parasites themselves to some of the prevalent antimalarial drugs. The recognition of the magnitude and the complicated nature of the task has resulted in the revival of research, and the false notion that malaria is vanishing, if not vanished, has been given up.

The discovery of the first treatment for malaria dates back to 1600, before the fever was given the name 'malaria'. Peruvian Indians were reported to have used the powdered bark from a tree, now known as Cinchona, for curing the fever (1). The use of this drug met with remarkable success but it was soon realised that the drug is effective in curing only certain types of intermittent

fevers. Italians called this fever "mal' aria" since, it was then widely believed that this was caused by the foul air common near marshy areas. The parasitic origin of the disease was discovered by Laveran (2), who first observed and described the infecting parasite in the red blood cell of malaria patients. Ronald Ross showed in 1897 that the female Anopheles mosquito is responsible for the transmittance of the disease. Since then, these vectors have become the target for the control and eradication of malaria.

Although the effectiveness of the Peruvian bark against malaria was known in 1600, it was only about two hundred years later that the active ingredient, quinine, was isolated from Cinchona. Quinine, isolated from its natural sources, has been the drug of choice for nearly 100 years. The difficulty of securing cheap supplies of quinine during the first world war stimulated research in synthetic antimalarial drugs and several synthetic drugs such as pamaquine, mepacrine and chloroquine were developed.

Among several other drugs, chloroquine has remained the drug of choice for curing malaria since the second world war. This is an excellent preventive and curative drug with minimal side effects, when compared to other available drugs. But unfortunately some strains of the parasites have developed the ability to survive and to multiply in spite of the administration of the drug (3-6). This phenomenon, termed as 'drug-resistance', is a serious one and needs to be tackled immediately before it results in a dramatic depletion of the available range of drugs for the prevention and treatment of malaria. At least nine species of the parasites are shown to be resistant to one or more of the fifteen effective antimalarial drugs in use (7). The conventional practice of synthesizing analogue molecules with minor structural variations and testing

them for improved pharmaceutical activity appears to be inadequate. It is necessary, therefore, to understand how antimalarial drugs act and what makes a parasite resistant to a particular drug. If these questions are answered satisfactorily, one can hope to tailor-make appropriate drugs - controlling anything which is undershould should be simpler.

#### **4.2.1 An outline of the pathology**

Malaria is a parasitic disease caused by the parasite Plasmodium, carried and transmitted by the mosquito. When a female Anopheles mosquito feeds on the blood after piercing the human skin, the sporozoites, the long thin cells of the parasites with a central nucleus and pointed ends, are injected into the wound and pass into the blood stream. While many of the sporozoites are destroyed by phagocytes in the blood stream, some enter the liver and undergo a process of development and multiplication known as pre-erythrocytic schizogony, and produce several thousands of merozoites. These merozoites enter the blood stream and invade the erythrocytes, where they feed on the hemoglobin. Merozoites have a vacuole which displaces the cytoplasm to periphery, while the nucleus is situated at the pole; thus the cytoplasm has an annular appearance and hence this stage is also called the ring stage. All the early stages of the parasite in the blood cells are called trophozoites. After a period of growth, the nucleus of the parasite multiplies and forms several merozoites. After this process is completed the red blood cells burst open and the merozoites are released into the blood stream. These merozoites invade the other uninfected red blood cells and the cycle repeats. The length of the erythrocytic phase is known as the schizogonic periodicity and differs with the species of the parasite, being 48 hours in P. vivax and 72 hours in P. falciparum, causing three or four day fever patterns. The pathogenesis of fever in malaria is still not well understood. Recent studies indicate that leucocytes release pyrogens

in response to endogenous stimuli due to the infectious agents. This, in a sequence of events, leads to a constriction of peripheral vessels and decreases heat dissipation, which results in a rise in the body temperature. Rapid and extensive destruction of erythrocytes may lead to anemia. Infected erythrocytes tend to clump together, interfering the circulation of the blood in capillaries and cause lesions in various organs through anoxia. Local disturbances can cause several impairments in the normal functions of the host.

#### **4.2.2 Action of Antimalarial drugs**

Attempts to understand the mode of action of antimalarial drugs started from as early as 1952. Quite naturally, researchers have looked at DNA as being a primary target of the drug. Clarke (8) has shown that while quinine inhibits the incorporation of radioactively labelled phosphate ( $^{32}\text{P}$ ) into the DNA of intra-erythrocytic parasites, no clear dosage-response correlation was seen; this led to the conclusion that "the action of quinine was not direct, but is mediated by the host cell". Polet and Barr(9) have postulated that the primary mechanism of action of quinine was inhibition of plasmodial DNA synthesis. Hahn et al. (10) have theorised that quinine acts as a DNA template poison and hence inhibits replication and transcription. They have also shown that another powerful antimalarial drug, chloroquine, forms molecular complexes with DNA and inhibits DNA-dependent nucleic acid polymerase activity in vivo and concluded that the mode of action of chloroquine as a blood schizontocide is a preferential inhibition of plasmodial DNA biosynthesis. On the basis of the parallelism between structural factors that govern intercalation to DNA and those that govern antimalarial potency, Hahn et al. (11) further concluded that intercalation binding of chloroquine to plasmodial DNA could be the molecular mechanism underlying the inhibition of schizontal DNA synthesis and, hence, the chemotherapeutic action of chloroquine.

The candidature of DNA as the primary target of the drugs became questionable on the basis of several observations. The quinoline class of drugs bind non-specifically to double-stranded and heat-denatured DNA from the host, the parasite and from various other sources (10, 12, 13). Stollar and Levine (14) have measured the association constant for chloroquine with calf thymus DNA by equilibrium dialysis. The value for the association constant,  $4.5 \times 10^3 \text{ M}^{-1}$  is much less than the value of  $2 \times 10^7 \text{ M}^{-1}$ , reported by Fitch *et al.* (15, 16) for drug binding to the parasites. The more powerful argument against DNA as the primary target of the drug is that mefloquine, an excellent schizontocide does not intercalate to DNA (17), but competitively inhibits chloroquine accumulation (18).

Mackerras and Ercole (19) had discovered as early as 1949 that the antimalarial drugs mepacrine and quinine affect the parasites only at those stages in their life cycle when the microorganisms are actively metabolising hemoglobin. This observation implicates hemoglobin degradation products in the action of the antimalarial drugs. It was observed that the first morphological change that occurs upon exposing the parasite to antimalarial drugs is in the organelle where hemoglobin undergoes digestion, namely the digestive vacuole (20, 21). Chloroquine has been found to bind to hematin. These observations led Macomber *et al.* (20) to propose that chloroquine may have more a direct injurious action on the parasite than just inhibiting DNA synthesis. They have also proposed that chloroquine accumulation, pigment clumping and the pharmacological effects all could arise from ferriprotoporphyrin binding to the drug. Fitch (22) exposed the red blood cells to  $10^{-8} \text{ M}$   $^{14}\text{C}$  labelled chloroquine and monitored the radioactivity in the cells and in the medium. It was observed that the  $^{14}\text{C}$  label level was approximately 14: 1 (cells : medium) for uninfected cells, around 600 : 1 in cells



infected with chloroquine-sensitive parasites, and 100:1 in the cells infected with chloroquine-resistant parasites. No degradation of chloroquine was found. This study suggests that the infected red blood cells might possess receptors for chloroquine, and that chloroquine resistance might be due to a decrease in the number, the affinity, or the accessibility of these receptors.

Fitch et al. were also able to provide further evidence for the idea that ferriprotoporphyrin IX (hemin) is the receptor for the quinoline class of antimalarial drugs (23). The affinity and specificity of hemin for chloroquine was found to be sufficient to account for chloroquine binding to erythrocytes infected with malaria parasites. It was possible to generate these receptor sites on uninfected erythrocytes by non-specific protease treatment, which was shown to have degraded hemoglobin and produced protoporphyrin. Further, very little or no hemoglobin degradation appears to occur in chloroquine-resistant strains. When the resistant strain reverts back to chloroquine susceptibility, the hemoglobin degradation and protoporphyrin reappear. These observations reinforce the suggestion that protoporphyrin-IX indeed is the receptor for the quinoline class of antimalarial drugs.

Meshnick et al. (24) had shown that hemin lyses Trypanosoma brucei, and that its lytic ability is not lost upon complexing with chloroquine (23). On exposure to chloroquine, red blood cells infected with parasites accumulate a chloroquine-hemin complex (25). Malaria parasites degrade hemoglobin and produce large amount of heme which is stored in the malaria pigment (26, 27). All these above observations led Fitch et al. (28) to propose that the antimalarial action of chloroquine is due to the accumulation of a toxic chloroquine-heme complex. Hemin, the byproduct of hemoglobin metabolism by the

parasite, can cause cell lysis. However, hemin in the self-aggregated form does not appear to cause any lysis (29), neither does it do so when sequestered by proteins. Hemin in micromolar concentrations, at neutral pH, undergoes aggregation to a significant extent (30), and also complexes easily with peptides and proteins (31, 32). All these observations highlight the point that a critical manipulation of such a molecular ensemble, composing the degradation products of hemoglobin and proteins, is essential for the survival of parasites, and any failure of this should result in the destruction of the parasite. Thus it appears that a technique that allows a direct monitoring the properties of this molecular ensemble with a minimum disturbance should prove useful in understanding the molecular events underlying the phenomenon. The necessity of in vivo or in situ spectroscopy, such as photoacoustic spectroscopy in the present instance, originates from several aspects of the system under study, such as: (i) isolated hemin in solution can exist in several states of aggregation depending on the concentration and on the pH of the medium used for isolation, while the interest is on its status in vivo (ii) the malaria pigment appears to be a heterogeneous population of hemin-protein complexes, part of which is soluble in alkaline medium while the other is soluble in acidic medium (27), (iii) a direct comparison between the drug-sensitive and drug-resistant parasites for differences, if any, and to monitor the drug-induced changes in the parasite themselves should be more meaningful than the study of their isolated constituents. Thus, we set ourselves to: (i) observe the changes that occur to endogenous hemin upon drug administration within the parasite, (ii) monitor the state in which hemin exists in the parasite, and (iii) investigate the differences between chloroquine-sensitive and resistant parasites. In addition, we found it worthwhile to study the spectral and equilibrium aspects of the drug binding to hemin in the solution phase.

### 4.3 Materials and Methods

The parasites Plasmodium berghei and P. chabaudi were isolated from the blood of heavily infected male Swiss-Webster mice, according to the procedure described by Fitch et al. (28). Blood from several mice was pooled and mixed with an equal volume of isotonic phosphate buffer medium, pH 7.4 (275 mosmol/l) containing 1 mg of heparin per ml. White blood cells were removed by passing this mixture through a column of Whatman CF11 cellulose powder. The erythrocytes were then recovered by centrifugation, suspended in 10 volumes of standard medium, and centrifuged again. Erythrocytes were lysed by suspending the pellet in 20 volumes of 0.015% (w/v) saponin in the medium and incubated at 37°C for 30 minutes. Parasites were isolated from the lysate by centrifugation and washed three times in 40 volumes of cold medium and centrifuged at 490 at 500 g. P. berghei were prepared by nitrogen decompression followed by saponin lysis of red blood cells, while only saponin lysis was used for P. chabaudi. Drug treatment was carried out by suspending the erythrocytes in the medium containing the desired drug for 30 minutes before proceeding for preparing parasites by lysing the cells (33, 34, 35). Hemozoin pigment was isolated from the parasite according to the procedure described by Yamada and Sherman (27). Samples of hemin, quinine, quinidine and chloroquine dipohosphate of high purity were obtained from commercial sources. PA spectra were run using the EG&G PAR Model 6001 and the EDT model OAS 400 spectrometers, with the modifications mentioned in the Chapter I. All the spectra were recorded at 40 Hz modulation frequency and 2 mm slitwidth, at the ambient temperature of 295 K. Parasites were used as lyophilized powders, dispersed in neutral alumina or dextrose. The spectral parameters of interest are the wavelength maxima of the band in the red region around 630 nm ( $\lambda_r$ ), the Soret band ( $\lambda_s$ ) around 400 nm, and their relative intensity (an internally normalized parameter that avoids any sample to sample variation in the observed PA signal strengths).

Circular dichroism spectra were recorded with a JASCO 3-20 spectropolarimeter at ambient temperature (295 K). Fluorescence spectra were recorded on a Hitachi model 650-1 OS spectrofluorimeter using a thermoregulated cell assembly. All CD and fluorescence measurements were made on freshly prepared hemin solutions within 30 minutes of mixing them, in order to avoid problems of time-dependent aggregation.

#### 4.4 Results and Discussion

In the PA study, the spectral parameters of interest are the wavelength of absorption maxima of the samples, and relative intensity of the two major absorption bands, namely the Soret and the red bands of the porphyrin, the chromophore of our interest present in the parasite. The PA signal depends on several factors besides the optical absorption coefficient of the sample. The particle size and volume of the gas in the cell, which in turn depends on the amount of the sample in the cell, also significantly alter the magnitude of the signal. Thus a direct comparison of PA signal intensity of different samples is prone to error. We take the Soret band intensity relative to red band intensity in the same spectrum, as an internally normalized parameter which is independent of the sample to sample variation. Thus we choose the ratio  $I_S/I_R$  where  $I_S$  and  $I_R$  are intensities of Soret and red bands respectively as a characteristic and reproducible parameter to compare various samples in this study. The photoacoustic signal is proportional to the optical absorption of the sample provided the optical absorption length  $\mu_a$  is greater than the sample thickness,  $l$ , or its thermal diffusion length  $\mu_s$ . But when  $\mu_a$  becomes less than that of either  $l$  or  $\mu_s$  the PA signal would become independent of  $\mu_a$ , and the signal varies nonlinearly with  $\mu_a$  in the near-saturation region. This can cause serious errors when comparing the signals with different strengths even in the

same spectrum. Thus it is necessary to ensure that the sample under study is not photoacoustically opaque. Figure 4.1 shows the PA signal strength ( $I_{PA}$ ) at 400 nm as a function of the amount of hemin in alumina. It can be seen that the signal varies linearly in the range of concentration studied, i.e. 0.8 to 6.6 mg of hemin per gram of alumina. We have also studied the modulation frequency dependence of the PA signal for the most concentrated sample and found it to vary as  $\omega^{-1}$ ; and a plot of  $\log$  versus  $\log I_{PA}^A(400)$  did not show any slope change at higher frequencies. Thus we have confirmed that PA saturation does not arise, in the concentration region investigated. All the samples of the parasites and hemozoin pigment were at concentrations of less than 3 mg/gram of alumina. The possibility of any spectral changes due to solid state charge-transfer is ruled out in the present cases as identical PA spectra in terms of  $\lambda_{max}$  and  $I_S/I_r$  are obtained regardless of whether alumina or glucose was used as the diluent. We also observed that the PA spectrum of the isolated and lyophilised parasites obtained from drug-free mouse erythrocytes is markedly different from that of the parasites isolated from the same cells exposed to antimalarial drugs (36). This observation highlights the point that antimalarial drugs do interact with the molecular ensemble which contains hemin within the parasite. This prompted us to carry out further investigation in order to understand the nature and consequence of such an interaction.

Figure 4.2 shows the PA spectra of hemin and the hemozoin pigment isolated from the parasites and of lyophilized parasites P. chabaudi, all in the solid state and dispersed in alumina. The presence of the red band in the 630-645 nm region in all these samples identifies the iron atom to be in the Fe(III) state (37). The spectrum of hemin reveals the sample to be essentially in the aggregated form, since the red band appears at 645 nm and a broad, apparently

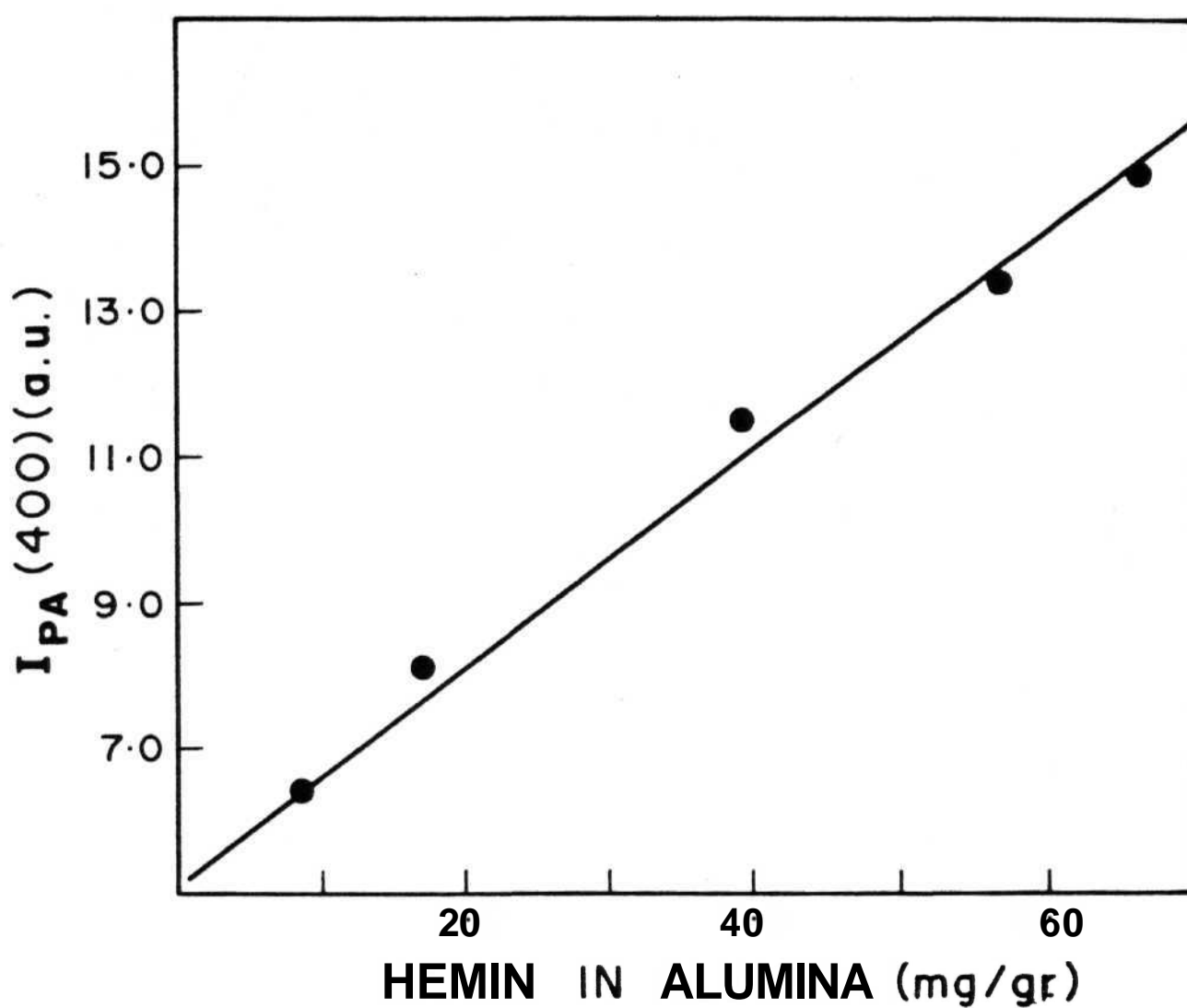


Figure 4.1 Plot of PA signal strength ( $I_{PA}$ ) at 400 nm as a function of the amount of hemin in alumina.

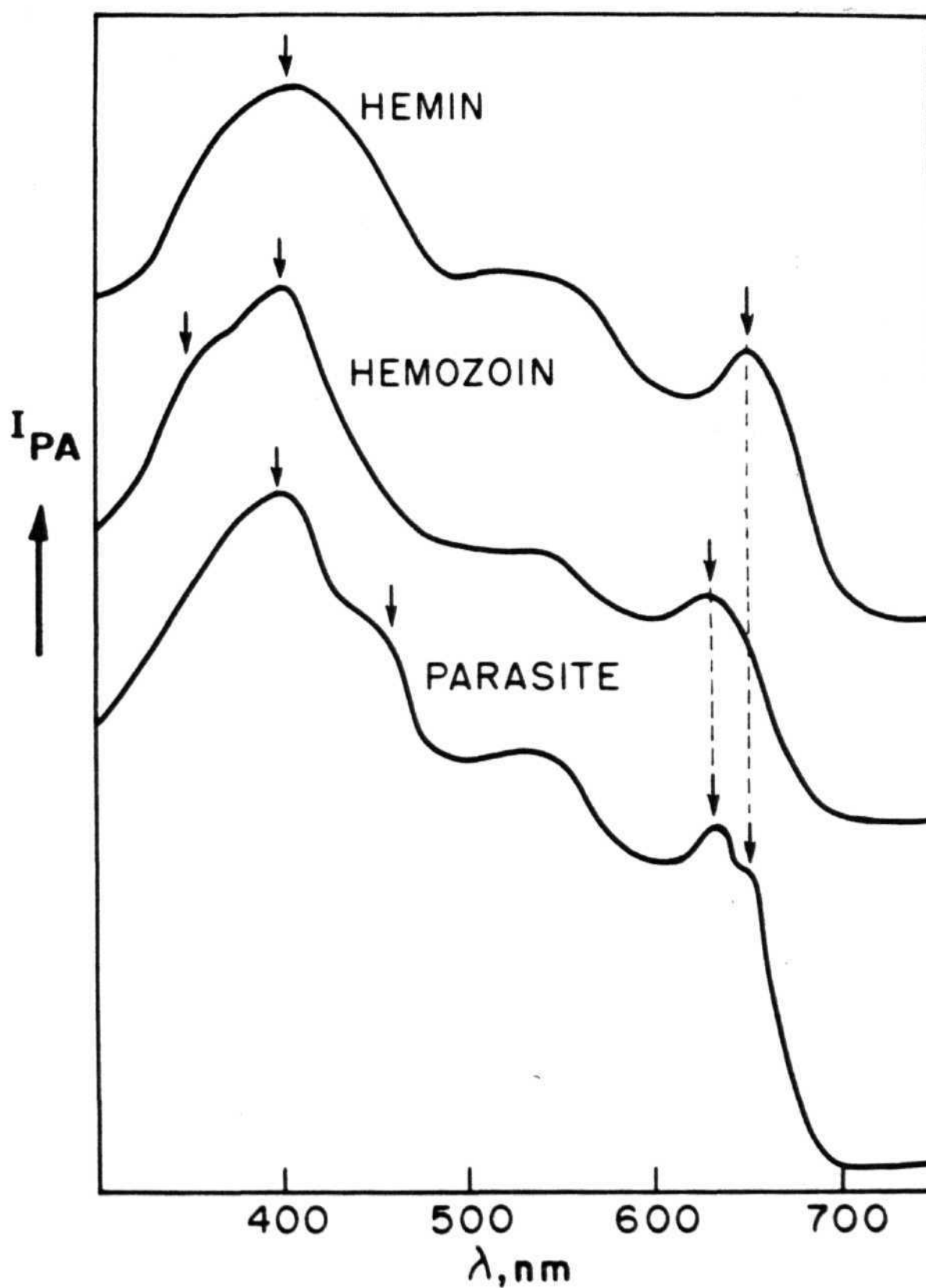


Figure 4.2 PA spectra of solid hemin, isolated hemozoin and parasites *P. chabaudi*, all in the solid state and dispersed in alumina.

composite solet band is seen around 400 nm; the spectrum resembles the optical absorption spectrum of hemin aggregates in solution (30, 31, 37). These observations allow us to conclude that hemin sample is essentially in the self-aggregated form. In contrast the red band is shifted to 630 nm, and the solet band is accompanied by characteristic shoulder near 370 nm, and the  $I_s/I_r$  ratio increases to over 2.5 in the case of the pigment, hemozoin, and is similar to that of the complex between serum albumin and hemin (see Table 4.1 for spectral details). The hemozoin PA spectrum is also similar to solution state spectra of the complexes of monomeric hemin with human serum albumin (31), with ferrileghemoglobin (38) in that the red band is seen at around 630 nm, and the solet band around 400 nm is accompanied by a shoulder near 370 nm. The intensity ratio,  $I_s/I_r$ , of both hemozoin and the hemin: albumin complex are distinctly higher than that of hemin aggregates (see Table 4.1). Kin consonance with the higher solet band absorption exhibited by monomeric hemin when compared to its aggregates (30, 37). These studies suggest that hemin in hemozoin is in a similar environment to those in its complexes with albumin or ligandin and allow us to conclude that the pigment is a noncovalent protein - sequestered complex of monomeric hemin, and confirm the earlier suggestion by Yamada and Sherman (27).

The PA spectrum of the parasite itself, as shown in Figure 4.2 in the lyophilized powder form, shows a band at 630 nm and a shoulder at 645 nm suggesting the presence of both the self-aggregated form and the protein complexed monomeric form of hemin. The shoulder at around 430 nm that accompanies the main solet band here can be attributed to the residual hemoglobin, or its partially degraded forms that still contain coordinated heme, present in the parasite at the time of isolation. The intensity ratio  $I_s/I_r$  of



Table 4.1: Summary of PAS data of Plasmodium and its components

Sample	$\lambda_{\gamma}, \text{ nm}$ (error $\pm 3 \text{ nm}$ )	$\lambda_{\delta}, \text{ nm}$ (error $\pm 3 \text{ nm}$ )	$I/I_s$	Remarks
a) Hemin, solid	645	400, broad	2.0	essentially aggregated, resembles the optical absorption spectrum of the aggregates in solution
b) Hemozoin, isolated from the parasite	630	400, shoulder at 370	2.5	monomeric hemin indicated; see (c) below
c) Hemin : BSA complex, lyophilized	630	-do-	2.5	monomeric hemin; resembles optical spectrum of the complex in solution
d) <u>P. chabaudi</u> , isolated and lyophilised; chloroquine-sensitive strain	645, 630	400, minor band $\sim 430$	2.1	both monomeric and aggregated heme indicated; 430 nm band suggestive of peptide-coordinated heme
e) <u>P. chabaudi</u> , chloroquine-resistant strain	645, 630	430	1.3	only peptide-coordinated heme indicated.
f) <u>P. berghei</u> , chloroquine-sensitive strain	645, 635	400	2.3	$I/I_s$ somewhat higher than in case (d); different parasite strain (also uncloned).
g) <u>P. berghei</u> , as above, but treated with chloroquine	640	370	3.0	blueshifted Soret band; hemin-drug interaction indicated.
h) <u>P. berghei</u> , as in (f), but treated with mefloquine	640	375	2.5	blueshifted Soret band; hemin-drug interaction indicated.

the parasite, is lower than that of the hemozoin and approaches that of hemin in solid state, dispersed in alumina (see Table 4.1). One would expect that the presence of pigment with its higher ( $I_s/I_r$ ) value, should increase the  $I_s/I_r$  for the parasite to some extent, depending on the amount of the pigment. The nearly equal value for hemin and parasite (see Table 4.1) can be attributed to two reasons. One is the absence of, or negligible amounts of, the pigment in the parasite, which does not appear to be the case; the parasite spectrum shows absorption at 630 nm indicative of the presence of the pigment. The other reason could be the formation of higher aggregates of hemin in the parasite than that of hemin dispersed in alumina. It is known that the hemin absorption at 400 nm decreases with increasing aggregation (30). Based on these, we suggest that endogenous hemin in the parasite occurs in part, as self-aggregates and in part as hemozoin, besides that present as residual hemoglobin. This agrees with, and lends credence to, the earlier view (27, 39 - 41) that the particulate form of the pigment in vivo might contain hemozoin, hematin aggregates, hemichrome, and to some extent reconciles this view with that of Home-wood et al. (42, 45), who stated that the pigment contains a heterogeneous array of molecules, some of which have surprisingly high molecular weights.

Figure 4.3 compares the PA spectrum of P. berghei isolated from mouse red blood cells that are incubated with or without antimalarial drugs such as chloroquine and mefloquine. The spectrum of this strain, in the absence of any drug treatment is essentially identical to that of P. chabaudi (Figure 4.1), excepting a somewhat higher  $I_s/I_r$  ratio, perhaps because of the species variation and the fact that we are dealing with an uncloned strain of P. berghei. Drug treatment is seen to have caused significant changes in the parasite spectrum; the solet band is blueshifted from 400 nm to 375 nm and the  $I_s/I_r$  ratio increases

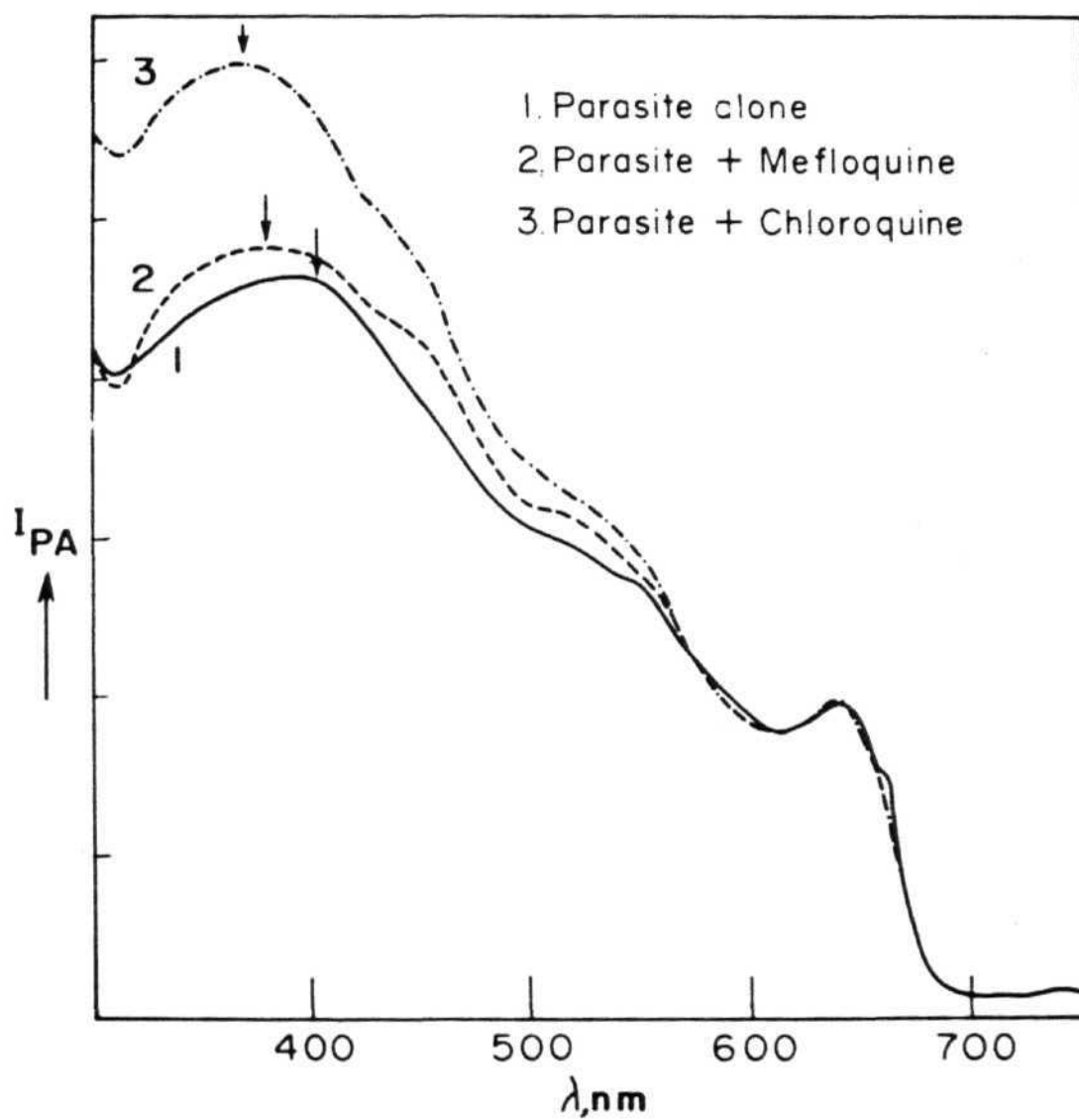


Figure 4.3 PA spectra of *P. berghei* isolated from infected mouse erythrocytes in the presence and absence of drugs.

significantly (see Table 4.1). It is clear from the spectra that the drug has affected the status of the endogenous hemin. The increase in the  $I_s/I_r$  ratio argues for a reduction in the population of self-aggregated hemin, while the solet band shift indicates hemin-drug interactions. Thus we believe that these results provide the first direct evidence for the presence of such a complex in the parasite. The drug-induced PA spectral changes are better reflected when a higher modulation frequency of 912 Hz is used, implying that a significant fraction of the absorbing species might lie closer to the surface. The stage of the parasites used here was not synchronized and it is therefore not certain whether this distribution is inherent due to the ring stage of the parasite or caused by drug addition.

That hemin and chloroquine can form a complex in the solution state has been suggested earlier (44, 46, 48). We have also carried out such investigations in solution state and have observed drug-induced optical activity in hemin, and a quenching of the fluorescence of the drug by added hemin. Figure 4.4 shows the circular dichroism spectra of hemin in the presence of quinine, and its diastereoisomer quinidine, in 0.02 M phosphate buffer of pH 7.4. It can be seen that a large negative cotton effect is induced in the solet band of the inherently achiral hemin molecule upon the addition of levorotatory quinine. The induced optical activity might arise either because of a perturbation of the hemin transitions by those of the drug, or by an exciton coupling between the bands of the hemin placed in the chiral environment provided by the chiral drug; the latter appears likely in the light of large ellipticities seen. Blauer has published a paper (47) while this thesis was being written; he has also observed a similar drug-induced CD and has attributed to the interaction of the drug with aggregated hemin. However, our results presented in Figure 4.4 have

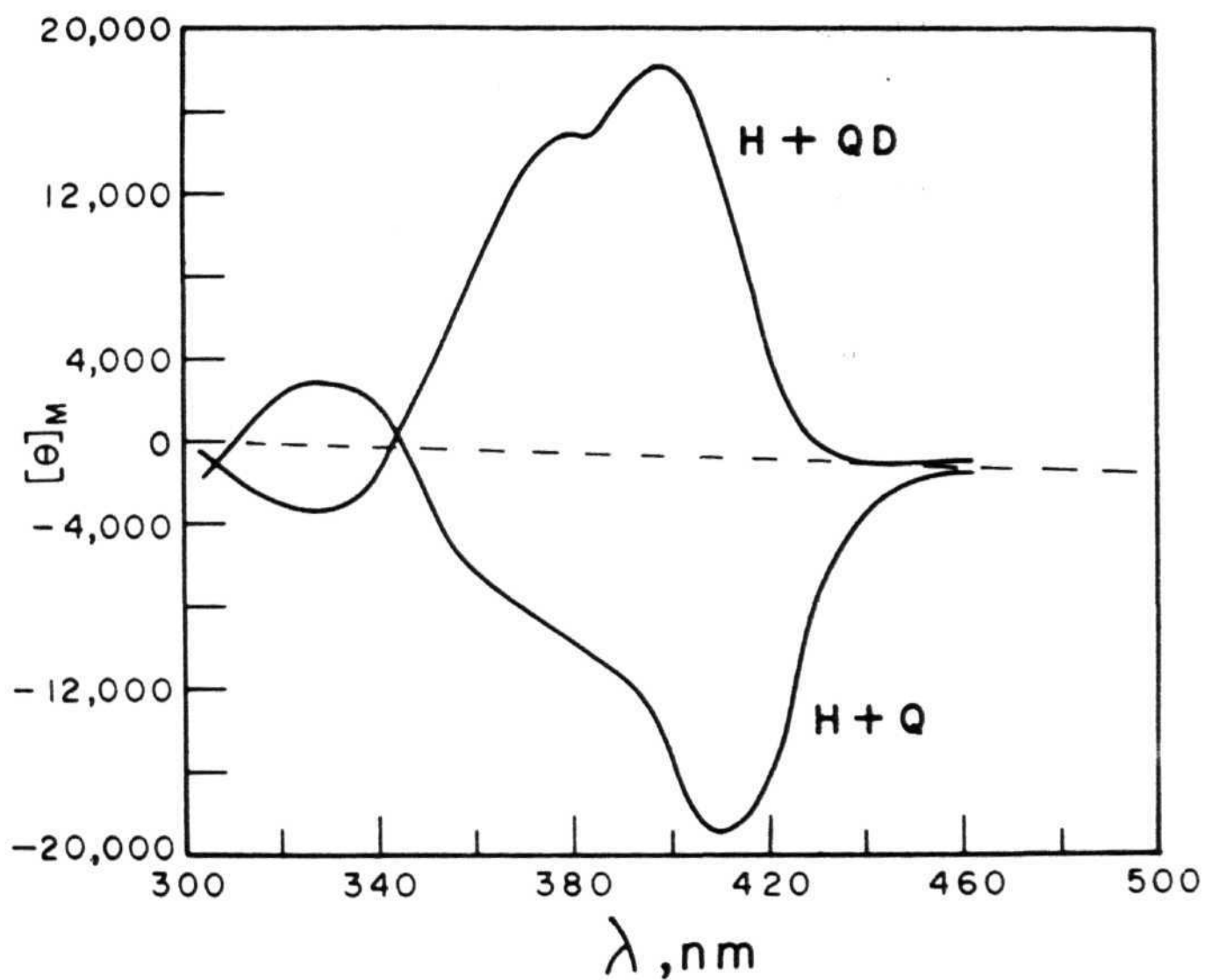


Figure 4.4 CD spectra of hemin (H),  $5 \times 10^{-5} \text{ M}$  in presence of  $4 \times 10^{-5} \text{ M}$  quinine (Q), or  $4 \times 10^{-5} \text{ M}$  quinidine (QD); pH 7.4, phosphate buffer  $[\theta]_{\text{M}}$  is molar ellipticity in  $\text{deg. cm}^2/\text{decimole}$  based on total hemin concentration.

been obtained with solutions of low concentrations where the aggregation of hemin is very unlikely. The spectra were recorded shortly after mixing the two components, in order to avoid any artifacts due to light scattering effects arising from time dependent aggregation. The observation of induced CD of hemin by the drug requires intimate contact between the interacting molecules. Gratifyingly, a similar and opposite effect is elicited by the diastereoisomer quinidine. The effect of chloroquine could not be studied by circular dichroism, since this drug is available only as a racemic mixture.

We have also studied the effect of hemin on the fluorescence properties of chloroquine. Chloroquine, in 0.02 M phosphate buffer at pH 7.4, fluoresces at 386 nm upon excitation with radiation of wavelength 290 nm. Figure 4.5 shows the fluorescence spectra of chloroquine as a function of added hemin. It can be seen that the addition of hemin quenches the fluorescence of chloroquine significantly. The hemin-dependent quenching of fluorescence was analysed by the Stern-Volmer equation. Figure 4.6 shows the plot of  $F_0/F$  against the concentration of hemin, where  $F_0$  and  $F$  are the fluorescence intensity without and with added hemin respectively, in arbitrary units. It can be seen that the plot shows a positive deviation from linearity. The quenching of fluorescence can arise due to collisions between the fluorophore and the quencher molecules, and/or due to the formation of a nonfluorescent 1 : 1 complex predating the excitation. If the quenching effect of either of these two kinds is much greater than the other, the quenching would follow the Stern-Volmer linear dependence of  $F_0/F$  on  $[Q]$ . If both of the modes, dynamic and static quenching, operate, then there will be a departure from linearity. We have found that the fluorescence intensity of the binary solution increases with temperature as shown in Figure 4.7; and have also observed that the steady

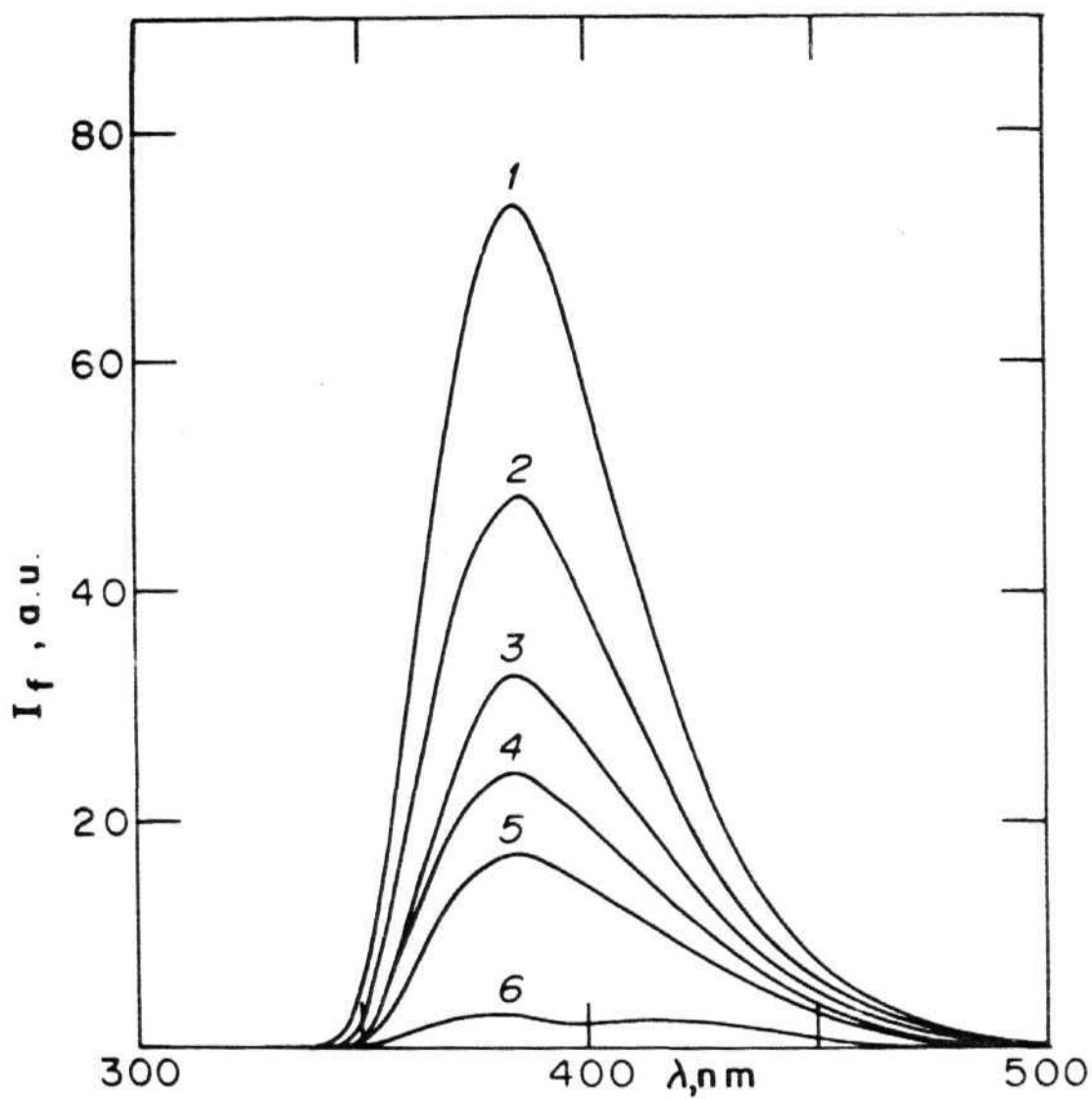


Figure 4.5 Fluorescence spectra of chloroquine in presence of hemin. Excitation wavelength 290 nm. Concentrations of hemin; 1 = 0.0M; 2 =  $7.45 \times 10^{-6}$  M; 3 =  $1.49 \times 10^{-5}$  M; 4 =  $2.23 \times 10^{-5}$  M; 5 =  $2.98 \times 10^{-5}$  M; 6 =  $7.45 \times 10^{-5}$  M. Chloroquine concentration was  $2.94 \times 10^{-4}$  M.

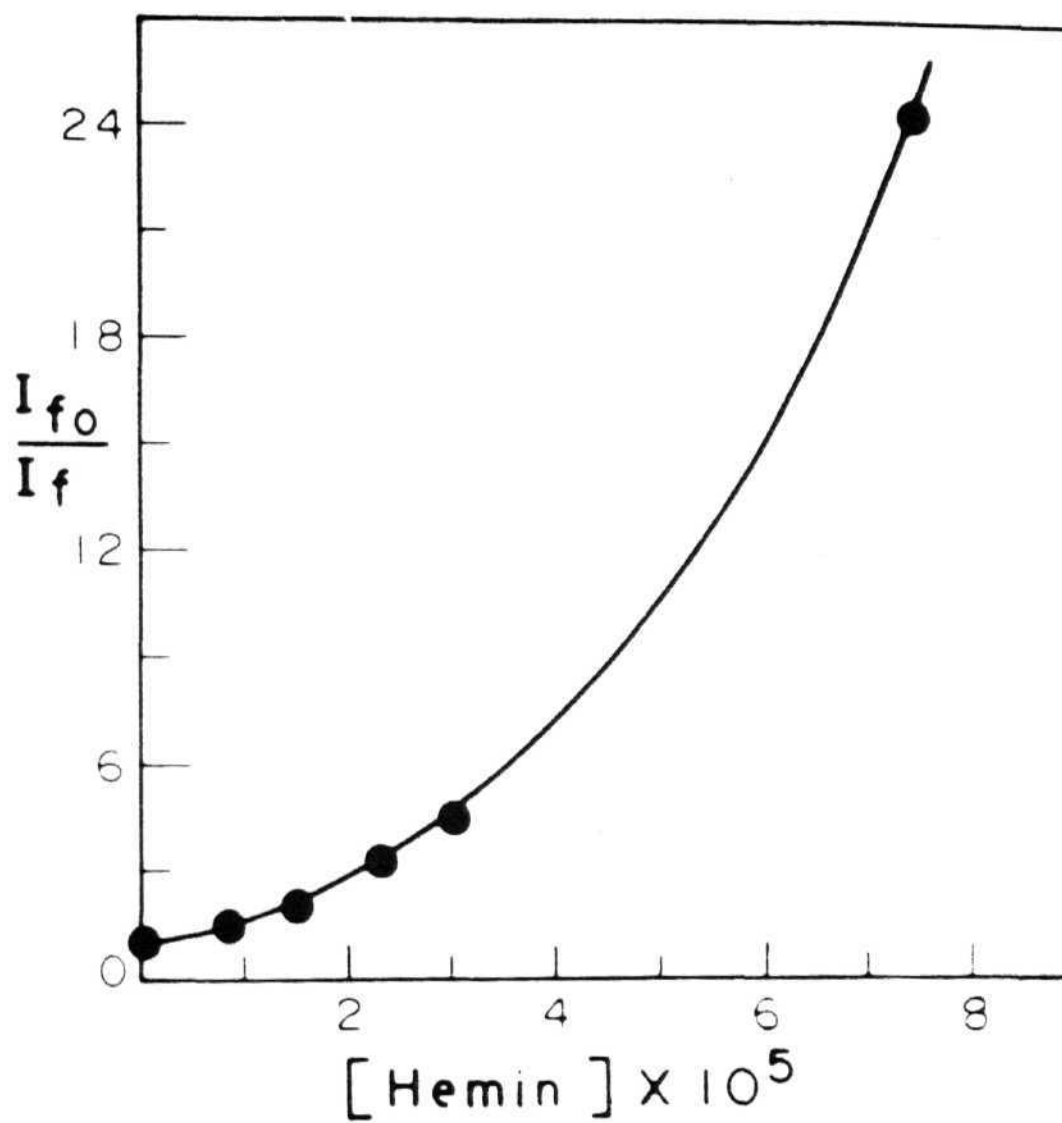


Figure 4.6  $F_0/F$  against the concentration of hemin;  $F_0$  and  $F$  are the fluorescence intensity without and with added hemin.



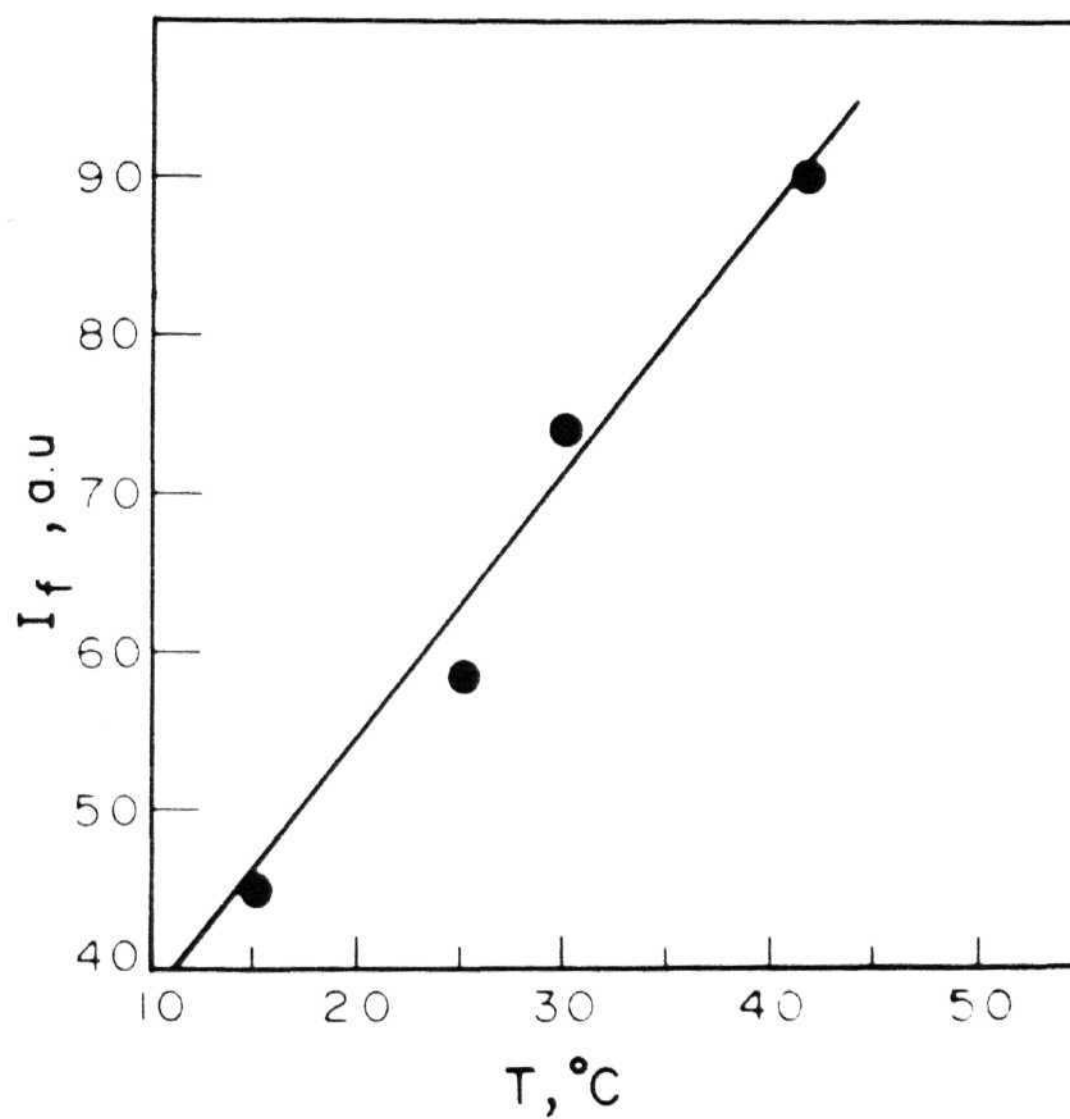


Figure 4.7 Temperature dependence of the fluorescence intensity of Chloroquine in the presence of hemin.

state fluorescence polarisation value remains almost invariant with increasing concentration of hemin. The dynamic quenching by hemin appears unlikely since, if it were to be operative, one would expect a drop in the fluorescence intensity with increasing temperature due to increased collisions. A non-fluorescent 1 : 1 complex also does not appear likely since the Stern-Volmer plot is nonlinear. This led us to analyse the fluorescence data on the basis of the formation of a 2 : 1, hemin : chloroquine complex, characterised by the formation constant  $K_f = [\text{complex}]/[\text{drug}][\text{hemin}]^2$ . The equilibrium concentrations of the complex, drug and hemin were calculated from their initial concentrations and the fluorescence intensities, for 10 different concentrations of hemin, and we obtained a value of  $K_f = 1.4 \times 10^7 \text{ M}^{-2}$  at 298 K. This lends credence to earlier suggestions (23, 48) and the value of  $K_f$  compares with the  $K_d$  values reported for binding of chloroquine to infected erythrocytes obtained by equilibrium dialysis measurements (23).

Figure 4.8 shows the PA spectrum of the clones of chloroquine-resistant parasites Plasmodium chabaudi. It can be seen that the spectrum is markedly different from that of the sensitive strain (Figure 4.1) showing the PAS can readily distinguish between drug-sensitive and -resistant parasites. Unlike the drug-sensitive strain, the resistant strain shows the solet maximum at about 430 nm and also a reduced  $I_e/I_s$  ratio of 1 . 3 (see Table 4.1). The latter is comparable to the value of 1.4 and 1.5 seen in the PAS of blood smears and erythrocytes (49) while the position of the solet band is similar to that seen in the optical spectra of heme coordinated to a peptide chain, e.g., hemoglobin and its derivatives (50). In the light of this, it appears that endogenous hemin in the resistant parasite might be largely in the form of coordinated to protein. Earlier workers have shown that when P. berghei becomes resistant to chloroquine

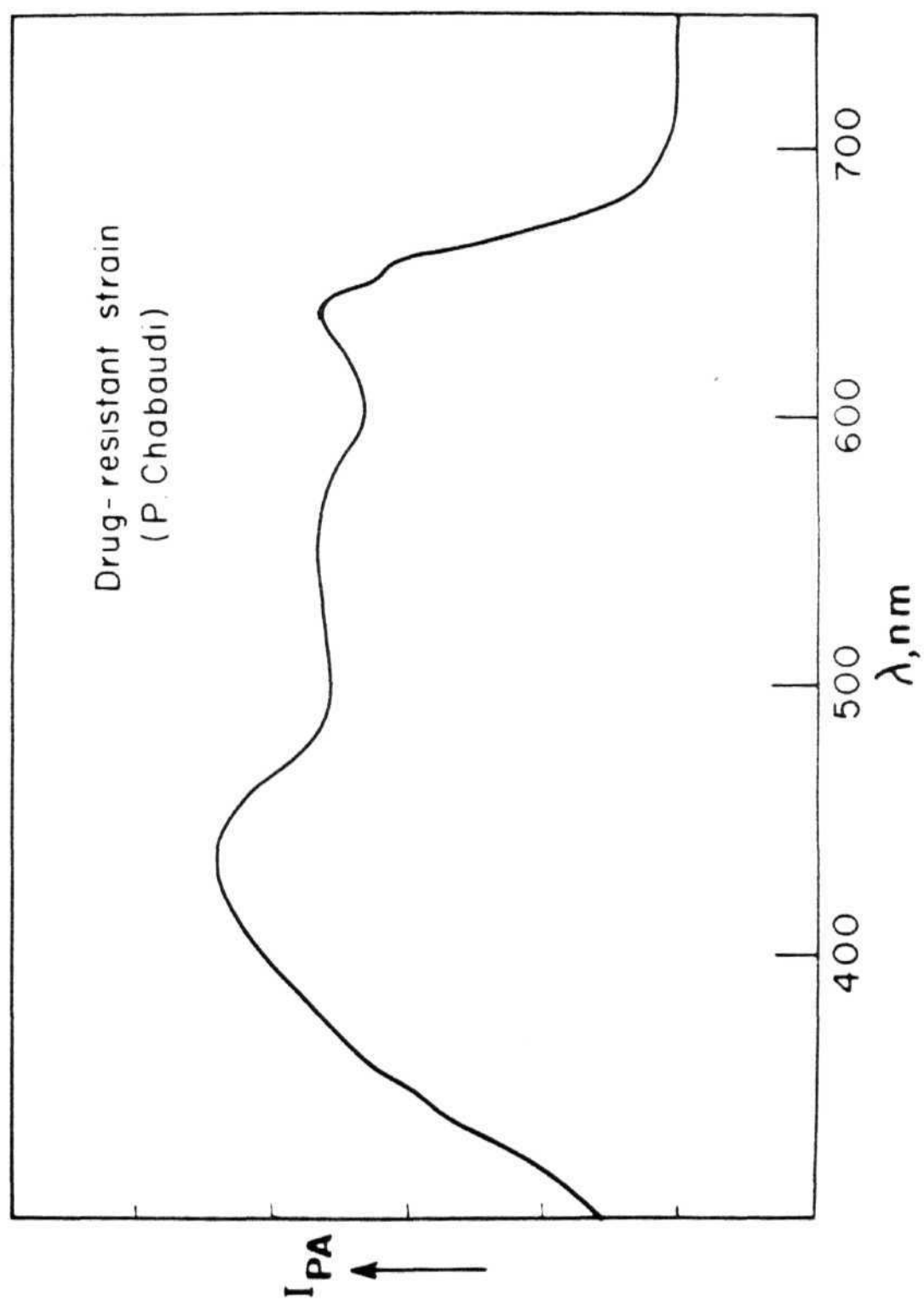
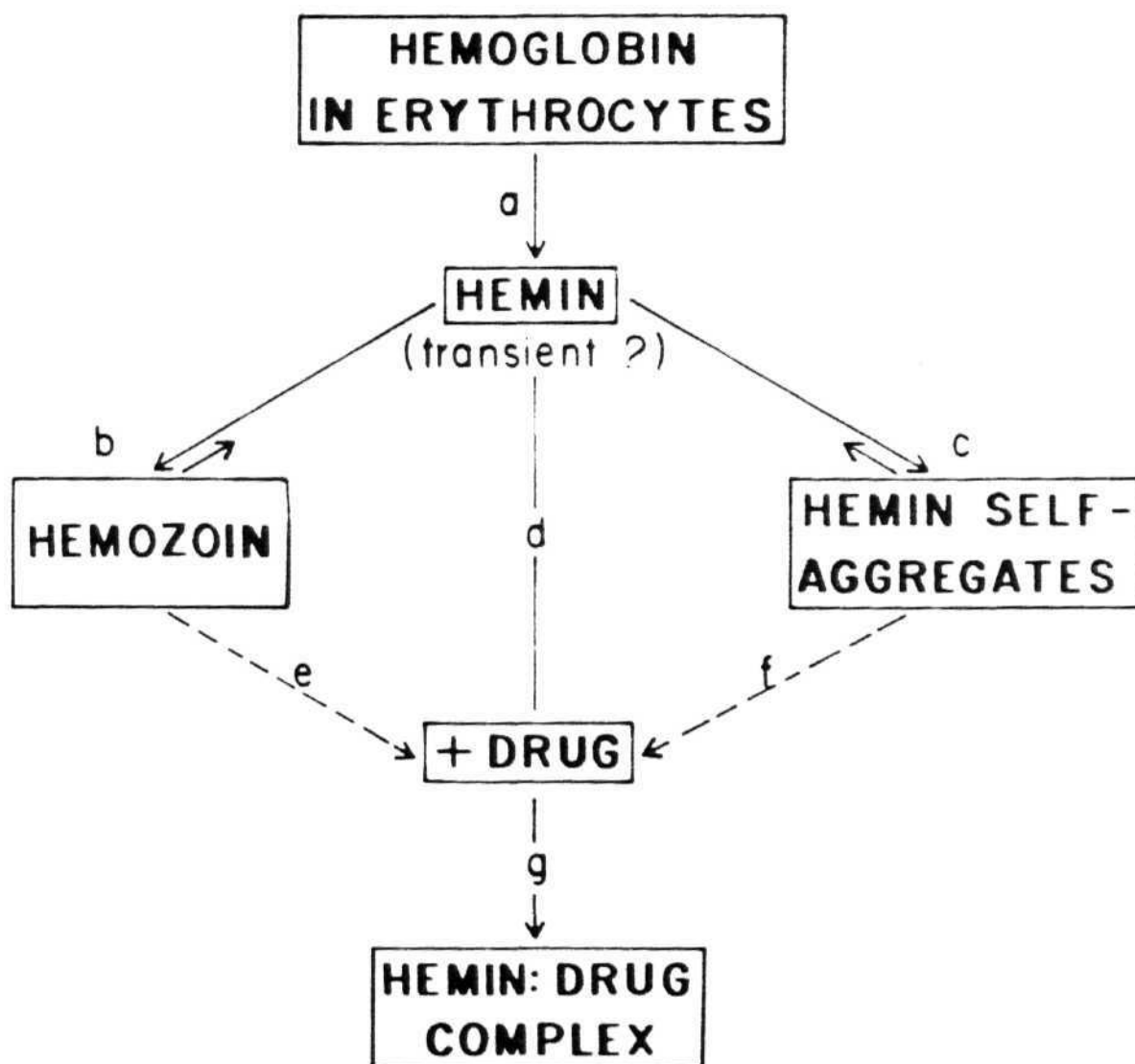


Figure 4.8 PA spectrum of clones of chloroquine-resistant parasites *P. chabaudi*.

the production of the pigment drops (51). Fitch and ChevJi (25) have argued that the molecular changes responsible for chloroquine resistance could involve either the process of hemoglobin degradation or the process of heme sequestration. In the light of our results, it appears likely that the drug resistance, at least in P.chabaudi, involves the former process in such a fashion that the degradation of hemoglobin occurs to a stage where the heme group is still held with the same integrity to the peptide chain as in the whole molecule.

Hemozoin preparations show two kinds of particles, one crystalline and the other particulate. The crystalline portion is soluble in 0.1 M NaOH and appears to be heme aggregate. Our PA results provide evidence for the presence of such heme aggregates in the parasite as well. We have also found that the hemolysis efficiency of 3-5 hours aged heme solution, i.e. essentially in the aggregated form, at 37°C to be extremely low. Thus neither the pigment nor the self-aggregated heme are membrane-lytic; and free heme which does lyse membranes, is not detected in the parasite. It is reasonable to conceive of the endogenous population of heme to be in equilibrium with its self-aggregates and hemozoin. The added drug may derive its partner from the species that are in such an equilibrium and form the lytic complex. The drug binding to the pigment or to residual hemoglobin itself does not seem to occur, though it does bind to protease-treated hemoglobin. In the light of these reports, and on the basis of our PAS results, we propose Scheme 1 as a model that is consistent with our present understanding of the mode of action of the quinoline class of drugs on the malaria parasite.

**SCHEME 1**

In brief, the model can be described as follows: (a) parasites metabolise host hemoglobin and produce the byproduct hemozoin, which is toxic to the parasite (b) this hemozoin binds to proteins and forms hemozoin, a non-toxic substance (c) hemozoin also undergoes extensive self-aggregation and becomes non-toxic. Thus the parasite survives, in spite of the toxin (free hemozoin) produced by itself. But when antimalarial drugs are administered, (d) the transitory hemozoin may strongly bind to the drug and a drug-hemozoin complex accumulates at the cost of hemozoin self-aggregates and hemozoin. This complex can cause cell lysis and destroy the parasite. However, it is still not clear whether (e) hemozoin, and/or (f) self-aggregates can also interact with the drug and form the lytic complex. Drug binding to the pigment appears unlikely but since the hemozoin-chloroquine complex can be isolated as a heteromolecular aggregated species, the possibility of the drug interacting with hemozoin self-aggregates (f) should also be considered until proved otherwise.

#### **4.5 Conclusion**

The study reported in this chapter provides the first direct spectral evidence for the presence of hemozoin self-aggregates in the parasites. The malaria pigment is shown to be a hemozoin-protein complex in which protoporphyrin is in an environment similar to those in its complexes with albumin and ligandin. Spectra of drug-treated parasites suggest that the drug interacts with endogenous hemozoin. On the basis of these observations and other earlier suggestions, we have proposed a scheme that is consistent with the current state of understanding of the mode of action of the quinoline class of antimalarial drugs. The spectra of chloroquine-resistant parasites, different from those of the sensitive strain, appear consistent with the interpretation that hemoglobin is degraded only partially in chloroquine-resistant parasites.

## REFERENCES

1. L.S. Bruce-Chwatt, 'Essential Malariology', William Heinemann Medical Books Ltd., London, 1980.
2. A. Laveran, Bull. Acad. Med. Paris, 9, 1235 (1880).
3. S.P. Ramakrishna, S. Prakash and D.S. Choudhury, Nature, 179, 974 (1954).
4. D.V. Moore and S.E. Lanier, Amer. J. Trop. Med. Hyg., 10, 5 (1961).
5. F. Hawking and K. Gammage, Trans. Roy. Soc. Trop. Hyg., 56, 263 (1962).
6. D.C. Warhurst and R.K. Kendrick, Nature, 213, 1048 (1967).
7. 'Antimalarial Agents' (Medicinal Chemistry series of monographs volume 12) P.E. Thompson and L.M. Werbel (Eds.), Acad. Press, New York, 1972.
8. D.H. Clarke, J. Exp. Med., 96, 451 (1952).
9. H. Polet and C.F. Barr, J. Pharmacol. Exp. Ther., 164, 380 (1968).
10. F.E. Hahn, R.L. O'Brien, S. Ciak, S.L. Allison, J.G. Olenick, Military Med., 131, 1071 (1966).
11. F.E. Hahn, in 'Mechanism of Action of Antimicrobial and Antitumor Agents', J.W. Corcoran and F.E. Hahn, (Eds.), Springer Verlag, 1975, p. 58.
12. W.E. Gutteridge and P.I. Trigg, 'Comparative Biochemistry of Parasites', H. Van den Bossche (Ed.), Acad. Press, New York, 1972, pp 199-218.
13. K.L. Yielding, L.W. Blodgett, H. Sterngran and D. Gaudin, Prog. Mol. Subcell. Biol., 2, 69 (1972).
14. D. Stollar and L. Levine, Arch. Biochem. Biophys., 101, 335 (1963).

15. CD. Fitch, R. Chevli and Y. Gonzalez, Life Sci., 14, 2441 (1974).
16. CD. Fitch, R.C.K. Ng and R. Chevji, Antimicrob. Agents Chemother., 14, 185 (1978).
17. M.W. Davidson, B.C. Griggs (Jr), D.W. Boykin and W.D. Wilson, Nature, 254, 632 (1975).
18. CD. Fitch, Proc. Helminthol. Soc. Wash., 39, 265 (1972).
19. M.3. Mackerras and Q.N. ErcoJe, Trans. Roy. Soc. Trop. Med. Hyg., 42, 443 (1949).
20. P.B. Macomber, hi. Sprinz and A.J. Tousimis, Nature, 244, 937 (1967).
21. D.C. Warhurst and D.3. Hockiey, Nature, 214, 935 (1967).
22. CD. Fitch, Proc. Nath Acad. Sci. (USA), 64, 1181 (1969).
23. A.C Chou, R. Chevji and C.D. Fitch. Biochemistry, 19, 1543 (1980).
24. S.R. Meshnick, K.P. Chang, A. Cerami, Biochem. Pharmacol., 26, 1923 (1977).
25. CD. Fitch and R. Chevli, Antimicrob. Agents Chemother., 19, 589 (1981).
26. 3.D. Fulton and C. Remington, J. Gen. Microbiol., 8, 157 (1953).
27. K.A. Yamada and I.W. Sherman, Exp. Parasitoh, 48, 61 (1979).
28. A.V. Orjih, H.S. Banyal, R. Chevli and CD. Fitch, Science. 214, 667 (1981).
29. B. Panijpan, personal communication, and our unpublished results.
30. Y. Inada and K. Shibata, Biochem. Biophys. Res. Com., 9, 323 (1962).



31. G.H. Beaven, S.H. Chen, A.D'Albis and W.B. Gratzner, Eur. J. Biochem., 41, 539 (1974).
32. E. Tipping, B. Ketterer, L. Christodoulides and G. Enderby, Biochem. J., 157, 461 (1976).
33. P.A. Kramer and S.E. Matusik, Biochem. Pharmacol., 20, 1619 (1971).
34. D.F.H. Wallach and M. Conley, 3. Mol. Med., 2, 119 (1977).
35. All the parasitic and pigment preparations were carried out at the Department of Biochemistry, Mahidol University, Bangkok (Thailand) by Dr B. Panijpan and his group.
36. D. Balasubramanian and Ch. Mohan Rao, Curr. Sci., 51, 111 (1982).
37. W.I. White, in 'The Porphyrins', D. Dolphin (Ed.), Acad. Press, New York, 1978, vol V, p.303.
38. C.A. Appleby, N.A. Nicola, S.G.R. Hurrell, S.S. Leach, Biochemistry, 14, 4444 (1975).
39. A. Searnpipatkul, P. Govitrapong, Y. Yuthavong and B. Panijpan, Experientia, 36, 1063 (1980).
40. W. Peters and R.W. Howells, in 'Rodent Malaria', R. Killick-Hendricks and W. Peters, (Eds.), Acad. Press, London, 1979, p 169.
41. A. Killejian, 3. Biol. Chem., 249, 4650 (1974).
42. C.A. Homewood, G.A. Moore, D. Warhurst and E.M. Atkinson, Anal. Trop. Med. Parasitol., 69, 283 (1975).
43. C.A. Homewood, S.M. Jewsbury and M.L. Chance, Comp. Biochem. Physiol., B 43, 517 (1972).

44. S.N. Cohen, K.O. Phifer and K.L. Yielding, Nature, 202, 805 (1964).
45. G. Blauer and H. Ginzburg, Biochem. Intl., 5, 519 (1982).
46. S. Moreau, B. Perly, 3. Biguet, Biochimie, 64, 1015 (1982).
47. G. Blauer, Biochem. Intl., 6, 777 (1983).
- 48., A. Jearnpipatkul and B. Panijpan, Chem. Biol. Interactions, 33, 83 (1980).
49. A. Rosencwaig, 'Photoacoustics and Photoacoustic spectroscopy', Wiley, New York, 1980.
50. M. A. Waterman, Methods Enzymol., 52, 456 (1978).
51. R. Ladda and H. Sprinz, Proc. Soc. Exp. Biol. Med., 130, 524 (1969).

## CHAPTER V\*

### SOME ONGOING PROJECTS

#### 5.1 ABSTRACT

Some vitamins and their derivatives appear to undergo photomodification in the solid state when exposed to uv radiation; such modifications seem to be absent, or highly attenuated, in the solution phase. PAS is shown to have a remarkable sensitivity in detecting such modifications.

The photoacoustic signal originates only when the molecule decays from the excited state by nonradiative deexcitation leading to the production of heat. Attempts to use this selective sensitivity of PA technique to study photosynthesis in isolated and oriented chloroplasts are briefly described.

---

\* Preliminary observations reported in this chapter are presented at the 'VII International Biophysics Congress', Mexico City, Mexico, August 1981.

## 5.2. Introduction

In this concluding chapter, we briefly describe two of our ongoing projects and comment on some future possibilities. The first one deals with the photodamage of vitamins while the second is an attempt to study some aspects of photosynthesis.

### 5.3 Photodamage of vitamins

There have been earlier unpublished observations that have hinted that certain vitamins might undergo photodamage in the solid state, while such damage seems to be absent or highly attenuated in the solution phase. This suggested the possibility of intermolecular interactions in the solid lattice as a governing factor. In the light of our experience in the use of PAS to study solid state reactions, we attempted to look at the photodamage that might occur to some vitamins in the solid phase - and we have initiated some work especially on thiamine and its derivatives (vitamin B<sub>1</sub>).

In one of our attempts to record the PA spectrum of thiamine, in a fashion analogous to the case of 3BCMU (see chapter III), we found subsequent spectra to be significantly different from the first recorded one, when the scanning was done from 700 nm downwards. We repeated the experiment with fresh samples and confirmed that the observed change is due to the photochemical reaction caused by the brief exposure of the sample to uv radiation while scanning the spectrum down to 200 nm. In another experiment the first spectrum was recorded from 500 nm to 200 nm, thereby allowing some photochemical modification during the scan; subsequent runs were stopped at 300 nm and cycled in the range of 500-800 nm. The absence of any further change in the subsequent spectra confirms

that the observed change in the spectra was indeed due to the photochemical reaction, induced by in situ exposure to uv radiation. Thiamin monophosphate, thiamin diphosphate and thiamin pyrophosphate also showed dramatic changes in their spectra after such exposure to the source lamp uv radiation. Figure 5.1 shows the first, second and third runs of thiamin pyrophosphate, recorded with no change in any of the instrumental parameters during the runs.

In an attempt to characterize the photoproduct, we recorded the nuclear magnetic resonance spectra of the sample in  $D_2O$  before and after the PA spectra were recorded. The NMR spectra showed no indication of any new product and were exactly superimposable. The sample was exposed to radiation of 300-200 nm for the short period of 30 seconds while recording the PA spectrum at a scan speed of 200 nm per minute; hence it is likely that the photoproduct formed could be too little to be detected by NMR spectroscopy. In order to increase the amount of the photoproduct, we exposed the sample to wide band uv radiation using a Model uv SL-25 multiband uv gun for several hours, but could not detect any difference in the NMR spectra; presumably a higher intensity of uv radiation is necessary to collect sufficient quantities of the product monitorable by NMR.

We are presently attempting to isolate the photoproduct using high performance liquid chromatography (HPLC) and to characterize the isolated compound by a variety of spectral methods. We have used the Waters HPLC instrument with a data module and a model 720 system controller. The column used was C-18 and the eluent was 0.2 M phosphate buffer, pH 5.3. Figure 5.2 shows the chromatograms obtained for irradiated and control samples. It can be seen that thiamin pyrophosphate (trace 1) shows two peaks, one major and a minor one; the latter could be due to the presence of thiamin monophosphate. Thiamin

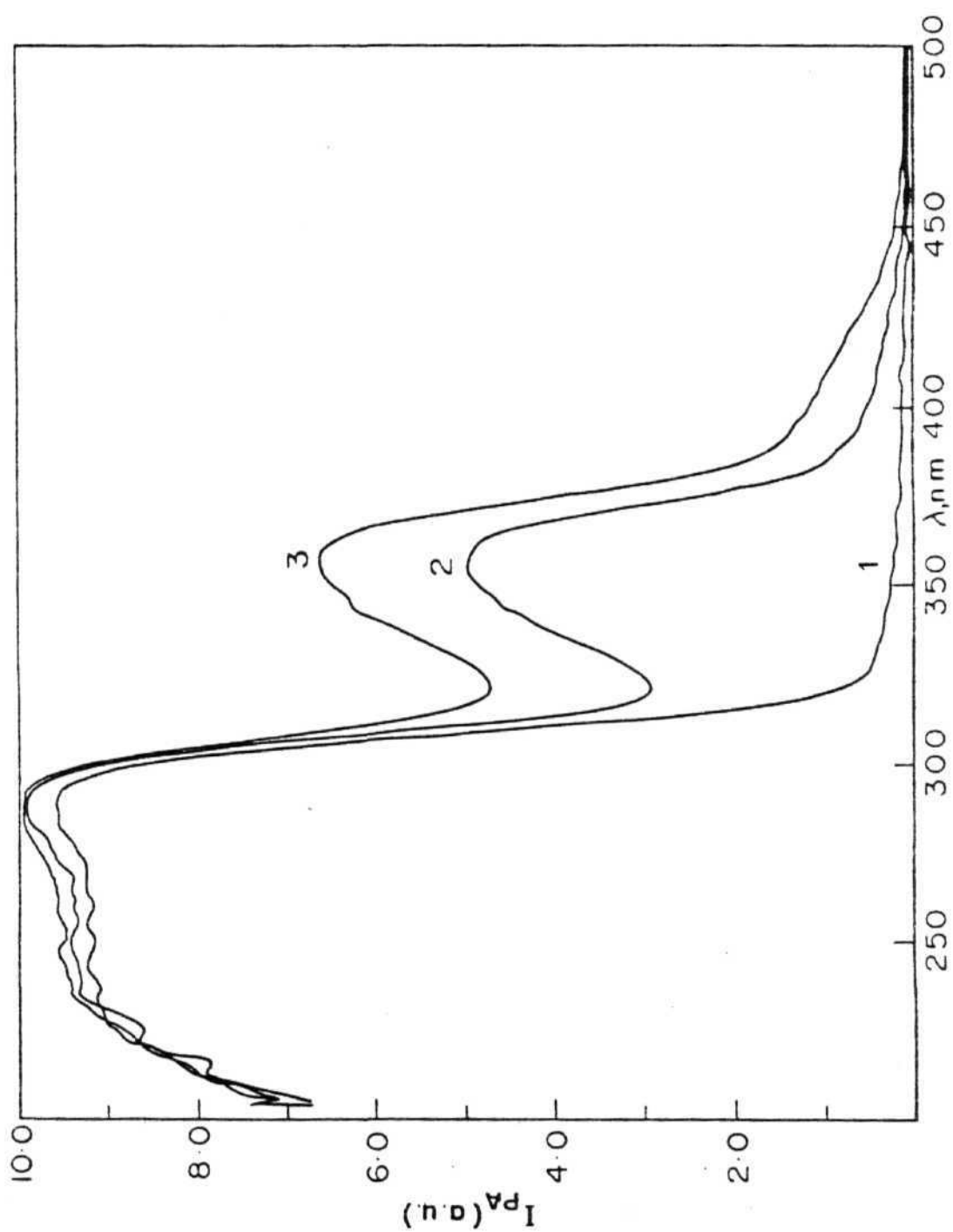


Figure 5.1. PA spectra of thiamin pyrophosphate. 1 is the first scan, 2 and 3 are second and third scans of the same sample.

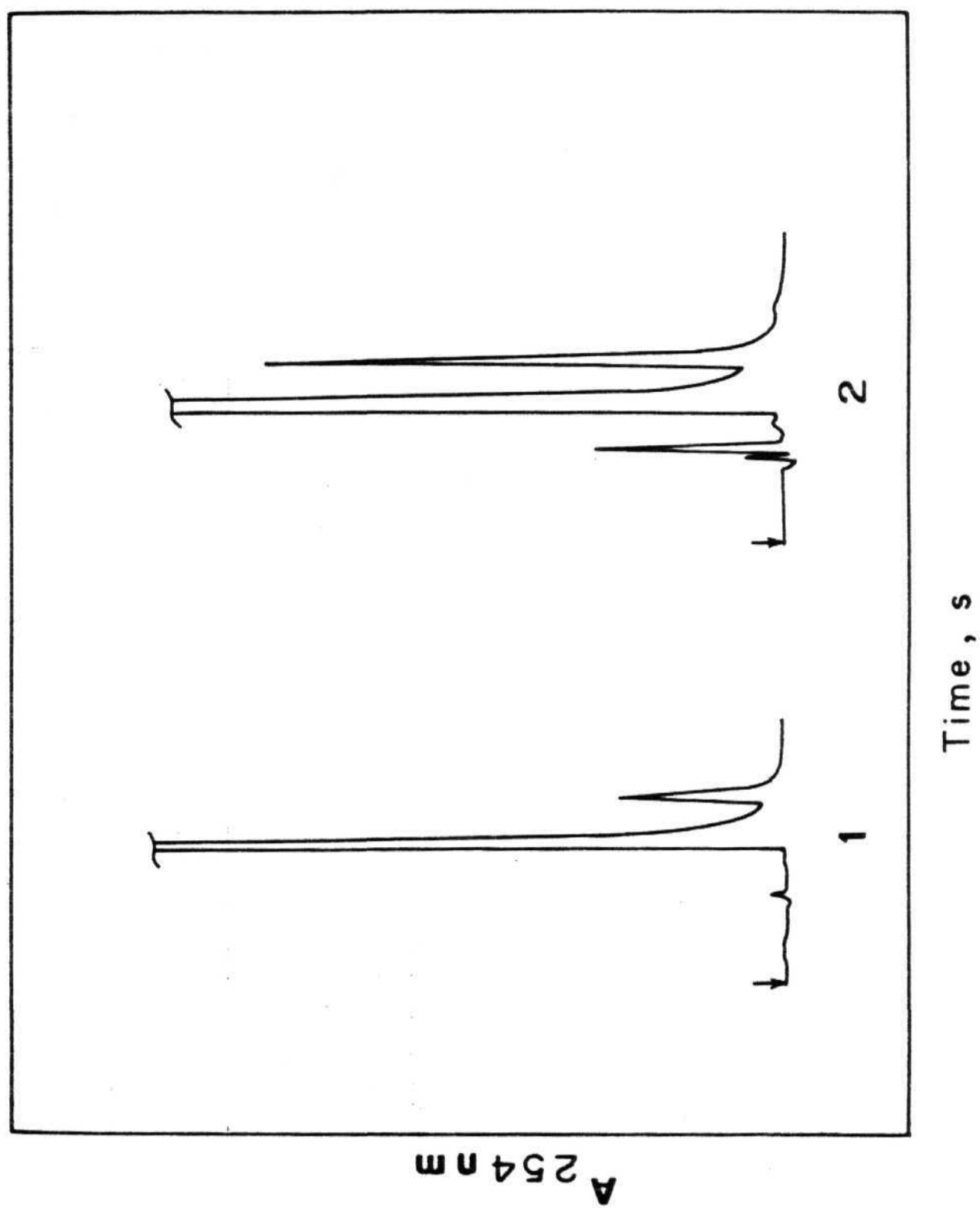


Figure 5.2 Chromatograms of thiamin (1) before and (2) after irradiation. C-18 column; 0.2 M phosphate buffer, pH 5.3.

pyrophosphate after exposure to uv radiation (trace 2) shows another peak, which might correspond to the photoproduct, eluting before thiamin pyrophosphate and thiamin monophosphate. It was necessary to expose the sample to uv radiation for nearly 24 hrs, with periodic mixing to ensure uniform exposure in order to detect the new peak in the chromatogram, corresponding to the photoproduct, while 30 seconds exposure was sufficient to detect the presence of the photoproduct in the PA experiment. This, we think, is due to the remarkable sensitivity of the PA method to surface modifications. Thiamin in solution (both at pH 1.0 and pH 7.4) shows negligible photomodification, while thiamin diphosphate shows no spectral change upon exposing to uv radiation. In contrast, thiamine in solid state undergoes detectable photomodification even when exposed to sunlight. These observations made on thiamin has prompted us to consider the possibility of exploring the PAS method to screen other vitamins for their photosensitivity. Figure 5.3 shows a similar cyclic set of runs of retinyl acetate, while Figure 5.4 shows similar spectra of tocopherol; it appears that both of these compounds also undergo extensive uv induced modification. Table 5.1 lists the samples we have screened for such photoactivity. It can be seen that several of the compounds tested show photodamage. Thus it appears that PAS can perhaps be effectively used to screen drugs and pharmaceuticals for their photoresistance or damage and to take appropriate precaution for the storage and packing of such samples that show photodamage.

#### 5.4 Photosynthesis

The second project is a study of some aspects of energy storage in photobiological systems. The PA signal, corrected for lamp intensity variations, is proportional to the product,  $\beta(\lambda) \eta(\lambda)$ , where  $\beta(\lambda)$  is the optical absorption coefficient and  $\eta(\lambda)$  is the efficiency of nonradiative decay at the wavelength  $\lambda$ .



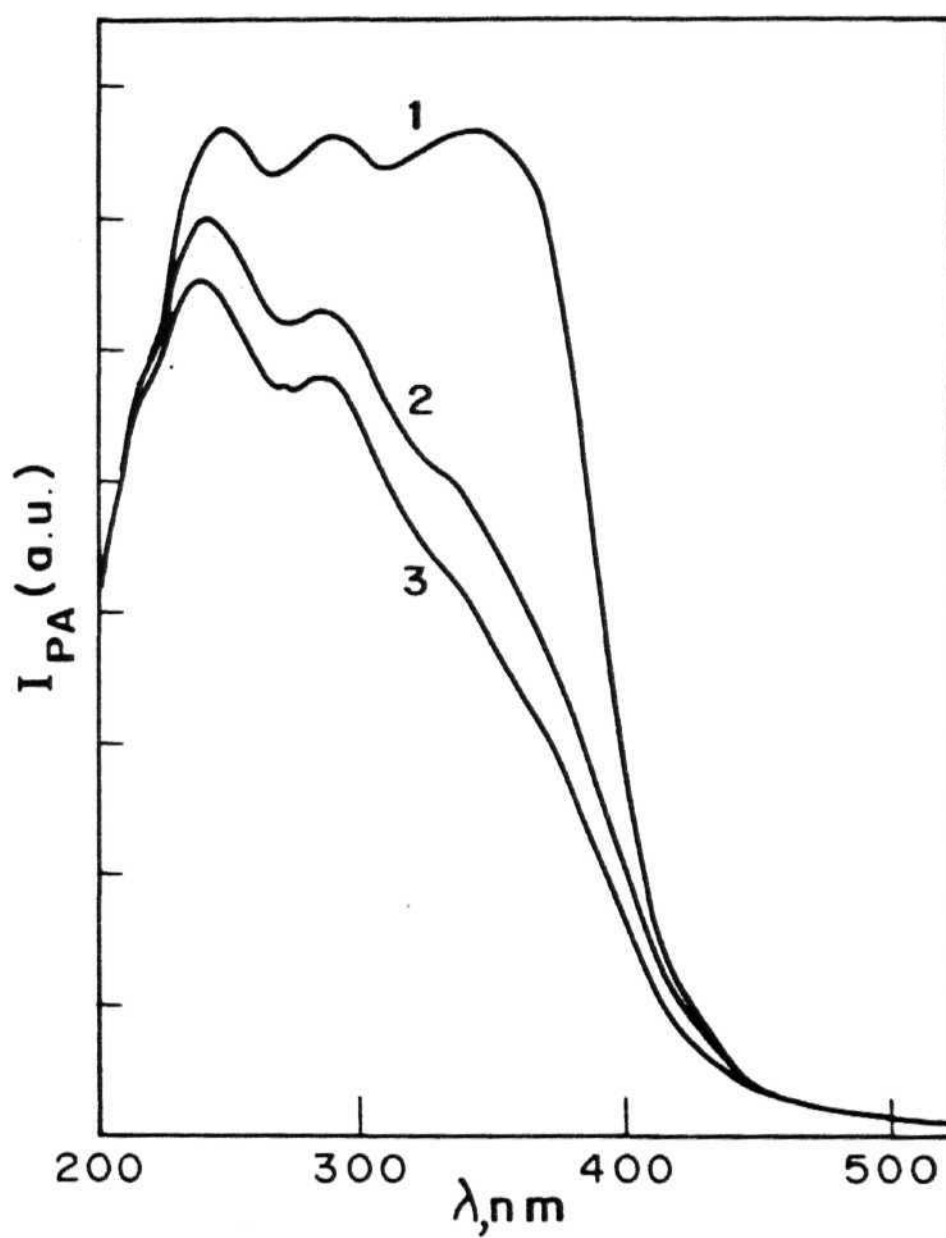


Figure 5.3 PA spectra of retinyl acetate. 1 is the first scan, 2 and 3 are second and third scans of the same sample.

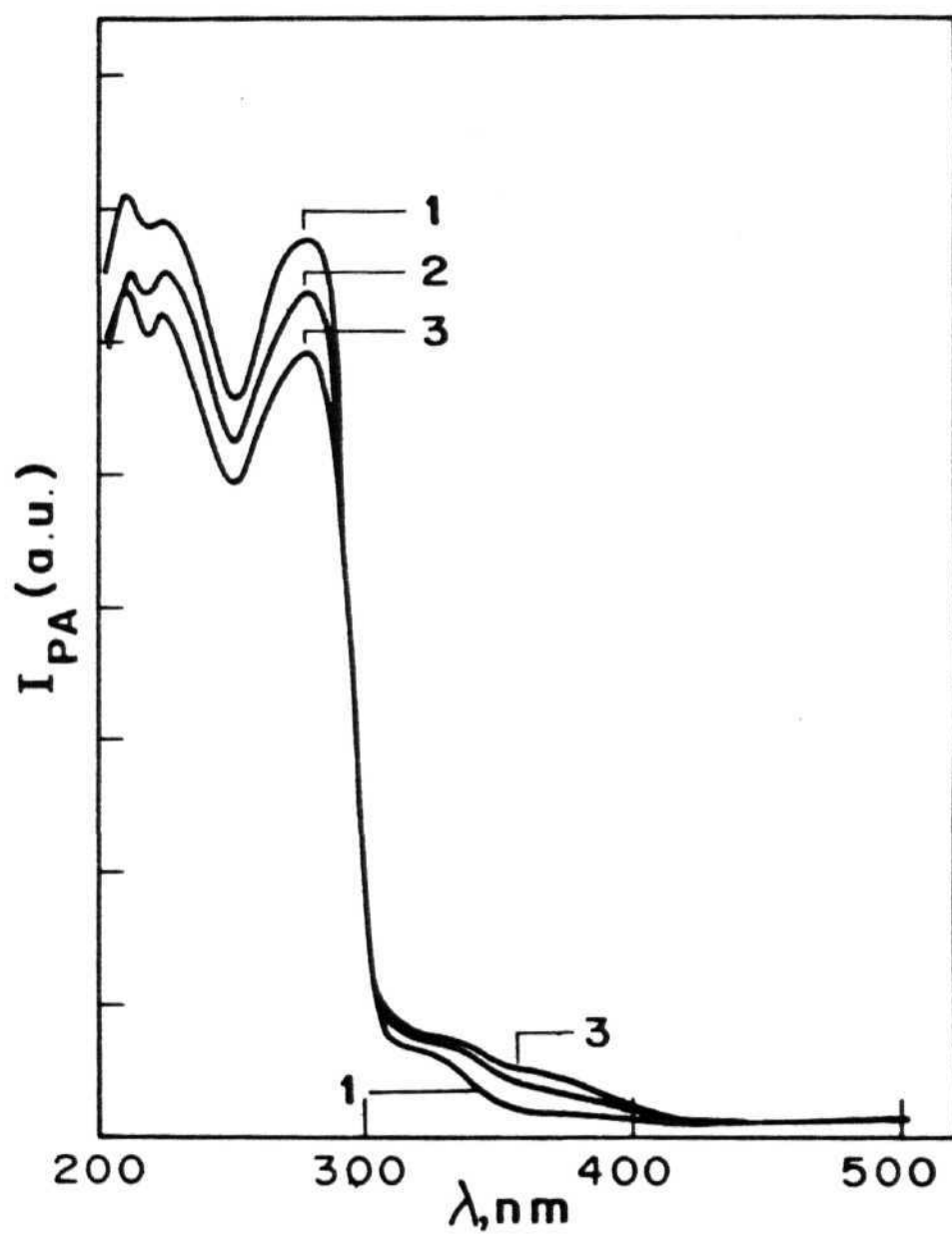


Figure 5.4 PA spectra of tocopherol. 1 is the first scan, 2 and 3 are second and third scans of the same sample.

TABLE 5.1 LIST OF VITAMINS THAT WERE SCREENED FOR POSSIBLE PHOTODAMAGE

Sl. No.	Sample	Photo-response	Appearance of new peaks and remarks
1. Retinol (S.A.) <sup>*</sup> (Vitamin A)		+	shows three peaks at 245, 295 and 345 nm; upon exposure total absorption decreases. 345, 245 peaks submerge, while 295 peak remains distinct.
2. Retinoic acid (S.A.)		+	absorption at 365 decreases and shifts to 350 nm.
3. Retinyl acetate (S.A.)		+	shows three peaks at 245, 295 and 345 nm, total absorption decreases upon exposure. Absorption at 345 submerges while 245 and 295 absorptions remain distinct.
4. Thiamin (S) <sup>*</sup> (Vitamin B <sub>1</sub> )		+	320 nm
5. Thiamin monophosphate (S)		+	362 nm; prolonged exposure results in shoulder at 312 nm.
6. Thiamin diphosphate (S)		+	355 nm
7. Thiamin pyrophosphate (S)		+	355 nm
8. Thiamin (solution pH ~ 1.0)		—	very little change observed around 320 nm.
9. Thiamin (solution pH 7.4)		—	-do-
10. Thiamin diphosphate (solution)		—	no change (contd...)

Sl. Nb.	Sample	Photo-response	Appearance of new peaks and remarks
11.	Thiamin (S, exposed to sun)	+	320 nm
12.	Thiamin pyrophosphate (S, exposed to sun)	+	355 nm
13.	Thiamin disulphide (S)	—	no change
14.	Oxythiamin (S)	+	315 nm
15.	Pyriothiamin (S)	+	350 nm
16.	Thiochrome	+	peak at 365 nm decreases with exposure and shifts to 355 nm.
17.	Riboflavin (S.A.) (Vitamin B <sub>2</sub> )	—	no change
18.	Cyano cobalamine (S.A.) (Vitamin B <sub>12</sub> )	—	no change
19.	Ascorbic acid (S.A.) (Vitamin C)	—	negligible increase in absorption around 325 nm
20.	Tocopherol (neat) (Vitamin E)	+	absorption at 230 and 280 nm decreases while there is slight increase in the absorption ~ 350nm.
21.	Menadione (Vitamin K)	+	shows a peak at 340 nm with a shoulder at 425 nm; absorption increases and shoulder shifts to 450 nm; absorption at 500 nm increases significantly.

\* S = solid state      S.A. = solid dispersed in alumina

The second term  $\eta(\lambda)$  is assumed to be equal to unity in the PA theory described in the first chapter. This is a reasonable assumption with routine samples, but in situations where the sample fluoresces (with an efficiency  $\phi_f$ ) or utilizes the energy of the excited state for driving photochemical reactions (with an efficiency  $\phi_{PC}$ ), the value of  $\eta$  would become less than unity (that is  $\eta + \phi_f + \phi_{PC} = 1$ ). For example a fluorescing molecule, fluorescein, which absorbs at 490 nm and fluoresces at around 520 nm (for fluorescein,  $\phi \approx 0$ ). Figure 5.5.a shows the PA spectrum of fluorescein in solution. Addition of potassium iodide to the fluorescein solution dramatically increases the PA signal at 490 nm (Figure 5.5 b). Potassium iodide does not absorb at 490 nm and hence cannot alter (3 (490). The observed increase in PA signal can be ascribed to a significant increase in  $\eta$  brought about by the quenching of the fluorescence by iodide ions. Similarly if a system utilizes the part of the absorbed energy in chemical reactions, but does not fluoresce (i.e.  $\phi > 0$ ,  $\phi_f = 0$ ) then the observed PA signal will be smaller, to the extent of energy stored in the process and the signal can again be recovered to its maximum value when the photochemical reactions are inhibited. Such an approach can be taken to study energy storage processes in the photosynthesis of green plants. Malkin and coworkers (see chapter 1) have carried out some pioneering work in this direction. The PA signal from isolated, photosynthetically active, chloroplasts represents only the fraction of the total energy absorbed, because the rest is used to drive photochemical reactions, and thus not available for heat production. If the chloroplasts are incubated with 3-(3,4-dichlorophenyl)-1,1-dimethylurea (DCMU), an electron transport inhibitor, then no storage of energy occurs and hence all the absorbed energy decays nonradiatively to yield an enhanced PA signal. The difference between the signals from the control and the poisoned chloroplasts contains information regarding the extent of energy storage; this difference being termed as 'photochemical loss'. Figure 5.6 shows the PA spectra

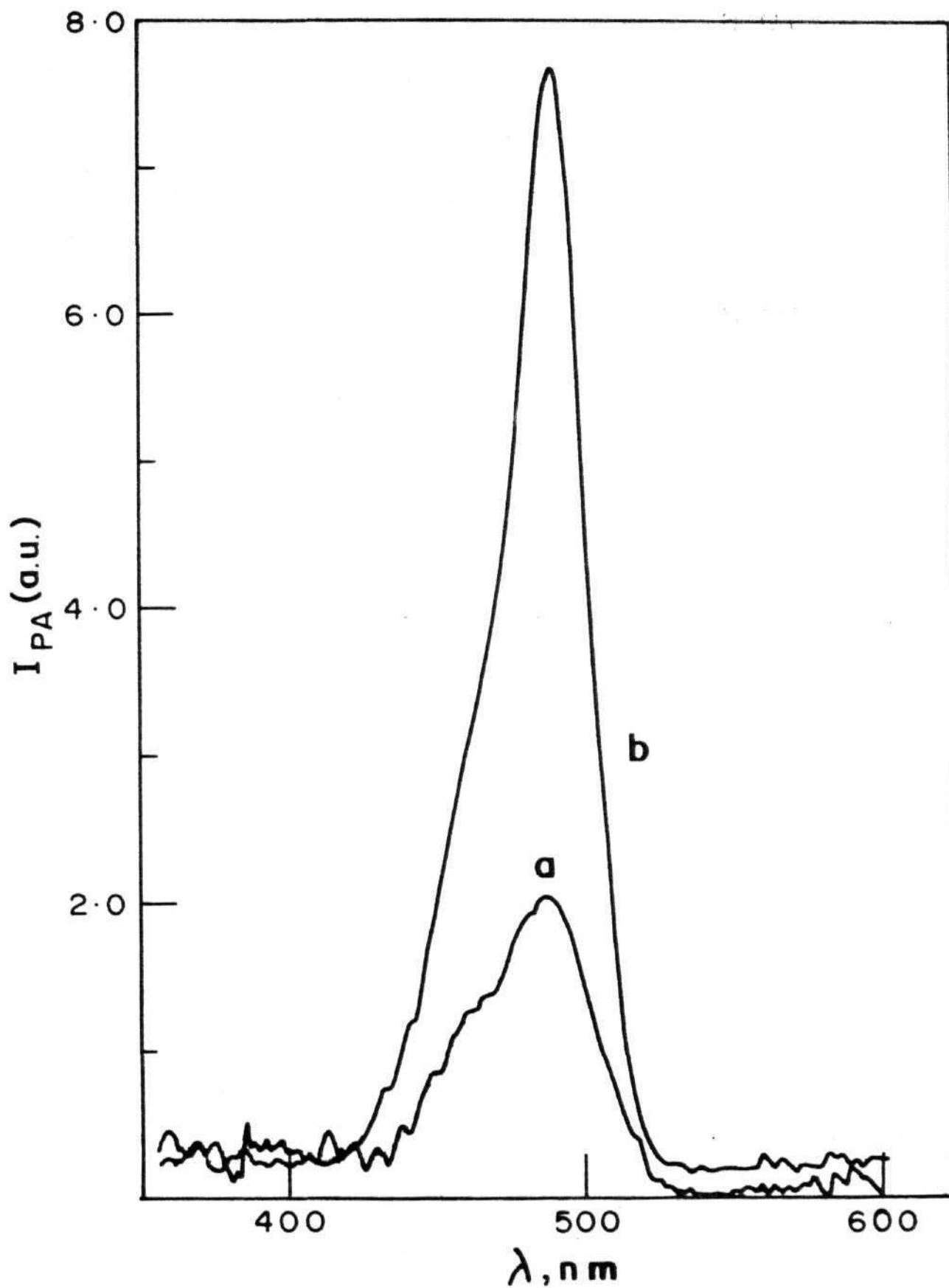


Figure 5.5 PA spectra of fluorescein in solution (a) without and (b) with added potassium iodide.

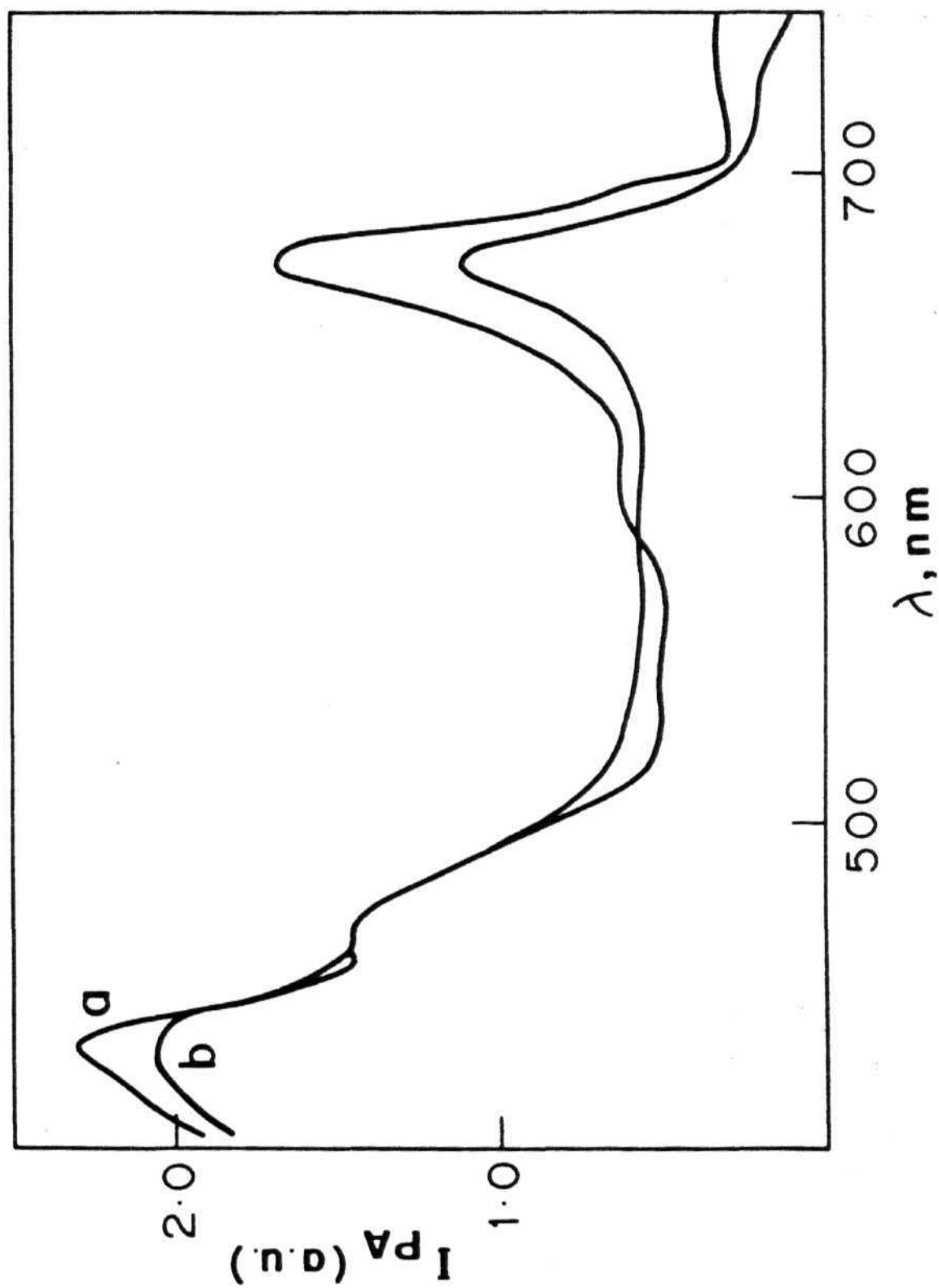


Figure 5.6 PA spectra of chloroplast suspension (a) with and (b) without the electron transport inhibitor, DCMU.

of Chloroplast suspensions in the presence and absence of DCMU. It can be seen that DCMU treatment enhances the PA signal, as expected. Our plans are to carry out a systematic study on the photosynthesis using various inhibitors that are known to inhibit the photosynthetic electron transport at various stages. We also intend to study the effect of the orientation of chloroplasts on their photosynthetic ability. There are several methods available for orienting chloroplasts, like stroking, or using electric or magnetic fields, we have chosen the magnetic orientation method for convenience. Chloroplasts or Chloroplast membrane preparations remain in a particular orientation as long as they are under the influence of a magnetic field. In order to "freeze" the chloroplasts in that orientation, we have taken the following approach. First, we suspended the chloroplasts in an appropriate buffer solution containing added bis-acrylamide, and placed the solution in a magnetic field of 13 kG provided by the pole gap of an ESR spectrometer. The acrylamide is allowed to polymerize into a gel while the chloroplasts are oriented in the magnetic field. After the completion of polymerization, the gel was removed from the magnetic field. Removal of the magnetic field would not cause any deorientation because the chloroplasts are now trapped in a phase where the translatory freedom of chloroplasts is drastically reduced. We could obtain a significant orientation of the chloroplasts using this method and verify it by recording the orthogonal polarization PA spectra (LDPA) for such samples. However the orientation obtained was not large enough to carry out further studies on energy storage. This, we think, is due to the slightly large pore size of the gel matrix wherein there may be considerable amount of space for each Chloroplast to move about, leading to partial deorientation. We are attempting to improve the orientation by a proper selection of pore sizes of the gel, the strength and duration of exposure to the magnetic field.



## 5. Concluding Remarks

The results presented in this thesis demonstrate the potential of photoacoustic spectroscopy: (i) in the study of surface changes as shown in the case of the measurement of surface acidity and photodamage of vitamins caused by very brief exposure to uv radiation; (ii) as a spectroscopic tool for solids for monitoring optical absorption, dichroism and photocalorimetry as shown in the study of the solid state photopolymerization of the diacetylene, BCMU; (iii) as a sensitive tool to study the nonradiative deexcitation processes as shown in the determination of the action spectrum of the photopolymerization of BCMU, and energy storage by photosynthesizing chloroplasts; (iv) in its successful application in the study of intact biological systems and to draw important conclusions as shown in the study of the malaria parasite.

Photoacoustic spectroscopy can be used to study several other photoresponsive systems, such as the photochemistry of substituted cinnamic acids and cumarins. Such a study can be expected to provide some insight into the factors effecting the solid state reactions. The action spectra of such reactions may provide valuable information in regard to the energy states involved in the reaction, and the effects of energy transfer on the solid state reaction, features that are not yet well understood. A systematic study of the photochemical loss, a measure of the extent of energy storage in the system, using various photosynthetic electron transport inhibitors and the study of effect of orientation of Chloroplast membranes and chloroplasts themselves on their photosynthetic ability, should be able to add to our understanding of photosynthesis in green plants.

Our study on the action of antimalarial drugs provided the first direct evidence for the presence of hemin self-aggregates along with the malaria pigment in the parasite and for the interaction of the drug with the endogenous hemin. This has led us to propose a comprehensive scheme of the mode of action of antimalarial drugs. While we have used lyophilized samples of parasites in this study, it would be certainly worthwhile to carry out further investigations on suspensions of the parasites growing in the appropriate medium. This study may lead to more concrete answers in regard to the action of antimalarial drugs. Also, we have observed spectral differences in the drug-sensitive and drug-resistant parasites. This difference may be exploited to screen blood samples of the malaria infected patients to discern information with regard to drug sensitivity. This appears at present rather difficult, since the strong hemoglobin absorption may mask the differences, but an analysis of the relative peak heights may still provide some clues. The remarkable sensitivity observed in the case of photoreaction of vitamins lends support to the hope that such a differentiation may not be impossible if one looks at blood smears.

The successful application of photoacoustic spectroscopy to more complicated chemical and biological systems is possible only with parallel improvement in the technique in terms of methodology and instrumentation. Since the PA signal strength is proportional to the intensity of the incident radiation, besides several other parameters, the signal strength for weakly absorbing sample can be increased by increasing the source intensity. Using lasers as light sources improves the sensitivity and also the resolution, since a narrow spectral bandwidth with sufficient power can be obtained. Biological samples such as tissues, parasites and organelles like chloroplasts are usually suspended in aqueous buffers. Since water has a high thermal capacity and a low thermal conductivity, its the thermal

diffusivity and hence the thermal diffusion length are very small. For example, the thermal diffusion length of water at a modulation frequency of 100 Hz is  $2 \times 10^{-3}$  cm. Since only the light absorbed within the thermal diffusion length can contribute to the PA signal, a large fraction of the absorbed energy for weakly absorbing samples in aqueous system goes undetected by the microphone. Use of piezoelectric detection system in this context has several advantages, since (i) the light absorbed in the entire sample contributes to the mechanical vibrations and results in a stronger signal, (ii) high modulation frequencies can be used which improve the time scale, and (iii) samples need not be contained in an airtight cell.

Another aspect of considerable interest in our laboratory is the study of the conformation and interaction of biomolecules. The study of conformational features of the biomolecules in model membranes, that are opaque or translucent, and in intact biological materials, is difficult due to optical opacity and light scattering problems. PA detection of circular dichroism in such samples may be quite useful. Modification of commercial spectrometers like EDT OAS 400 and EG&G PAR 6001 spectrometers should be straight forward. Such modification decreases the light intensity at the sample, and could pose a serious problem when recording the spectra of samples with low absorptivity; use of photoelastic modulator may prove to be useful in this context.

## VITAE

Chintalagiri Mohan Rao was born on 19th January 1954 at Hanamkonda, Warangal District, Andhra Pradesh. After his schooling at **Huzurabad**, he graduated from the Arts and Science College, Warangal in 1975 and received his M.Sc. degree in Chemistry from the Kakatiya University, Warangal in 1977 during which time he was awarded a National Merit Scholarship of the Government of India. He registered for his Ph.D. degree in Chemistry at the University of Hyderabad in 1977. During the period 1977-79 he was a Junior Research Fellow and during 1979-81 a Senior Research Fellow of the University Grants Commission. Presently he is a Senior Research Fellow of the Council of Scientific and **Industrial** Research, at the Centre for Cellular and Molecular Biology, Hyderabad. He was awarded the '**Young Scientist Award**' of A.P. Academy of Sciences for the year 1982.

## **LIST OF PUBLICATIONS**

1. Investigation of acidity of catalyst surfaces by photoacoustic spectroscopy  
Ch. Mohan Rao and D. Balasubramanian  
**Spectroscopy Letters** 13, 329-337, 1980.
2. Photoacoustic spectroscopy of biological systems  
D. Balasubramanian and Ch. Mohan Rao  
**Photochemistry and Photobiology** 34, 749-752, 1981.
3. Biological applications of photoacoustic spectroscopy  
D. Balasubramanian and Ch. Mohan Rao  
**Current Science** 51, 111-117, 1982.
4. **Study** of a solid state reaction by photoacoustic spectroscopy  
Ch. Mohan Rao and D. Balasubramanian  
**J. Physical Chemistry** 86, 939-943, 1982
5. Interaction of antimalarial drugs with hemin  
B. Panijpan, Ch. Mohan Rao and D. Balasubramanian  
(Manuscript submitted)
6. The malaria parasite monitored by photoacoustic spectroscopy  
D. Balasubramanian, Ch. Mohan Rao and B. Panijpan  
(Manuscript submitted)

### Papers presented in symposia and meetings

1. Photoacoustic studies on some photoreactive systems  
Ch. Mohan Rao and D. Balasubramanian  
Fourth Indian Photobiology Symposium, Mahabaleshwar, April, 1981.
2. Biological applications of photoacoustic spectroscopy: studies on photo-damage and on pigment orientation in chloroplasts.  
D. Balasubramanian and Ch. Mohan Rao  
VII International Biophysics Congress and III Pan-American Biochemistry Congress, Mexico City, Mexico, August 1981.
3. Solid state polymerization diacetylenes studies by photoacoustic spectroscopy.  
D. Balasubramanian and Ch. Mohan Rao  
Annual meeting of American Chemical Society, New York City, August 1981.
4. Photoacoustic study of the malaria parasite: mode of action of the chloro-quine class of drugs.  
B. Panijpan, Ch. Mohan Rao and D. Balasubramanian  
'III International Conference on Photoacoustic and Photothermal spectroscopy', Paris, April 1983.